Using Encoding to Reduce the Errors in Quantum Spin Chains

Catherine Keele

A thesis presented for the degree of

Doctor of Philosophy

School of Engineering, Physical and Mathematical Sciences

Royal Holloway, University of London

September 2021

Declaration

I, Catherine Keele, hereby declare that this thesis and the work presented in it is entirely my own. Where I have consulted the work of others, this is always clearly stated.

Signed:

Date: 08/09/2021

Acknowledgements

There are many people I would like to thank for their support and encouragement throughout my PhD. Primarily, I'd like to thank my supervisor, Dr Alastair Kay, for his unwavering support and unending patience, and for never making me feel stupid (even if sometimes my questions were!). I'd also like to thank my sister and my mum for always believing that I could do it. To the people who have been on this journey with me, I am grateful for the time spent talking about anything but the PhD! Special thanks go to Amy, Laura, Lydia, and Nicola for being my 'girl gang'; to Tabby for providing everlasting entertainment; to Liam for always providing a positive perspective; to everyone from office 253 for welcoming me to the department; and finally to Gemma, who I started my journey into physics with. My thanks would be incomplete without acknowledging Nick, and mentioning how supremely grateful I am for his constant care and support. The pandemic and multiple lock-downs would have been unbearable without his company and sense of humour.

Using Encoding to Reduce the Errors in Quantum Spin Chains

Catherine Keele

Abstract

Quantum computation is on the horizon, and promises to revolutionise the world of computing. With vastly more computing power, we will be able to simulate systems that are larger and significantly more complex than those we can currently simulate. We will also be able to solve problems that cannot be solved with classical computation. Within such quantum devices we require a way to transfer quantum states between registers. Quantum spin chains have been introduced as a solution to this, but their physical realisations will be subject to noise and errors associated with construction. In extreme cases, this noise could render spin chains unusable. We introduce a way to model this noise to show exactly how damaging it is to spin chains. We then present an encoding technique that can be used to reduce the effects of noise and fabrication defects in quantum spin chains. Our technique is easily applicable and particularly useful in situations where the number of qubits is not high enough for full error correction. We also demonstrate our technique on different systems to show the improvement that can be made.

Contents

List of Figures

0.1 List of Variables

For convenience, the variables used in this thesis are detailed below. This is not an exhaustive list, but covers much of the notation used throughout the thesis as a whole. Individual chapters may introduce additional variables.

- N: The number of sites in a chain
- n: The specific site number we refer to (our convention is to label these 1 through to N, where 1 is the initial site and N is the final site)
- J_n: The coupling strength between sites n and $n+1$, (the $\frac{1}{2}(X_nX_{n+1}+Y_nY_{n+1})$ term in the Hamiltonian).
- B_n: The strength of magnetic field on site n, (the $\frac{1}{2}Z_n$ term in the Hamiltonian).
- $|0\rangle$: A single spin in the relaxed state
- $|0\rangle^{\otimes N} \equiv |\mathbf{0}\rangle$: A chain of length N where all spins are in the relaxed state
- $|1\rangle$: A single spin in the excited state
- $|\mathbf{n}\rangle$: A chain where only the spin at site n is excited
- $|\psi\rangle$: The state on a single qubit or encoding region
- $|\boldsymbol{\psi}\rangle$: The state over a set of qubits
- H: The Hamiltonian
- H_i: The Hamiltonian in the i-excitation subspace
- $\mathcal{Q}$: The superoperator describing some general noise
- $\mathcal{Q}_D$: The superoperator describing the dephasing noise
- $\mathcal{Q}_A$: The superoperator describing amplitude damping noise
- X, Y, Z: The pauli-X,-Y,-Z matrices respectively

- S_i: The ith excitation subspace
- $S_{i,j}$: The subspace including excitations in the i and j excitation subspaces
- Γ_z: Dephasing strength parameter
- Γ_x: Amplitude damping strength parameter
- ρ: The density matrix
- $|\rho\rangle$: The density vector
- t_0: The optimal extraction time for perfect state transfer, i.e when fidelity = 1.
- M: Size of encoding region
- Λ: Set of sites belonging to the decoding region

Chapter 1

Introduction

1.1 Introduction

Since the introduction of personal computers to the market in 1977, their size has reduced dramatically and they have become increasingly more powerful [1]. This is largely due to the growth of the semi-conductor industry and the ability to manufacture ever smaller transistors. Computers are now used in almost every aspect of daily life, from personal devices such as mobile phones, all the way up to supercomputers. For many people today, it is hard to imagine a world without computers and we experience the benefits of them every day. Computers have contributed to every sector of human existence, creating invaluable contributions to the worlds of medicine, education, manufacturing, and research, among many others. However, many of the world's greatest problems have such complexity that they cannot be solved by classical computation, and instead require something with vastly more computing power. Examples of these problems are the modelling of organic systems and chemical reactions. Organic systems are generally very complex [2], which makes simulating them time-consuming at best and impossible at worst. Quantum computation could allow us to simulate such systems, leading to leaps in our understanding of biological systems and the chemical interactions used in pharmacology. These quantum computers provide vastly more computing power, that classical computers can never achieve, due to time limitations, and we call this quantum supremacy [3], [4]. The idea of a computer based on quantum mechanics was first introduced by Richard Feynman in 1981 [5], who envisioned creating a device that could simulate the physical world - meaning to simulate quantum physics. Since then, the area of quantum computing has become very popular in the academic world for both experimentalists and theoreticians, and within industry, with large competitors such as Google and IBM competing to win the race for full-scale quantum computation. Quantum computing continues to be an exciting area of research for both academic research and industry and [6], [7], [8], [9], and [10] provide just a small snapshot of the exciting world of quantum computation.

Quantum computation is a vast topic, and if it is to be eventually realised, we must break it down into various smaller topics. The particular part of quantum computing

that we cover here is the topic of state transfer, which refers to the transfer of states between quantum registers. To complete such a task, one can use quantum *spin chains* (see Chapter 2). These quantum spin chains are subject to errors due to imperfect construction, which can negatively affect the quality of the transfer (Chapter 3). Further to this, any physical system will be subject to noise, which also reduces the transfer quality significantly (Chapter 4). In this thesis, we present a technique that provides significant improvement on quality of transfer in the presence of these two issues. Our technique is simpler than the quantum error correction schemes that are currently available, and uses less qubits. Therefore our technique is more applicable to current quantum devices, where qubit numbers are small.

We now give an overview of what the reader will find in this thesis. In this Chapter, we introduce the concepts required to understand quantum computation, and the current experimental realisations. In Chapter 2, we introduce spin chains as a method for transferring quantum states. We give a measure of success for the systems and techniques we describe and outline much of the more in-depth methods described in each of Chapters 3 and 4. In Chapter 3, we demonstrate the effects of random errors on an otherwise perfect chain, and introduce our encoding method for mitigation of these errors. In Chapter 4, we develop a method that allows us to consider systems with noise and we demonstrate that our encoding can also be applied to noisy systems with improvement in fidelity of transfer. In Chapter 5, we extend our technique to higher excitation subspaces.

1.2 Qubits

To understand the concept of quantum computing, we must first discuss the basic component of the quantum computer - the *qubit*, and we introduce these via the more familiar *classical computing*. Classical computing is well understood and utilises *bits* to store and manipulate data. A bit is a system that exists in one of two states; on/off, up/down, high/low, etc, where the classical computing realisation of these is usually a small electronic device, called a transistor. Physically, a transistor is a device that can

allow current to pass or not - giving our two states and effectively acting as a switch. The states of a bit are given as 0 and 1 (0 being the 'off' state and 1 being the 'on' state). Qubits, however, are not confined to being in *either* the state 0 or the state 1, they may instead exist in a *superposition* of the two states. To make sense of this, we introduce $|0\rangle$ and $|1\rangle$ as the qubit states that are somewhat equivalent to the 0 and 1 of a classical qubit. The notation $|\ \rangle$ is explained in detail in Section 1.3, but for now we will ignore it to instead gain some conceptual understanding of what a superposition state is. We note here that $|0\rangle$ is often known as the *ground state*, and $|1\rangle$ as the *excited state*. We can write the total state on a qubit as

$$|\psi\rangle = \alpha|0\rangle + \beta|1\rangle \tag{1.1}$$

where $|\alpha|^2 + |\beta|^2 = 1$ and α and β give the proportion of each of the composite states present in the superposition, such that if we have $\alpha = 1$ and $\beta = 0$ then we have the state $|\psi\rangle = |0\rangle$ and effectively have the classical state, 0. Similarly, if $\beta = 1$ and $\alpha = 0$, the we have the classical 1 state. This superposition only remains in place as long as no measurement is made on the system. Once a measurement has been performed on a qubit, the superposition no longer holds and the system remains in the state $|0\rangle$ with probability $|\alpha|^2$ or the state $|1\rangle$ with probability $|\beta|^2$. We can represent all possible states of a qubit on surface the Bloch sphere, where $\alpha = \cos\frac{\theta}{2}$ and $\beta = \sin\frac{\theta}{2}e^{i\phi}$ and the angles θ and ϕ are indicated on the Bloch sphere in Fig. 1.1, where $0 \leq \theta \leq \pi$ and $0 \leq \theta \leq pi$. It then becomes clear that qubits have the ability to hold much more information and can exist in infinitely many states (limited only by the ability to distinguish states that are close together on the surface of the Bloch sphere), where a bit can only exist in two states.

1.3 Vector Space, Dirac Notation, and Multiple Qubits

Although a qubit is interesting in itself, for us to move towards quantum devices and quantum computation, we will need multiple qubits in a single device. Therefore,

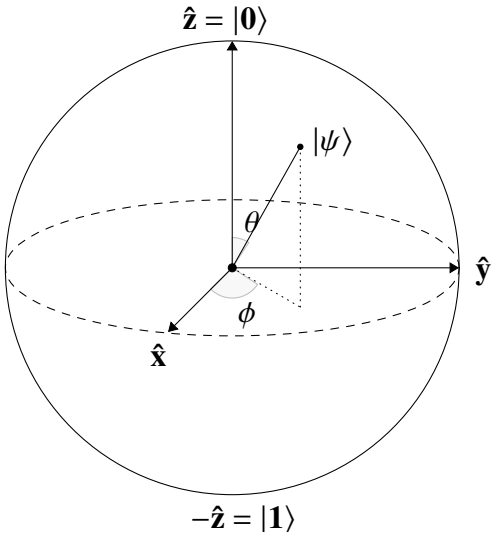

Figure 1.1: *The Bloch sphere, where all possible states of a qubit can be described as a location on the surface in terms of the angles θ and ϕ, where $0 \leq \theta \leq \pi$ and $0 \leq \theta \leq pi$.*

we require some important mathematical concepts to allow us to treat multiple qubits. Here we will introduce vector spaces along with Dirac notation (that allows us to write vectors more succinctly) and then demonstrate how we can consider multiple qubits. We introduce the vector space $\mathbb{C}^n$, which is the space of all $n-$tuples of complex numbers $(z_1, z_2, \ldots, z_n)$, i.e. vectors of n complex elements. We have already seen this used in $|0\rangle$ and $|1\rangle$ where the notation $|\ \rangle$ is used to describe a column vector. In the specific case of the single qubit states $|0\rangle$ and $|1\rangle$ they are given as

$$|0\rangle \equiv \begin{bmatrix} 1 \\ 0 \end{bmatrix}, |1\rangle \equiv \begin{bmatrix} 0 \\ 1 \end{bmatrix}. \tag{1.2}$$

This can be extended to consider a general vector $|w\rangle$, colloquially known as a *ket*, which describes the column vector

$$|w\rangle \equiv \begin{bmatrix} w_1 \\ w_2 \\ \vdots \\ w_n \end{bmatrix}. \tag{1.3}$$

We also introduce $\langle v|$, known as a *bra*, as the row vector

$$\langle v| \equiv \begin{bmatrix} v_1^* & v_2^* & \dots & v_n^* \end{bmatrix}, \tag{1.4}$$

where converting between row and column vector requires taking the hermitian conjugate, i.e. the complex conjugate of each element, such that $\langle A| = |A\rangle^\dagger$. We can take the inner product of these vectors as such

$$\langle v|w\rangle = v_1^* w_1 + v_2^* w_2 + \cdots + v_n^* w_n \tag{1.5}$$

which produces a scalar value. We can also use this notation to give the outer product as

$$|v\rangle\langle w| = \begin{bmatrix} v_1 w_1^* & v_1 w_2^* & \dots & v_1 w_n^* \\ v_2 w_1^* & v_2 w_2^* & \dots & v_2 w_n^* \\ \vdots & \vdots & \ddots & \vdots \\ v_n w_1^* & v_n w_2^* & \dots & v_n w_n^* \end{bmatrix} \tag{1.6}$$

which results in a matrix.

As we have seen, a single qubit or spin site can be represented as $|0\rangle$ or $|1\rangle$ (or a superposition of the two), and has the vector space $\mathbb{C}^2$, but often the case is that we want to build a system that contains more than one qubit, so we need to understand how to represent multiple qubits. If we consider two qubits, $|0\rangle_A$ and $|0\rangle_B$, we can write the system containing both of these as $|0\rangle_A \otimes |0\rangle_B$ where the tensor product is given by

$$\begin{bmatrix} 1 \\ 0 \end{bmatrix}_A \otimes \begin{bmatrix} 1 \\ 0 \end{bmatrix}_B \rightarrow \begin{matrix} 1_A \times \begin{bmatrix} 1 \\ 0 \end{bmatrix}_B \\ 0_A \times \begin{bmatrix} 1 \\ 0 \end{bmatrix}_B \end{matrix} \rightarrow \begin{bmatrix} 1 \\ 0 \\ 0 \\ 0 \end{bmatrix}_{AB} \tag{1.7}$$

where the subscripts are used to make the ordering clear. The same method is used for

larger systems, so a system containing N qubits all in the state $|0\rangle$ is given by

$$|0\rangle_1 \otimes |0\rangle_2 \otimes ... \otimes |0\rangle_N = |0\rangle^{\otimes N} \tag{1.8}$$

such that the vector that represents this has 2^N entries. It is important to note that the tensor product can be written in multiple ways. The notation used above is easy to understand but long, so we simplify to $|0\rangle \otimes |0\rangle = |0\rangle|0\rangle = |00\rangle$. When we begin to talk specifically about spin systems we define $|\boldsymbol{\psi}\rangle = |0\rangle^{\otimes N}$ or $|\boldsymbol{\psi}\rangle = |\mathbf{0}\rangle$ where all qubits in the system $|\boldsymbol{\psi}\rangle$ are in the relaxed state. This is particularly useful when if we need to represent arbitrarily long systems.

1.4 Operators

We have introduced a qubit, and demonstrated that we can consider a system containing multiple qubits, but as of yet we have not introduced a method to act upon these qubits and alter their states. This is where we introduce operators, starting with the Pauli matrices and later introducing the time evolution operator (Section 1.8) - a key component in state transfer, which we will introduce later (Section 2.2). The ability to manipulate quantum states happens via operators, which may be represented as matrices. Some of the most useful of these are the Pauli matrices, which are given by

$$X = |0\rangle\langle 1| + |1\rangle\langle 0| \equiv \begin{bmatrix} 0 & 1 \\ 1 & 0 \end{bmatrix}, \tag{1.9}$$

$$Y = \begin{bmatrix} 0 & -i \\ i & 0 \end{bmatrix}, \tag{1.10}$$

$$Z = |0\rangle\langle 0| - |1\rangle\langle 1| \equiv \begin{bmatrix} 1 & 0 \\ 0 & -1 \end{bmatrix}. \tag{1.11}$$

Is it also useful to include the 2×2 Identity matrix in these

$$\mathbb{1} = \begin{bmatrix} 1 & 0 \\ 0 & 1 \end{bmatrix}. \tag{1.12}$$

We can now see that by allowing the Pauli-X matrix to act on the $|1\rangle$ state (by matrix multiplication) we will get the $|0\rangle$ state, therefore it acts as a quantum NOT gate (changing a state from $|0\rangle$ to $|1\rangle$ and vice versa),

$$X|1\rangle = \begin{bmatrix} 0 & 1 \\ 1 & 0 \end{bmatrix}\begin{bmatrix} 0 \\ 1 \end{bmatrix} = \begin{bmatrix} 1 \\ 0 \end{bmatrix}. \tag{1.13}$$

Similarly, if we allow the Identity operator to act on one of the states, it will return the state unchanged. An important note to make, is that if we consider the operator X_i, this means that we apply the X operator to the i^{th} spin and the Identity operator to all other spins in the system, so that in reality we have $X_i = \mathbb{1}_1 \otimes \mathbb{1}_2 \otimes \ldots X \ldots \otimes \mathbb{1}_{N-1} \otimes \mathbb{1}_N$. These operators are often combined to create more complicated operations, such as the Hamiltonian, which will be discussed in more detail in Section 2.2.

1.5 The Computational Basis

When working within a vector space, we must make it clear what basis we use. Here we introduce our chosen basis. Using the tensor product to represent a system with multiple qubits leads to a natural choice. We demonstrate our chosen basis using a system containing 3 qubits, where have the following states according to excitation number.

$$\left.\begin{aligned} |0\rangle \otimes |0\rangle \otimes |0\rangle = |000\rangle \end{aligned}\right\} S_0 \tag{1.14a}$$

$$\left.\begin{aligned} |0\rangle \otimes |0\rangle \otimes |1\rangle = |001\rangle \\ |0\rangle \otimes |1\rangle \otimes |0\rangle = |010\rangle \\ |1\rangle \otimes |0\rangle \otimes |0\rangle = |100\rangle \end{aligned}\right\} S_1 \tag{1.14b}$$

$$\left.\begin{aligned} |0\rangle \otimes |1\rangle \otimes |1\rangle &= |011\rangle \\ |1\rangle \otimes |0\rangle \otimes |1\rangle &= |101\rangle \\ |1\rangle \otimes |1\rangle \otimes |0\rangle &= |110\rangle \end{aligned}\right\} S_2 \tag{1.14c}$$

$$\left.\begin{aligned} |1\rangle \otimes |1\rangle \otimes |1\rangle &= |111\rangle \end{aligned}\right\} S_3. \tag{1.14d}$$

We have also divided the basis into sets which span subspaces S_n, where n is the excitation number. If we compute the tensor products and write them as the columns of a matrix, ordered as in Eqs. (1.14), we get

$$Basis = \begin{bmatrix} 1 & 0 & 0 & 0 & 0 & 0 & 0 & 0 \\ 0 & 1 & 0 & 0 & 0 & 0 & 0 & 0 \\ 0 & 0 & 1 & 0 & 0 & 0 & 0 & 0 \\ 0 & 0 & 0 & 0 & 1 & 0 & 0 & 0 \\ 0 & 0 & 0 & 1 & 0 & 0 & 0 & 0 \\ 0 & 0 & 0 & 0 & 0 & 1 & 0 & 0 \\ 0 & 0 & 0 & 0 & 0 & 0 & 1 & 0 \\ 0 & 0 & 0 & 0 & 0 & 0 & 0 & 1 \end{bmatrix}. \tag{1.15}$$

Usually it is more useful to be able to separate the systems into the excitation subspaces, so it is convenient to swap some columns around so that those representing a particular number of excitations are adjacent. In this particular case, that means swapping columns 4 and 5 and the matrix above converts between the two orderings. If we then decide to only consider systems with 0 excitations or 1 excitation, we can restrict this matrix and take S_0 and S_1

$$S_{0,1} = \text{span}(|000\rangle, |001\rangle, |010\rangle, |100\rangle). \tag{1.16}$$

We are able to consider parts of this matrix separately as we have a block matrix where all elements in the rows and columns adjacent to the block are 0. More generally, as

long as a matrix commutes with the total Z operator such that

$$\left[A, \sum_{n=1}^{N} Z_n\right] = 0, \tag{1.17}$$

where $[A, B] = AB - BA$, it can be divided into separate subspaces, given by the eigenvalues of B. We can demonstrate that this is true by considering the case where $N = 3$.

Example 1. If we consider the case where $N = 3$, then we can expand the part $\sum_{n=1}^{N} Z_n$ to give

$$\sum_{n=1}^{3} Z_n = (Z_1 \otimes \mathbb{1}_2 \otimes \mathbb{1}_3) + (\mathbb{1}_1 \otimes Z_2 \otimes \mathbb{1}_3) + (\mathbb{1}_1 \otimes \mathbb{1}_2 \otimes Z_3), \tag{1.18}$$

$$\sum_{n=1}^{3} Z_n = \begin{bmatrix} 3 & 0 & 0 & 0 & 0 & 0 & 0 & 0 \\ 0 & 1 & 0 & 0 & 0 & 0 & 0 & 0 \\ 0 & 0 & 1 & 0 & 0 & 0 & 0 & 0 \\ 0 & 0 & 0 & -1 & 0 & 0 & 0 & 0 \\ 0 & 0 & 0 & 0 & 1 & 0 & 0 & 0 \\ 0 & 0 & 0 & 0 & 0 & -1 & 0 & 0 \\ 0 & 0 & 0 & 0 & 0 & 0 & -1 & 0 \\ 0 & 0 & 0 & 0 & 0 & 0 & 0 & -3 \end{bmatrix}. \tag{1.19}$$

We can then take the eigenvectors and eigenvalues of this matrix, we have eigenvalues: $\{\lambda\} = +3, +1, +1, +1, -1, -1, -1, -3$ which correspond to the eigenvectors:

$$\{|\lambda\rangle\} = \begin{bmatrix} 1 \\ 0 \\ 0 \\ 0 \\ 0 \\ 0 \\ 0 \\ 0 \end{bmatrix}, \begin{bmatrix} 0 \\ 1 \\ 0 \\ 0 \\ 0 \\ 0 \\ 0 \\ 0 \end{bmatrix}, \begin{bmatrix} 0 \\ 0 \\ 1 \\ 0 \\ 0 \\ 0 \\ 0 \\ 0 \end{bmatrix}, \begin{bmatrix} 0 \\ 0 \\ 0 \\ 0 \\ 1 \\ 0 \\ 0 \\ 0 \end{bmatrix}, \begin{bmatrix} 0 \\ 0 \\ 0 \\ 1 \\ 0 \\ 0 \\ 0 \\ 0 \end{bmatrix}, \begin{bmatrix} 0 \\ 0 \\ 0 \\ 0 \\ 0 \\ 1 \\ 0 \\ 0 \end{bmatrix}, \begin{bmatrix} 0 \\ 0 \\ 0 \\ 0 \\ 0 \\ 0 \\ 1 \\ 0 \end{bmatrix}, \begin{bmatrix} 0 \\ 0 \\ 0 \\ 0 \\ 0 \\ 0 \\ 0 \\ 1 \end{bmatrix}, \tag{1.20}$$

Where we have ordered these from lower excitation number to higher excitation number. Now we can see that the system divides into subspaces, where the different eigenvalues refer to systems with different excitation number.

For much of this thesis, we remain in the single excitation subspace, and as such, we take the first four vectors representing the first four states, as in Eq. (1.16) as above. We can write these in a more concise format using ket notation

$$S_{0,1} = \text{span}\big(|\mathbf{0}\rangle, |\mathbf{1}\rangle, |\mathbf{2}\rangle, |\mathbf{3}\rangle\big) \tag{1.21}$$

where the number in bold gives the location of the excitation and the $|\mathbf{0}\rangle$ is the all zero case. It is important to note here that $|0\rangle$ and $|\mathbf{0}\rangle$ are generally not equivalent; the former describes a single qubit in the spin down state and the latter describes a number of qubits all in the spin down state. Similarly $|1\rangle$ represents a single excited qubit and $|\mathbf{1}\rangle$ represents a system of qubits where only the qubit in position 1 is excited. We now demonstrate how the states of multiple qubit systems can be represented in Dirac notation.

Example 2. Representing a superposition with kets

Let's consider the case where we have the state $|\psi\rangle = \alpha|\mathbf{0}\rangle + \beta|\mathbf{2}\rangle$ (where $N = 3$) which indicates a superposition between the $|000\rangle$ and the $|010\rangle$ states (a superposition on qubit two). As a single column vector this can be written as

$$|\psi\rangle \equiv \begin{bmatrix} \alpha \\ 0 \\ \beta \\ 0 \end{bmatrix}. \tag{1.22}$$

in the $S_{0,1}$ subspace. So we can see that the α will always be present in the first position (which indicates the zero excitation subspace, S_0) and the β will appear in the position indicating where the excitation is. Of course this corresponds to the case where we have a chain of 3 qubits, and can be generalised to larger N. We also note that this case is

specific to a single excitation located on only one qubit, which will not be true as the system goes through Hamiltonian evolution. Later we introduce encoding and decoding regions where instead we have a single excitation, initially spread over a number of sites.

1.6 Pure States, Mixed States, and the Density Operator

Much of what we have discussed up to now, is assuming that the state of a system is *pure*, however, in general that will not be the case - and particularly not when we introduce noise. We therefore introduce the reader to the concept of *pure states* and *mixed states* and show how these can be described with the density operator. A pure state is a state that is completely known and satisfies the condition that $\mathrm{Tr}(\rho^2) = 1$. In the case of the pure state, the density operator is given by

$$\rho = |\psi\rangle\langle\psi|. \tag{1.23}$$

A mixed state, by contrast, is one where the state is not completely known and is an ensemble of different pure states. Mixed states satisfy $\mathrm{Tr}(\rho^2) < 1$. The density operator for a mixed state is given as

$$\rho = \sum_j p_j |\psi_j\rangle\langle\psi_j|. \tag{1.24}$$

For a single qubit state, we can see what a density operator may look like. Our qubit state is $|\psi\rangle = \alpha|0\rangle + \beta|1\rangle$, then the density matrix is given as $\rho = |\psi\rangle\langle\psi|$. Multiplying this out, we get

$$\rho = |\alpha|^2|0\rangle\langle 0| + \alpha\beta^*|0\rangle\langle 1| + \alpha^*\beta|1\rangle\langle 0| + |\beta|^2|1\rangle\langle 1| \tag{1.25}$$

$$\rho = \begin{bmatrix} |\alpha|^2 & \alpha\beta^* \\ \alpha^*\beta & |\beta|^2 \end{bmatrix}. \tag{1.26}$$

The density operator evolves as $\rho' = U\rho U^\dagger$, where ρ' is the density operator at a later time, and U is the evolution operator.

1.7 Fidelity

Often in quantum systems, it is necessary to transfer a state from one qubit to another, but to do so we require a measure of how well a state has been transferred. Here we introduce *fidelity* as a measure of success

$$F = \langle \psi_{desired} | \rho | \psi_{desired} \rangle, \tag{1.27}$$

where $\rho = |\psi\rangle\langle\psi|$ is the density operator and fidelity is essentially a measure of how close a state is to the desired state and a perfectly transferred state will have a fidelity of 1. Usually, the measure we are interested in is the *average fidelity*, which gives the fidelity averaged over all input states, and we will denote this as $\overline{F}$. In Section 2.2, we will introduce spin chains as a way of transferring states through quantum systems, and to allow us to see the merit of these spin chains, we first demonstrate the calculation of fidelity for semi-classical communication. Semi-classical communication means that we measure a qubit state, then transfer that information classically, before applying the communicated state to a second qubit. We note that for spin chains to be useful to us, they must provide a fidelity that is higher than transferring the state semi-classically. Starting with a single qubit in the superposition state

$$|\psi\rangle = \cos\frac{\theta}{2}|0\rangle + \sin\frac{\theta}{2}e^{i\phi}|1\rangle, \tag{1.28}$$

where $0 \leq \theta \leq \pi$ and $0 \leq \theta \leq pi$, we can measure this in the $z-$basis, such that we measure the state $|0\rangle$ with probability $\cos\frac{\theta}{2}^2$ or the state $|1\rangle$ with probability $\sin\frac{\theta}{2}^2$. Such measurement destroys the information that was stored within the superposition. We then communicate the measured state to the receiver, who then recreates the state $|0\rangle$ or $|1\rangle$ so that the output is

$$\rho = \cos^2\frac{\theta}{2}|0\rangle\langle 0| + \sin^2\frac{\theta}{2}|1\rangle\langle 1|. \tag{1.29}$$

Then, from Eq. (1.27), the fidelity is given by

$$F = \cos^2\frac{\theta}{2}\cos^2\frac{\theta}{2} + \sin^2\frac{\theta}{2}\sin^2\frac{\theta}{2}. \tag{1.30}$$

We now average over all the possible initial states of the first qubit by integrating over all values of θ and ϕ given by the Bloch sphere 1.1, so that

$$\overline{F} = \frac{1}{4\pi}\int_0^{2\pi}\int_0^{\pi} F\sin\theta d\theta d\phi = \frac{2}{3}. \tag{1.31}$$

Therefore, we can achieve an average fidelity of $\overline{F} = \frac{2}{3}$ for semi-classical communication.

1.8 Introduction to Quantum Mechanics

Although we have already introduced many of the essential concepts for understanding this thesis, we take a short detour to provide a more complete overview of quantum mechanics. Therefore, we introduce some of the fundamental concepts we will need later via the 6 postulates of quantum mechanics. These postulates allow us to give an overview of the concepts of state space, evolution, measurement, and composite systems.

> **Postulate 1:** Any isolated quantum system can be completely described by a so-called *state vector*, $|\psi\rangle$, of length 1.

We have already demonstrated that we can describe the state of a single qubit, but we extend this to any closed quantum system. This does not mean that we instantly know the state of any given quantum mechanical system – indeed, that is a much more complex problem than anything we will discuss here. It does, however, introduce a method by which we can describe a system, without necessarily knowing anything about it. Not only can any closed quantum system be described by a state vector, but the superposition of two state vectors is also a valid state vector of a system. If we have two possible states of a system, given by $|\psi_1\rangle$ and $|\psi_2\rangle$, then $|\psi\rangle = a_1|\psi_1\rangle + a_2|\psi_2\rangle$ is also a state of that same system. Indeed, this is more intuitively demonstrated by considering one of

the simplest quantum systems, in which we have much interest: a qubit. A single qubit has a two-dimensional state space, and we have introduced the states $|0\rangle$ and $|1\rangle$ as an orthonormal basis. Then, we are able to write any vector in the qubit state space as $|\psi\rangle = \alpha|0\rangle + \beta|1\rangle$, which is known as a *superposition state*.

> **Postulate 2:** Every observable quantity of a physical system $\mathcal{A}$ can be described by an operator, $\hat{\mathcal{A}}$, that acts on the state vector, $|\psi\rangle$.

In Section 1.4 we demonstrated some basic operators that can act on single qubits, but this can be extended to operators that can act on more complicated states. Some observables that one could be interested in are: *position*, *energy*, or *momentum*, all of which can be described by an operator. The operator for position in one dimension is generally written as $\hat{X} = x$ and for momentum we have $\hat{\mathcal{P}} = i\hbar\frac{\partial}{\partial_x}$. In three-dimensions the momentum operator is given by $\hat{\mathcal{P}} = -i\hbar\nabla$ where ∇ is the gradient operator. Such operator acts directly on the state vector as $\hat{\mathcal{A}}|\psi\rangle$. For two physical quantities to be simultaneously observable, the two observables in question must commute. The commutation relation is given as $[\hat{\mathcal{A}}, \hat{\mathcal{B}}] = 0$ where $[\hat{\mathcal{A}}, \hat{\mathcal{B}}] = \hat{\mathcal{A}}\hat{\mathcal{B}} - \hat{\mathcal{B}}\hat{\mathcal{A}}$. For the position and momentum operators, this becomes $[\hat{X}, \hat{\mathcal{P}}] = i\hbar$ meaning that the two quantities are not simultaneously observable. This lack of commutation for the position and momentum operators is what leads to the uncertainty principle.

> **Postulate 3:** The result of the measurement of an observable $\mathcal{A}$ will be an eigenvalue of $\hat{\mathcal{A}}$

This statement, in particular, explains the *quantum* nature of quantum mechanics. Any time we take a measurement of a system, its energy is confined to being one of the eigenvalues of the operator itself. This means that energy is quantised, and can only take very particular discrete values, given by the eigenvalues a_n.

> **Postulate 4:** When a measurement of observable $\mathcal{A}$ is made on the state vector $|\psi\rangle$, the probability of getting the eigenvalue a_n is given by $|\langle a_n|\psi\rangle|^2$

This describes another of the fundamental reasons that the quantum world behaves differently from the classical world. Instead of dealing with certainty, we are dealing with probability, and one can only predict the result of a certain measurement with some probability as given above. This statement assumes no degeneracy in the eigenvalues of $\mathcal{A}$.

> **Postulate 5:** Immediately after the measurement has obtained eigenvalue a_n, the state of the system is the eigenvector $|a_n\rangle$

We know from Section 1.2 that we cannot directly observe or measure a quantum state, and that once we attempt to, the information held within the superposition is lost and the system remains in a particular state. This postulate describes such phenomena and reinforces the idea that we can only make predictions on the superposition state and therefore quantum mechanics is highly probabilistic in nature.

> **Postulate 6:** Time evolution of a quantum system is found by solving the time-dependent Schrödinger equation.

This is perhaps the most important postulate we consider here, and it is what allows us to evolve a system through time. We begin by introducing the Schrödinger equation as

$$i\hbar\frac{d|\psi\rangle}{dt} = H|\psi\rangle, \tag{1.32}$$

where H is known as the Hamiltonian and describes the energies present in the system. The Hamiltonian will be introduced in more detail in Section 2.2. We can use the general solution to a differential equation to give

$$|\psi(t)\rangle = e^{-\frac{iHt}{\hbar}}|\psi(0)\rangle, \tag{1.33}$$

where we set $\hbar = 1$ for the rest of our work. This then demonstrates how a state evolves according to some Hamiltonian H, and we can introduce a unitary evolution operator

$U = e^{-iHt}$ that evolves a state through time so that

$$|\psi'\rangle = U|\psi\rangle. \tag{1.34}$$

This then concludes our introduction to the postulates of quantum mechanics. The reader may find a much more complete explanation of all relevant concepts in [11].

1.9 Experimental Realisations

In the previous sections, we have introduced many concepts required to understand quantum computation, however we have introduced them purely as a theoretical framework. To utilise these ideas, we need to actually be able to build a physical quantum computer, and in the following section, we demonstrate that the idea of quantum computation is not purely theoretical. The main benefit of qubits over their classical counterpart, is that they can be simultaneously in the states $|0\rangle$ and $|1\rangle$, with different probability amplitudes, assuming one of these values when measured. To actually harness the power of these superposition states and use them in quantum computation, we need a physical implementation of these qubits. Here we introduce an overview of some of the most promising examples of these, including Nuclear Magnetic Resonance (NMR) devices, ion traps, superconducting qubits, and quantum dots.

NMR

One of the first potential physical implementations of a quantum computer was based on the use of liquid NMR (Nuclear Magnetic Resonance) systems. These liquid NMR systems use molecules containing atoms that behave as spin-$\frac{1}{2}$ particles, suspended in liquid. These particles can then be acted on using NMR technology [12]. These particles will line up with an external magnetic field and the parallel and anti-parallel alignments provide the two qubit states required. Inter-atomic bonds provide interaction between qubits that can be useful for forming quantum gates. A five qubit quantum computer has been demonstrated in liquid NMR in [13], and in [14], a three qubit chain

is demonstrated. Although these systems started off promisingly due to the research already available on NMR techniques, there are limitations to liquid NMR. A particular limitation is that these systems don't scale well [15], which leads to problems if one wants to implement complex gates which require multiple qubits. Another limitation is given by the high ratio of gate operation time over decoherence time, which needs to be low in order to have accurate information processing. These systems are also difficult to reset after operations have been performed.

Recently, liquid NMR has been overtaken somewhat by solid state NMR, which utilises the properties of lattice structures within crystals as opposed to molecules in liquids. These systems have particular advantages in that they can be operated at room temperature and have long decoherence times. A more in-depth discussion of solid-state NMR is presented in [16] and both liquid and solid-state NMR are discussed in [15].

Ion Traps

Trapped ions were another of the early potential realisations for quantum hardware [17]. The system involves a set of cold ions interacting with laser light in a linear trap. The states of the qubit are given by the internal states of the ion. Manipulation of individual qubits happens via interaction with laser beams, and the strong Coulomb interaction aids with qubit-qubit interactions. As qubit-qubit interaction happen via interaction with a common mode, we are not limited to nearest neighbour interactions. Trapped ions have the benefit of having a long decoherence time, due to the internal ion states being relatively well isolated from the environment [18]. There are limitations to ion traps as qubits, and some of such limitations are presented in [19]. The authors specifically make note of spontaneous emission from such atomic qubits, however this can be taken into account in one's choice of ion. These ion traps are not so easily scalable, and as such scalability relies on using multiple traps connected using photons, or by physically transferring ions to another register [20]. This means that the idea of state transfer is less relevant to such devices. A demonstration of an ion trap quantum computer can be found in [20].

Superconducting Qubits

Solid state qubit devices have come a long way in the past 15 years [21], and using these, artificial atoms can be created and used as qubits. The energy levels can be engineered via Josephson junctions. Superconducting qubits are used in IBM's Quantum computer - IBMQ [22]. In [23], the authors present a solid state system based on Josephson arrays. They demonstrate the fidelity of state transfer that can be achieved from such systems and also consider the effects of imperfect manufacture. They consider errors of the order $\epsilon = 0.1$ for bond disorder and an absolute variance of 0.025 for site disorder, both of which turn out to be quite damaging.

Quantum Dots

Quantum dots are small pieces of semiconductor material where electrons can be confined to some space by a potential. Is has been shown that quantum spin chains can be implemented using quantum dots in [24], although due to physical limitations they present spin chains of length $N \leq 10$. In [25], the authors also propose implementation of a universal set of gates using these quantum dots.

Photonic Systems

Photonic lattices (arrays of coupled waveguides, [26]) currently provide some of the best experimental realisations of quantum state transfer. State transfer over 19 sites is demonstrated in [27]. Perfect State Transfer (Section 2.4) is also demonstrated using photonic lattices in [28], where the authors also discuss noise as propagation loss - which is analogous to amplitude damping (Section 4.5.3), which we consider later.

Chapter 2

Spin Chains

2.1 Introduction

Quantum computation promises to revolutionise the world of computing, and in doing so, will lead to significant advancements in many other fields. Although this new breed of computation seems far-fetched and mystical, the real-world applications of such computation cannot be understated. For quantum computation to be realised, we need a way to transfer quantum states from one location to another - much like wires in a classical computer. However, we are not dealing with classical computation, we are instead dealing with quantum computation, and to transfer quantum states, the wires themselves must be quantum mechanical in nature. We gave an overview of the experimental realisations of qubits in Section 1.9 and we note that many of the interaction present are nearest neighbour interactions, which leads to a natural solution for transferring states along a chain of qubits linked by such nearest neighbour interactions. In this chapter, we introduce concepts required for understanding state transfer. We first introduce the reader to spin chains and how these can transfer a state perfectly. We introduce the different systems we will be considering in Chapters 3 and 4. We then go through the encoding method first introduced in [29] that we will be extending in our work.

2.2 Spin Chains

To transfer quantum information between registers in a quantum computer, we require a system that is quantum in itself. We can use a 1-dimensional chain of qubits as a system to transfer information from one end to the other. By using a 1-dimensional chain, we can use the nearest neighbour interactions, which are often found in experimental realisations of such systems, and we can maximise our transfer distance. These nearest neighbour interactions lead to natural choices of Hamiltonian, which are the XX-Hamiltonian or the Heisenberg Hamiltonian - we choose the XX here. Choosing the XX Hamiltonian allows us to demonstrate our techniques using a specific Hamiltonian, but we note that the techniques can be used with any excitation preserving Hamiltonian. We now describe the protocol for such transfer. If we start with a chain of N sites, such that

each site contains a qubit in its relaxed state, then the overall state of the system is $|\boldsymbol{\psi}\rangle = |\mathbf{0}\rangle = |0\rangle^{\otimes N}$. This system is governed by a system Hamiltonian, which describes the energies present. Our system is given by the nearest neighbour (XX) Hamiltonian

$$H = \frac{1}{2}\sum_{n=1}^{N-1} J_n(X_nX_{n+1} + Y_nY_{n+1}) - \frac{1}{2}\sum_{n=1}^{N} B_nZ_n, \tag{2.1}$$

where the J_n give the coupling strengths between adjacent sites and the B_n give the on site energies. We also have that

$$\left[H, \sum_{n=1}^{N} Z_n\right] = 0, \tag{2.2}$$

so that we are able to consider excitation subspaces separately, and indeed for much of this thesis we will remain in the single excitation subspace. As we are able to separate our system into subspaces, we introduce H_1 as the part of the Hamiltonian that belongs to the single excitation subspace. We can then introduce a state to a site at one end of the chain so that the state of the system is now $|\boldsymbol{\psi}\rangle = |\psi\rangle|0\rangle^{\otimes N-1}$. This system can then be evolved through time using our evolution operator $U = e^{-iH_1t}$, and for transfer to be successful we require that the final state of the system is as close as possible to $|\boldsymbol{\psi'}\rangle = |0\rangle^{\otimes N-1}|\psi\rangle$, up to some phase $e^{i\phi}$ which can be removed after evolution by application of some single qubit unitary operator. Our initial state $|\boldsymbol{\psi}\rangle$ is given by

$$|\boldsymbol{\psi}\rangle = \alpha|\mathbf{0}\rangle + \beta|\mathbf{1}\rangle, \tag{2.3}$$

where the 1st qubit is in a superposition of the states $|0\rangle$ and $|1\rangle$ and all other qubits are in the $|0\rangle$ state. As the $|\mathbf{0}\rangle$ state is an eigenstate of the Hamiltonian, the problem simplifies to become the transfer of a single excitation from one end of the chain to the other $|1\rangle|0\rangle^{\otimes N-1} \rightarrow |0\rangle^{\otimes N-1}|1\rangle$. As we are now considering the transfer of a single excitation, we introduce the states

$$|\mathbf{n}\rangle = |0\rangle^{\otimes n-1}|1\rangle|0\rangle^{\otimes N-n}, \tag{2.4}$$

which give an excitation on site n. In particular, in the single excitation subspace and with the basis given by Eq. (2.4) the Hamiltonian in Eq. (2.1) is given by

$$H_1 = \begin{pmatrix} B_1 & J_1 & 0 & \dots & 0 & 0 & 0 \\ J_1 & B_2 & J_2 & \dots & 0 & 0 & 0 \\ 0 & J_2 & B_3 & \dots & 0 & 0 & 0 \\ \vdots & \vdots & \vdots & \ddots & \vdots & \vdots & \vdots \\ 0 & 0 & 0 & \dots & B_{N-2} & J_{N-2} & 0 \\ 0 & 0 & 0 & \dots & J_{N-2} & B_{N-1} & J_{N-1} \\ 0 & 0 & 0 & \dots & 0 & J_{N-1} & B_N \end{pmatrix}. \tag{2.5}$$

This gives us a tridiagonal $N \times N$ matrix with the on-site energies on the diagonal and the coupling strengths off-diagonal.

2.3 Measure of Success

As we intend to use these spin chains to send some quantum state from one end to the other, we need to be able to quantify the quality of transfer. We previously introduced *fidelity* as a measure of the transfer success in Section 1.7, where the maximum value is 1. Here we first demonstrate the fidelity of *excitation transfer*, F_{ex} and then extend this to the average fidelity of *state transfer*, $\overline{F}$. Fidelity is essentially a measure of the closeness of two states, so we can see how far our evolved state is from our desired state.

2.3.1 Fidelity of Excitation Transfer

To give a measure of fidelity for excitation transfer we begin with a state $|\psi\rangle = \alpha|\mathbf{0}\rangle + \beta|\mathbf{1}\rangle$ and apply the evolution operator so that $|\psi'\rangle = U|\psi\rangle$. Using the same justification as above, we can consider just the evolution of a single excitation, meaning that our desired state, at some later time, is $|\psi'_{desired}\rangle = |\mathbf{N}\rangle$, where we have a single excitation on site

N. The fidelity is then given by

$$F_{ex} = |\langle \mathbf{N}|e^{-iH_1 t}|\mathbf{1}\rangle|^2, \tag{2.6}$$

where again we are remaining in the single excitation subspace. The fidelity of state transfer is a slightly more involved calculation than that of excitation transfer, as we want to average over all possible input states.

2.3.2 Average Fidelity of State Transfer

For state transfer via spin chains to be useful, we want to provide a fidelity that is better than semi-classical communication - that is, measuring a state and classically communicating such measurement before applying that state to a second qubit, which is given in Section 1.7. In terms of the density operator, the fidelity of excitation transfer is given by

$$F_{ex} = \langle \boldsymbol{\psi}_{desired}|\rho'|\boldsymbol{\psi}_{desired}\rangle, \tag{2.7}$$

where ρ' is the final density matrix, given by $\rho' = U\rho U^\dagger$ and $|\boldsymbol{\psi}_{desired}\rangle$ is the desired state. As the task is to transfer a state from one end of a 1-dimensional chain to the other, we only care about the state on the final qubit after the time evolution. Therefore, we take the partial trace over all states other than the last site

$$\rho'_N = \mathrm{Tr}_{1,2,\ldots,N-1}\rho'. \tag{2.8}$$

Further explanation of the partial trace can be found in Appendix A. We remind ourselves that the input state on the first qubit is $|\psi\rangle = \alpha|0\rangle + \beta|1\rangle$ and take this chance to write this instead in terms of θ and ϕ such that

$$\alpha = \cos\frac{\theta}{2} \tag{2.9}$$

$$\beta = \sin\frac{\theta}{2}e^{i\phi}. \tag{2.10}$$

We now have

$$F_{ex}(\theta,\phi) = \langle\psi|\rho'_N|\psi\rangle, \tag{2.11}$$

where $|\psi\rangle = \cos\frac{\theta}{2}|0\rangle + \sin\frac{\theta}{2}e^{i\phi}|1\rangle$, and we can now integrate over all possible input states so

$$\overline{F} = \frac{1}{4}\int_0^{2\pi}\int_0^{\pi} F_{ex}(\theta,\phi)\sin\theta d\theta d\phi. \tag{2.12}$$

The integral removes all terms with $e^{i\phi}$ or similar, so the final average fidelity is

$$\overline{F} = \frac{1}{6}\left(3 + 2\sqrt{F_{ex}} + F_{ex}\right). \tag{2.13}$$

We note that the minimum value for the average fidelity of state transfer is $\overline{F}_{min} = \frac{1}{2}$ as the component belonging to the zero subspace will always transfer perfectly.

2.4 Perfect State Transfer

When a system is able to transfer a state with a fidelity of 1 for arbitrary length, it can achieve Perfect State Transfer (PST) [30], [31], [32], [33], [34], [35]. In this section we discuss the conditions that are necessary and sufficient for PST, as given in [33]. We restrict ourselves to consider the 1D chain and we allow it to evolve with no external control during evolution (naturally we require some control before and after evolution to introduce the initial state, remove the final state, and correct any phase picked up during transfer). We also restrict to the single excitation subspace. Given that we have restricted ourselves to evolving a system with no external control, we can use the Hamiltonian in Eq. (2.5) to give us an indication of what parameters we have access to in improving transfer. It's clear then that the only opportunity to alter the system is to play with the coupling strengths J_n and the on-site energies B_n.

Lemma 1. *For a PST chain, the Hamiltonian is mirror symmetric such that* $J_n^2 = J_{N-n}^2$ *and* $B_n = B_{N+1-n}$,

Proof. Working in the single excitation subspace, we can write the Hamiltonian in terms

of its eigenvectors and eigenvalues

$$H_1 = \sum_{n=1}^{N} \lambda_n |\lambda_n\rangle\langle\lambda_n|, \tag{2.14}$$

where λ_n are the eigenvalues and $|\lambda_n\rangle$ are the eigenvectors. Using the notation in Eq. (2.4) we can write our initial state as $|\mathbf{1}\rangle$ and our desired state as $|\mathbf{N}\rangle$. We can write these in terms of their eigenvectors as

$$|\mathbf{1}\rangle = \sum_{n=1}^{N} \alpha_n |\lambda_n\rangle \tag{2.15}$$

$$|\mathbf{N}\rangle = \sum_{n=1}^{N} \beta_n |\lambda_n\rangle. \tag{2.16}$$

The intended evolution of the initial state is given by

$$e^{-iH_1 t_0}|\mathbf{1}\rangle = e^{i\phi}|\mathbf{N}\rangle, \tag{2.17}$$

where ϕ is some arbitrary phase that can be removed by applying some unitary operator on the last qubit. If we rewrite this in terms of the eigensystem, we have

$$\sum_{n=1}^{N} e^{-i\lambda_n t_0}|\lambda_n\rangle\langle\lambda_n|\left(\sum_{n=1}^{N}\alpha_n|\lambda_n\rangle\right) = e^{i\phi}\left(\sum_{n=1}^{N}\beta_n|\lambda_n\rangle\right), \tag{2.18}$$

which we can simplify to give

$$\sum_{n=1}^{N} e^{-i\lambda_n t_0}\alpha_n|\lambda_n\rangle = e^{i\phi}\sum_{n=1}^{N}\beta_n|\lambda_n\rangle. \tag{2.19}$$

Then we can see that we must have

$$e^{-i\lambda_n t_0}\alpha_n = e^{i\phi}\beta_n \tag{2.20}$$

for all values of n. As the exponential terms are just phases, we can see that for Eq. (2.20) that we must have $|\alpha_n|^2 = |\beta_n|^2$. We can then use this to gain information on the

elements of the Hamiltonian given by Eq. (2.5). We can use

$$\langle \mathbf{1}|H_1^m|\mathbf{1}\rangle = \sum_{n=1}^{N} \lambda_n^m |\alpha_n|^2 = \langle \mathbf{N}|H_1^m|\mathbf{N}\rangle \tag{2.21}$$

where m is an integer, to give us information on each of the elements. For $m = 1$ this tells us that $B_1 = B_N$. For $m = 2$ we get that $B_1^2 + J_1^2 = B_N^2 + J_{N-1}^2$, therefore $J_1^2 = J_{N-1}^2$. As we increase m, we reveal more information, and eventually see that the Hamiltonian must be mirror symmetric. □

Lemma 2. *If t_0 is the perfect state transfer time, and there is a phase, ϕ, we have $e^{-it_0\lambda_n^s} = e^{i\phi}$ for the symmetric subspace and $e^{-it_0\lambda_n^a} = -e^{i\phi}$ for the anti-symmetric subspace.*

Proof. We assume for simplicity that all $J_n > 0$. This mirror symmetry means that the Hamiltonian commutes with the symmetry operator

$$S = \sum_{n=1}^{N} |\mathbf{n}\rangle\langle \mathbf{N+1-n}|, \tag{2.22}$$

where $S^2 = \mathbb{1}$, so that we can further divide H_1 into symmetric and anti-symmetric subspaces. The symmetric subspace govern particles that can occupy the same space, such as bosons, where the antisymmetric subspace governs fermions - which cannot occupy the same space and are constrained by the Pauli exclusion principle. Each of these spaces has its own eigenvectors, given by $|\lambda_n^s\rangle$ for the symmetric subspace and $|\lambda_n^a\rangle$ for the anti-symmetric subspace. As before, we decompose the initial state into its eigenvectors, this time separating the symmetric and anti-symmetric subspaces, such that

$$e^{-iH_1t_0}|\mathbf{1}\rangle = \sum_n e^{-i\lambda_n^s t_0}\alpha_n^s|\lambda_n^s\rangle + e^{-i\lambda_n^a t_0}\alpha_n^a|\lambda_n^a\rangle. \tag{2.23}$$

We can then give our target state as

$$e^{i\phi}|\mathbf{N}\rangle = e^{i\phi}S|\mathbf{1}\rangle = e^{i\phi}\left(\sum_{n=1}^{N}\alpha_n^s|\lambda_n^s\rangle - \alpha_n^a|\lambda_n^a\rangle\right) \tag{2.24}$$

Equating these shows us that $e^{-i\lambda_n^s t_0} = e^{i\phi}$ and $e^{-i\lambda_n^a t_0} = -e^{i\phi}$, which gives conditions for all $\alpha_n \neq 0$. This also means that at time t_0, the states transfer perfectly to their mirror opposite pair, leading to perfect transfer from site 1 to site N.

□

Lemma 3. *If the chain has PST at time t_0, the the eigenvalue spacing is given by*

$$\lambda_n - \lambda_{n-1} = (2m_n + 1)\pi/t_0 \tag{2.25}$$

where m is a positive integer, where we assume eigenvalues are are ordered such that $\lambda_n < \lambda_{n+1}$.

Proof. This condition comes from the fact that the symmetry of the eigenvectors alternates due to the structure of the Hamiltonian, which is proven in [36]. So we have that

$$e^{-i\lambda_n t_0} = e^{-i\lambda_{n-1} t_0} e^{-i(2m_n+1)\pi} = -e^{-i\lambda_{n-1} t_0}, \tag{2.26}$$

which gives the alternating sign. □

This concludes the conditions that are necessary and sufficient for Perfect State Transfer.

There are also many chains that do not exhibit PST, but instead exhibit 'pretty good' or 'almost perfect' state transfer [37], [38], where the fidelity is arbitrarily close to 1.

2.5 Chain Types

Throughout this thesis, we apply our techniques to a number of different systems to demonstrate their versatility. Here, we introduce the four chains we will be using. We note that all systems are given by the Hamiltonian in Eq. (2.1), we just alter the coupling strengths between sites. On-site energies are initially set to 0 throughout. We use two systems that allow Perfect State Transfer (PST) and two that do not. In each case, we set the maximum coupling strength equal to 1 and rescale all other couplings according

to this upper bound. In the following sections we introduce such chains, starting with the Uniform chain, followed by the Linear PST system, the Apollaro chain, and the Quadratic PST chain. The specific chains that we will consider are:

- Uniform (Section 2.5.1)
- Linear PST (Section 2.5.2)
- Apollaro (Section 2.5.3)
- Quadratic PST (Section 2.5.4)

and their coupling strengths for $N = 51$ are shown in Fig. 2.1.

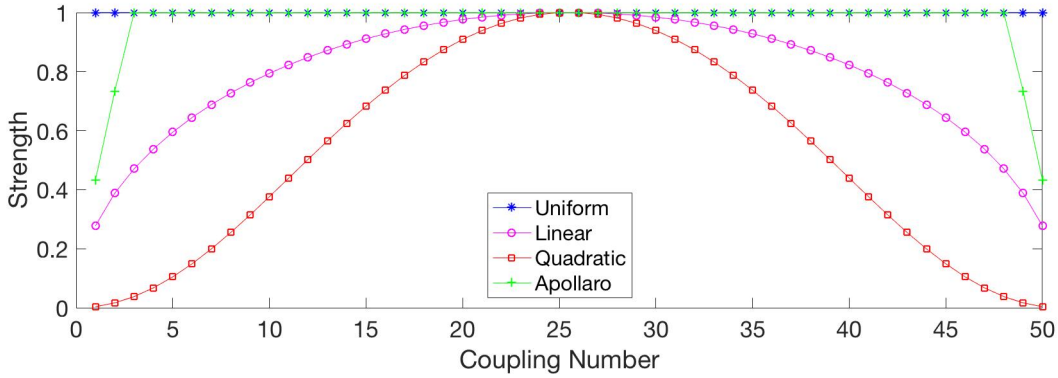

Figure 2.1: *Coupling strengths of various different chain types with maximum coupling strength set to 1. Linear and Quadratic chains allow for PST whilst the Apollaro and Uniform chains do not*

2.5.1 Uniform Chains

The first chain we present is the Uniform chain, where all coupling strengths are set to the maximum coupling strength of 1. The Uniform chain is the simplest that we will consider, with no modulation of couplings required, and provides fast transfer. This is the case first presented in [30], where we see that PST can be achieved for $N = 2, 3$ but is impossible for higher N (proven in [39]), we demonstrate this in Fig. 2.2a. We can also present the results for $N = 2$ and $N = 3$. In this case, the eigenstates of the Hamiltonian are given by

$$|\lambda_k\rangle = \sqrt{\frac{2}{N+1}} \sum_{n=1}^{N} \sin\left(\frac{\pi k n}{N+1}\right) |\mathbf{n}\rangle \tag{2.27}$$

and the eigenvalues by

$$\lambda_k = -2\cos\left(\frac{k\pi}{N+1}\right). \tag{2.28}$$

We know that fidelity from site 1 to site N is given by $F_{ex} = |\langle \mathbf{N}|e^{-iHt}|\mathbf{1}\rangle|^2$, where we can rewrite the evolution operator in terms of the eigenvectors as

$$e^{-iHt} = \sum_{k=1}^{N} e^{-i\lambda_k t}|\lambda_k\rangle\langle\lambda_k|, \tag{2.29}$$

which then gives the fidelity as

$$F_{ex} = |\frac{2}{N+1}\sum_{k=1}^{N}\sin\left(\frac{\pi k}{N+1}\right)\sin\left(\frac{\pi kN}{N+1}\right)e^{-i\lambda_k t}|^2. \tag{2.30}$$

For $N = 2, 3$ the solutions are $F_{ex} = \sin^2 t$ and $F_{ex} = [\sin\frac{t}{\sqrt{2}}]^4$. Given that we know we cannot obtain PST for higher than $N = 3$, what are the benefits of considering a system like this? Primarily, being a simple system without the need for initial tuning of the couplings, we believe it will be easier to physically implement, along with being more robust as all coupling strengths are maximum. The uniform chain has a fast transfer speed, which will become important when we consider noise in Chapter 4. We also consider chains that do not allow PST because we aim to see how much we can improve the transfer fidelity, therefore we do not necessarily need our chains to initially transfer with high fidelity.

We also note that the uniform chain can produce higher average fidelity if one is willing to wait arbitrarily long, as shown in [30]. We choose to limit the transfer time here to $t \leq N$.

2.5.2 Linear PST Chain

In [31], Christandl *et. al.* present a set of modified couplings that allow PST for all N. Starting with a chain of length N, they associate this to a ficticious spin-$(N-1)/2$ particle and relabel the basis vectors as $|\mathbf{m}\rangle$, where $m = -\frac{1}{2}(N-1)+n-1$. This means that the initial site can be labelled as both $|n = 1\rangle$ and $|m = -\frac{1}{2}(N-1)\rangle$. Similarly, the

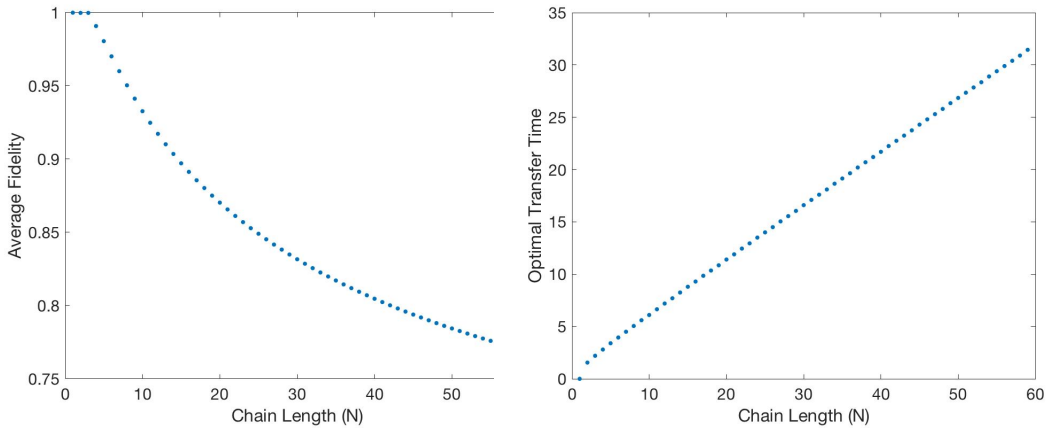

(a) *Average fidelity* (b) *Transfer time*

Figure 2.2: *Plots showing the transfer time and average fidelity for a uniform chain of various lengths, where we have evolved through the time window* $0 \leq t_0 \leq N$.

output site can be labelled as both $|n = N\rangle$ and $|m = \frac{1}{2}(N-1)\rangle$. We know from Section 2.2 that we can evolve a system like this with a Hamiltonian of the form

$$H = \sum_{n}^{N-1} \frac{J_n}{2}(X_n X_{n+1} + Y_n Y_{n+1}) - \frac{1}{2}\sum_{n=1}^{N} B_n Z_n. \tag{2.31}$$

We can represent this Hamiltonian by the Hamiltonian of the ficticious spin-$\frac{1}{2}(N-1)$ particle, $H = \lambda S_x$ where S_x is the angular momentum operator and λ is a constant. Then the matrix elements will be given by

$$J_n = \frac{\lambda}{2}\sqrt{n(N-n)}. \tag{2.32}$$

We then have evolution given by

$$U = e^{-i\lambda t S_x}, \tag{2.33}$$

meaning that the probability amplitude for state transfer is

$$F(t) = |\langle \mathbf{N}|U|\mathbf{1}\rangle|^2 = \left| -i \sin \frac{\lambda t}{2} \right|^{2(N-1)}, \tag{2.34}$$

and perfect transfer is obtained at time $t = \frac{\pi}{\lambda}$.

Example 3. We demonstrate this for the case of $N = 5$. In this case, our basis vectors are relabelled as $|-2\rangle, |-1\rangle, |0\rangle, |1\rangle, |2\rangle$ and we consider a spin $S = 2$ particle. We can then construct S_x. The elements of S_x are given by

$$\langle m'|S_x|m\rangle = (\delta_{m',m+1} + \delta_{m'+1,m})\frac{1}{2}\sqrt{S(S+1) - m'm}. \tag{2.35}$$

We can clearly see from the above equation that only the elements where $|m| - |m'| = 1$ will be filled, and all others will be 0. We can then calculate those elements such that

$$\langle -1|S_x|-2\rangle = 1 \tag{2.36}$$

$$\langle 0|S_x|-1\rangle = \frac{\sqrt{6}}{2} \tag{2.37}$$

$$\langle 1|S_x|0\rangle = \frac{\sqrt{6}}{2} \tag{2.38}$$

$$\langle 2|S_x|1\rangle = 1. \tag{2.39}$$

We know that the Hamiltonian will be real and symmetric, so we don't need to calculate the rest of the elements. We can see then that our Hamiltonian will be

$$H = \begin{bmatrix} 0 & 1 & 0 & 0 & 0 \\ 1 & 0 & \frac{\sqrt{6}}{2} & 0 & 0 \\ 0 & \frac{\sqrt{6}}{2} & 0 & \frac{\sqrt{6}}{2} & 0 \\ 0 & 0 & \frac{\sqrt{6}}{2} & 0 & 1 \\ 0 & 0 & 0 & 1 & 0 \end{bmatrix}. \tag{2.40}$$

From this example that the couplings we have calculated are indeed given by Eq. (2.32). We choose to rescale these so that the maximum coupling strength is 1, so our new couplings are given by

$$J_n = \frac{2\sqrt{n(N-n)}}{N}, \tag{2.41}$$

for even N, and

$$J_n = \frac{2\sqrt{n(N-n)}}{\sqrt{N^2-1}}, \tag{2.42}$$

for odd N. In this thesis we always use odd chain lengths, which will give an optimal extraction time of

$$t_{Lin} = \frac{\pi}{4}\sqrt{N^2 - 1}. \tag{2.43}$$

This chain is likely to be much more susceptible to errors due to the extremal couplings being much smaller than those in the centre. We can also assume that any errors associated with building the device will lead to less-than-perfect transfer. However, starting with a system than allows perfect transfer will allow us to clearly see how much damage is done by noise and fabrication errors.

2.5.3 Apollaro Chain

We include the chain presented in [40], which we call the *Apollaro* Chain after the first author, as a compromise between the Uniform and Linear PST chains. The Apollaro chain is a uniform chain with the two extremal couplings (x being the coupling between sites 1 and 2 and sites N and $N-1$, y being between sites 2 and 3, and $N-1$ and $N-2$) at each end modulated to give better transfer. We give a short overview on how the values of x and y can be calculated, but for more detail we direct the reader towards the original paper. We start by noting that for a uniform chain, the eigenvalues are given by $\lambda = 2\cos k$ where the values of k are given by

$$k = \frac{\pi n}{N+1}, \tag{2.44}$$

with $n = 1, \ldots, N$. Then by altering the couplings x and y away from 1 such that $x, y \leq 1$, a shift is introduced on the eigenvalues, so that now

$$k = \frac{\pi n + 2\varphi_k}{N+1}. \tag{2.45}$$

For convenience the shifted variable

$$q \equiv \frac{\pi}{2} - k \in \left(-\frac{\pi}{2}, \frac{\pi}{2}\right) \tag{2.46}$$

is used, having allowed values

$$q_m = \frac{\pi m - 2\varphi_{q_m}}{N+1}, \tag{2.47}$$

where $m = -\frac{N-1}{2}, \ldots \frac{N-1}{2}$. The phase shifts are given by

$$\varphi_{q_m} = \tan^{-1}\left[\frac{y^2 \sin 2q_m}{x^2 - (2-y^2)(1-\cos 2q_m)}\right] - 2q_m, \tag{2.48}$$

where $\varphi_{q_m} = 0$ for $x = y = 1$, therefore recovering the uniform chain. Then Eqs. (2.48) and (2.47) can be solved iteratively and we can use the values of q_m to calculate the transition amplitude between sites 1 and N. This transition amplitude is given by

$$u(t) = \left| \sum_m P_{q_m} e^{i(\pi m - t \sin q_m)} \right|, \tag{2.49}$$

where

$$P_q = \frac{2}{N+1+2\varphi'_q} \times \frac{x^2 y^2}{x^4 + (4-x^2-2y^2)^2 \tan^2 q - 16(1-y^2)\sin^2 q} \tag{2.50}$$

and

$$\varphi'_q = -2 + \frac{2y^2[x^2 + 2(2-x^2-y^2)\sin q]}{x^4 + 4[y^4 - x^2(2-y^2)]\sin^2 q + 16(1-y^2)\sin^4 q}. \tag{2.51}$$

Although, this is not a PST chain, the quality of transfer is very high for arbitrary length of chain (reaching ≈ 0.995 for a chain of $N = 51$). The authors state that 'almost perfect' transfer can be achieved for for arbitrary length N, where by 'almost perfect' they state that the fidelity is above 0.99. Therefore, we are able to compromise between simplicity (all central couplings are uniform) and high fidelity transfer. The specific values of x and y change depending on the chain length, and are given in [40] for $N = 51$, but for lower N, we follow the above method to calculate.

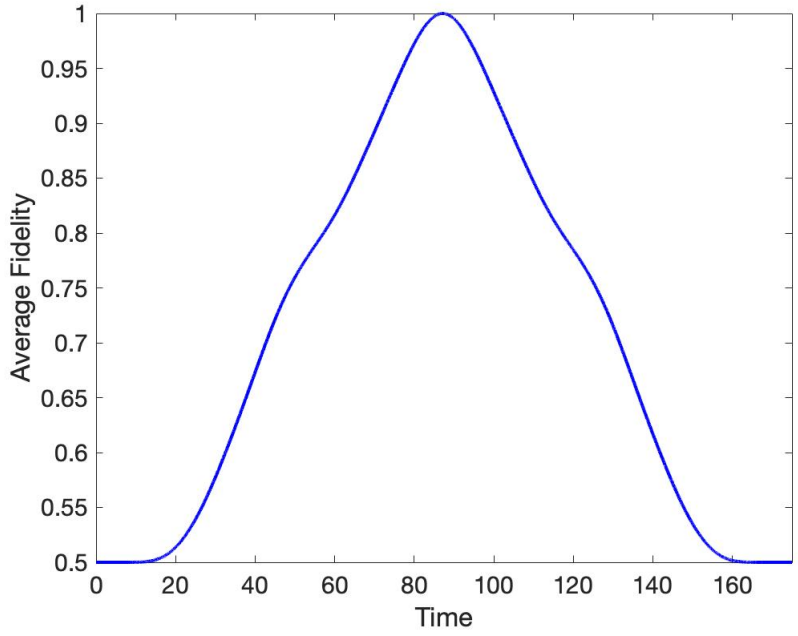

Figure 2.3: *Average fidelity of transfer for the Quadratic chain with* $N = 15$

2.5.4 Quadratic Chain

There are infinitely many different PST chains for fixed N, in fact any chain that satisfies the particular set of conditions presented in [33] is able to achieve PST at some time, t_0, although there is an argument that it should achieve PST in a 'reasonable time' to be useful (see Section 2.5.5). In [41], Zwick *et al.* discuss a number of these chains in the context of random errors on the couplings. In this paper, there are two systems in particular that stand out in their ability to transfer a state in the presence of these errors; the Linear chain and the Quadratic chain [42]. We have already discussed the Linear chain, but we also decide to include the Quadratic chain as another PST system. This chain has eigenvalues given by $\lambda_n^{quadratic} = (-1)^{n-k_0}(n-k_0)^2$, where k_0 is the centre of the spectrum. Using the Inverse Eigenvalue Problem, as described in [36] we can retrieve the coupling strengths. Although allowing PST, the Quadratic chain has a large t_0, which could prove to be problematic later when we consider noise. We show the average fidelity of transfer for this chain in Fig. 2.3.

2.5.5 A Comparison of Extraction Time

As well as transfer fidelity, extraction time is also an important consideration for each of these chain types. First, the chain must transfer the state in a reasonable time, as we cannot afford to wait forever for the state to arrive. Second, the arrival time must be somewhat predictable, as we need to know what time to extract without having the ability to 'see' when the state has arrived. If we consider first the idea of a reasonable extraction time, we need to first discuss what we mean by *reasonable*. We can first introduce an earlier method of transferring a state, known as a *swapping channel*, which can act as a limit on the maximum time we are willing to wait. Then we can discuss the earliest possible arrival time. We then discuss each of our chosen chains in turn.

The *swapping channel*, as given in [43], is a system where swap gates are applied to successive pairs of qubits to swap the state from one end of the channel to the other. We can use this as a benchmark for our systems, as we know that spin chains can transfer faster than these swapping channels [44], and if the spin chain is slower than this, we would use a swapping channel instead. The time required for the state to be transferred in this case is the time taken to operate a swap gate, multiplied by the $N-1$ swaps required. If we consider the ideal swap case, where every swap can occur with the same maximum coupling strength as the Linear PST chain, J_{max}, then the time for each swap to take place is $t = \frac{\pi}{2J_{max}}$. For the $N-1$ swaps to take place, we then have a total transfer time of

$$t_{max} = \frac{(N-1)\pi}{2J_{max}}. \tag{2.52}$$

This can therefore act as the maximum transfer time, and we aim for our transfer to be faster than this.

Ideally, we want our transfer time to be as fast as possible, particularly as the effects of noise get worse over time (we will show this more explicitly in Chapter 4). So it is useful to find some minimum arrival time, such that we are able to properly evaluate the arrival times of the chains we have selected. In [44] and [45], the authors discuss both the Quantum Speed Limit (QSL) and the time required to transfer a state along a

swapping channel. We choose to use these transfer times as the upper and lower bound to our evolution later. The minimum time to transfer a state is given in [44], as

$$t_{min} = \alpha(N-1) + \beta, \tag{2.53}$$

where $\alpha = 0.34$ and $\beta = 3.64$. These values are found numerically by introducing some threshold ϵ for infidelity and then defining t_{min} as the smallest value of t for each N where the infidelity is $< \epsilon$. We have therefore introduced our minimum and maximum arrival times.

Uniform Chain

To effectively evaluate the average fidelity of transfer, we need to know the arrival time of the state on the final qubit. In a system without errors, we can easily evolve the system through time for various chain lengths and find the optimal arrival time for each length. We confine ourselves to the time interval discussed above in this system. Higher fidelity can be achieved if one is willing to wait longer, but we limit ourselves to a more realistic solution, therefore finding the first 'peak' in fidelity. We display such results for transfer time and fidelity for the uniform chain in Fig. 2.2. We have given the optimal transfer time for the Linear PST case, so we can now compare that to the transfer time of the Uniform chain. In his original paper [30], Bose gave a theoretical prediction of the arrival time for the first revival as

$$t_{Uni} \approx \frac{(N + 0.8089N^{\frac{1}{3}})}{2J_{max}}, \tag{2.54}$$

where J_{max} is the maximum coupling strength (in our case this is 1), and we will see that this transfers faster than the Linear chain, as shown in 2.1.

Linear PST

We have introduced our minimum and maximum transfer times in the section above, but now we discuss in more detail the transfer times of each of our chosen systems.

In [35], Yung discusses the quantum speed limit and proves that the Linear chain gives the fastest possible transfer time for a perfect state transfer chain. We will introduce the reader to an explanation of why this is true here, and more detail can be found in the original paper. If we begin by noting that in Section 2.4, we demonstrated that for perfect state transfer to occur, we must have

$$e^{-i\lambda_n t} = \pm e^{i\phi}, \tag{2.55}$$

for all n, which gives us an infinite number of solutions according to the eigenvalue spectra we can produce from this. One of the most well-known solutions is the Linear PST chain, which we have selected as one of our example chains. If there are so many possible spectra, then we can start to consider which of these would have the fastest transfer. Yung introduces the efficiency η, which can be quantified using the maximum coupling strength and the transfer time so that

$$\eta = \frac{J_{max} t_0}{\tilde{J_{max}} \tilde{t_0}}, \tag{2.56}$$

where $\tilde{J_{max}}$ and $\tilde{t_0}$ are the maximum coupling strength and the optimal transfer time for the Linear PST chain, which we use to compare all other PST chains. Now, we will demonstrate that for all other chains $\eta \geq 1$, therefore showing that the Linear PST is the fastest. If we order the eigenvalues such that $\lambda_1 > \lambda_2 > ... > \lambda_N$, then we can define the difference between successive eigenvalues as $\Delta_n \equiv \lambda_n - \lambda_{n+1}$, and then the range of the eigenvalue spectrum is $\Delta_E \equiv \lambda_1 - \lambda_N = \sum_{n=1}^{N-1} \Delta_n$. Then from Eq. (2.55), the transfer time is limited by the smallest energy interval $\Delta_{min} = min\{\Delta_n\}$ and so $t_0 \geq \frac{\pi}{\Delta_{min}}$. For the Linear chain this is $\tilde{t_0} = \frac{\pi}{\tilde{\Delta_{min}}}$. Now we can rewrite our efficiency as

$$\eta \geq \frac{J_{max} \tilde{\Delta_{min}}}{\tilde{J_{max}} \Delta_{min}}. \tag{2.57}$$

If we scale the eigenvalue spectra so that $\tilde{\Delta_{min}} = \Delta_{min}$, then $\eta \geq 1$ if $J_{max} \geq \tilde{J_{max}}$. As we rescale all chains such that the maximum coupling strength is 1, this becomes a

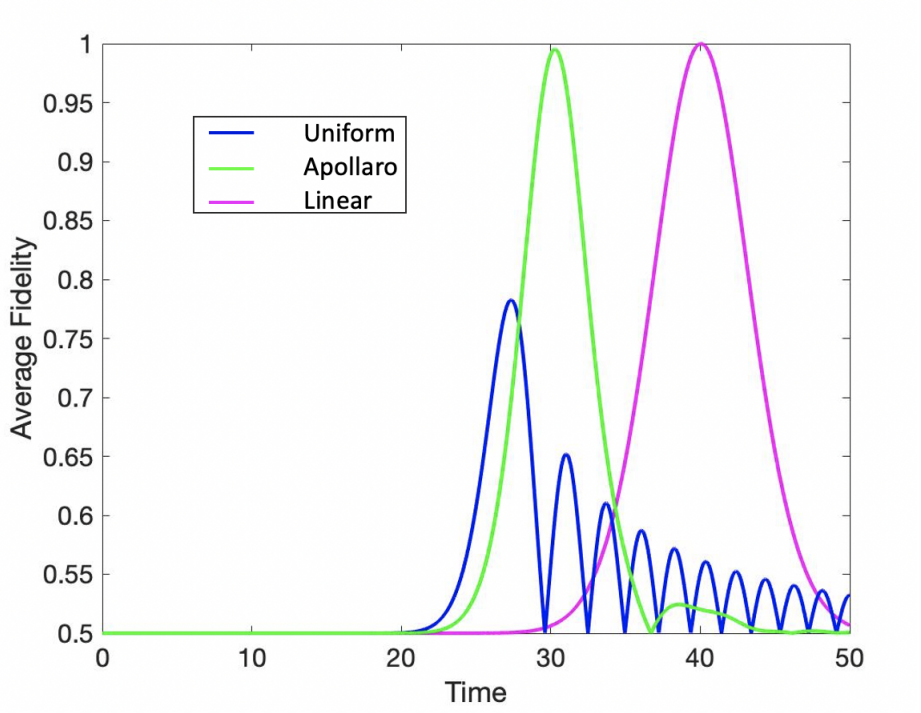

Figure 2.4: *A comparison of arrival time for the Uniform (blue), Apollaro (green), and Linear PST (magenta) chains, for* $N = 51$. *We do not include the quadratic chain as the arrival time is significantly later*

constraint on time and says that $\tilde{t_0} \geq t_0$. This then demonstrates that the Linear chain is the fastest chain that allows for PST and the transfer time is given in Section 2.5.2 as

$$t_{Lin} = \frac{\pi}{4}\sqrt{N^2 - 1}.$$

Apollaro

The third chain we will consider is a compromise between the Uniform chain and the Linear PST chain. There is no straightforward way of predicting an appropriate arrival time for this chain. Although we cannot give a prediction for the arrival time in shorter chains, we can assume that the arrival time will fall somewhere between the arrival times of the Linear PST chain and the Uniform chain, given the nature of its couplings. We have shown the evolution of a chain of $N = 51$ for the Uniform chain, Linear PST chain, and the Apollaro chain in Figure 2.4.

Quadratic PST

As the Quadratic chain leads to PST, it is somewhat easier to give an arrival time (given that the state must arrive with fidelity of 1 at some point). If we consider a chain with eigenvalues of $\lambda = 0, \pm 1, \pm 2^2, \ldots, \pm \frac{N-1}{2}^2$, where N is odd, we know that this will achieve perfect state transfer at time $t = \pi$. However, we have chosen to rescale our maximum coupling strengths so that $J_{max} = 1$. To then give a demonstration of the minimum transfer time in this case, we use the method outlined in [46]. We have the Hamiltonian of this system given by H and the symmetry operator given by S. We know that the trace of H^2S is the sum of the eigenvalues squared (counted with multiplicities)

$$\mathrm{Tr}(H^2S) = \sum_{n=1}^{N} \lambda_n^2 (-1)^{n+1} = 2\left(\sum_{n=1}^{\frac{N-1}{2}} (-1)^n n^4 \right) (-1)^{\frac{N-1}{2}}, \tag{2.58}$$

where the second equality is possible as we have pairs of eigenvalues. We also find that

$$\mathrm{Tr}(H^2S) = 4J^2_{\frac{N-1}{2}} \leq 4J^2_{max}. \tag{2.59}$$

We can then write

$$4J^2_{max} \geq \frac{N+1}{16}(N^3 - N^2 - 5N + 5), \tag{2.60}$$

where we have simplified the final part in Eq. (2.58). We can now rescale our couplings such that $J_{max} = 1$ and we get

$$t_0 \geq \frac{\pi}{8}\sqrt{(N+1)(N^3 - N^2 - 5N + 5)}. \tag{2.61}$$

We now have an expected arrival time for the quadratic system and it is clear that this arrives much later than the other chains we have chosen. We initially considered this chain as it performs well against fabrication errors [47], but we will later see that the late arrival time makes it a less useful candidate. We give a final overview of the transfer times compared to the t_{max} given in Eq. 2.52 in Table 2.1

	Uniform	Linear	Apollaro	Quadratic
$\frac{t}{t_{max}}$	$\frac{1}{\pi}$	$\frac{1}{2}$	$\frac{1}{\pi}$	$> N$

Table 2.1: *Comparison of extraction times of various chain types with respect to* t_{max}

2.6 Encoding Method

Much of the work presented in this thesis is based on encoding and decoding strategies. Therefore, we present the basis of this technique here. The optimal encoding strategy that we apply and modify is that presented in [29].

Where previously we have introduced the theory of sending a state or single excitation through the system and retrieving it with some fidelity; we now present the theory of sending this as an encoding. This means that we choose a certain number of spins that are controlled by a sender and encode our state over those spins within the single excitation subspace. We can then choose to extract this state at a single site or over a number of spins that a receiver controls. Then, instead of starting with the state $|\boldsymbol{\psi}\rangle = \alpha|\mathbf{0}\rangle + \beta|\mathbf{1}\rangle$, we begin with

$$|\boldsymbol{\Psi}\rangle = \alpha|\mathbf{0}\rangle + \beta|\boldsymbol{\psi}\rangle \tag{2.62}$$

where $|\boldsymbol{\psi}\rangle = \sum_{n=1}^{M} \delta_n|\mathbf{n}\rangle$ and M is the number of spins we encode over, and all other sites are in the $|0\rangle$ state. After time evolution, the state of the chain is then

$$|\boldsymbol{\psi}'\rangle = \alpha|\mathbf{0}\rangle + \beta\sum_{k=1}^{N}\eta_k|\mathbf{k}\rangle \tag{2.63}$$

where the output state can have the excitation spread over all sites. If we have the receiver controlling the same number of sites as the sender, it is possible to decode over these sites. We introduce the set of sites belonging to the decoding region as Λ. The receiver applies a unitary U_Λ to their set of spins, where the part of the unitary applied to the $|0\rangle$ component of each site returns $|0\rangle$ so that

$$U_0^\Lambda|\mathbf{0}\rangle = |\mathbf{0}\rangle. \tag{2.64}$$

The part of the unitary acting on the non-zero component gives

$$U_1^{\Lambda} \sum_{k\in\Lambda} \eta_k |\mathbf{k}\rangle = |\mathbf{N}\rangle \sqrt{\sum_{k\in\Lambda} |\eta_k|^2}. \tag{2.65}$$

Then our total final state is given as

$$U_\Lambda |\boldsymbol{\psi}'\rangle = |\boldsymbol{\psi}'_U\rangle = \alpha|\mathbf{0}\rangle + \beta \sum_{k\notin\Lambda} \eta_k |\mathbf{k}\rangle + \beta \sqrt{\sum_{k\in\Lambda} |\eta_k|^2} |\mathbf{N}\rangle \tag{2.66}$$

where the first part of the final state gives the $|\mathbf{0}\rangle$ component, the second part gives any part of the excitation not on the spins controlled by the receiver, and the final part is controlled by the receiver. Now we have our output state, we can find an expression for the average fidelity of transfer. We start by finding the output density matrix

$$\begin{aligned}
\rho' = |\alpha|^2 |\mathbf{0}\rangle\langle\mathbf{0}| + \alpha^*\beta \sum_{k\notin\Lambda} \eta_k |\mathbf{k}\rangle\langle\mathbf{0}| + \alpha^*\beta \sqrt{\sum_{k\in\Lambda} |\eta_k|^2} |\mathbf{N}\rangle\langle\mathbf{0}| \\
+\alpha\beta^* \sum_{k\notin\Lambda} \eta_k^* |\mathbf{0}\rangle\langle\mathbf{k}| + |\beta|^2 \sum_{k\notin\Lambda} |\eta_k|^2 |\mathbf{k}\rangle\langle\mathbf{k}| + |\beta|^2 \sum_{k\notin\Lambda} \eta_k^* \sqrt{\sum_{k\in\Lambda} |\eta_k|^2} |\mathbf{N}\rangle\langle\mathbf{k}| \\
+\alpha\beta^* \sqrt{\sum_{k\in\Lambda} |\eta_k|^2} |\mathbf{0}\rangle\langle\mathbf{N}| + |\beta|^2 \sum_{k\notin\Lambda} \eta_k \sqrt{\sum_{k\in\Lambda} |\eta_k|^2} |\mathbf{k}\rangle\langle\mathbf{N}| + |\beta|^2 \sum_{k\in\Lambda} |\eta_k|^2 |\mathbf{N}\rangle\langle\mathbf{N}|.
\end{aligned} \tag{2.67}$$

We can then take the partial trace, (see Appendix A for details), noting that we have removed any terms where the inner product is 0, and all remaining terms have an inner product equal to 1.

$$\begin{aligned}
\mathrm{Tr}(\rho') = |\alpha|^2 |0\rangle\langle 0| + \alpha^*\beta \sqrt{\sum_{k\in\Lambda} |\eta_k|^2} |1\rangle\langle 0| + |\beta|^2 \sum_{k\notin\Lambda} |\eta_k|^2 |0\rangle\langle 0| \\
+\alpha\beta^* \sqrt{\sum_{k\in\Lambda} |\eta_k|^2} |0\rangle\langle 1| + |\beta|^2 \sum_{k\in\Lambda} |\eta_k|^2 |1\rangle\langle 1|.
\end{aligned} \tag{2.68}$$

If we rewrite this as a matrix such that

$$\rho'_N = \begin{bmatrix} |\alpha|^2 + |\beta|^2 \sum_{k\notin\Lambda} |\eta_k|^2 & \alpha\beta^* \sqrt{\sum_{k\in\Lambda} |\eta_k|^2} \\ \alpha^*\beta \sqrt{\sum_{k\in\Lambda} |\eta_k|^2} & |\beta|^2 \sum_{k\in\Lambda} |\eta_k|^2 \end{bmatrix}, \tag{2.69}$$

then we can see that the fidelity of excitation transfer is given as

$$F_{ex} = \sum_{k\in\Lambda} |\eta_k|^2. \tag{2.70}$$

To average over all possible input states we take

$$F = \langle\psi|\rho'_N|\psi\rangle, \tag{2.71}$$

and then integrate over all possible values of α and β given by the Bloch sphere. We are then left with

$$\overline{F} = \frac{1}{6}\left(3 + 2\sqrt{\sum_{k\in\Lambda} |\eta_k|^2} + \sum_{k\in\Lambda} |\eta_k|^2\right). \tag{2.72}$$

In the absence of noise, we can simply use Eq. (2.13) to find the average fidelity of state transfer.

To apply the optimal encoding and decoding strategy, we use the method outlined by Haselgrove in [29], which involves finding the singular value decomposition (SVD) of a modified time evolution operator. We have already defined the time evolution operator as

$$U = e^{-iHt}, \tag{2.73}$$

which automatically evolves the system to the optimal time for extracting the state. Although, we are not necessarily considering the optimal extraction time but rather some approximate time which we estimate should produce high fidelity transfer. Then the fidelity at this time is maximised as

$$\max_{|\psi\rangle,|\phi\rangle} |\langle\phi|U|\psi\rangle| \tag{2.74}$$

where $|\phi\rangle$ gives the state of the decoding region and $|\psi\rangle$ the encoding. The time evolution operator is modified by applying the projection operators for the encoding state space P_{in} and the decoding state space P_{out}. These projectors are given by

$$P_{in} = \sum_{n=1}^{M} |\mathbf{n}\rangle\langle\mathbf{n}| \tag{2.75}$$

$$P_{out} = \sum_{n\in\Lambda} |\mathbf{n}\rangle\langle\mathbf{n}| \tag{2.76}$$

where M is the size of the encoding zone, and Λ is the set of spins belonging to the decoding region. Now our modified time evolution operator is

$$\tilde{U} = P_{out} U P_{in}. \tag{2.77}$$

After applying the projection operators, we have fidelity of excitation transfer given by

$$F_{ex} = |\langle\boldsymbol{\phi}|\tilde{U}|\boldsymbol{\psi}\rangle|. \tag{2.78}$$

Maximising $|\boldsymbol{\phi}\rangle$ happens by selecting some $r|\boldsymbol{\phi}\rangle = \tilde{U}|\boldsymbol{\psi}\rangle$, so that $|r|$ gives the fidelity. We can find the maximum value of r by taking the SVD of $\tilde{U}_{t_0}$, where the maximum of r will be the maximum singular value. Taking the SVD means factorising the matrix into three new matrices. This gives us three components: the left-singular vectors $\overrightarrow{v_i}$, the right-singular vectors $\overrightarrow{w}_i^*$, and the singular values s_i, where the columns of the left and right singular values are orthonormal and the singular values are the non zero entries in a diagonal matrix and are positive real. The singular value decomposition is given in [48] as

$$A = \sum_{i=1}^{r} s_i v_i w_i^*, \tag{2.79}$$

where w and v are orthonormal sets and s_k are positive real numbers. The vectors $w_1, w_2, ..., w_r$ and $v_1, v_2, ..., v_r$ are the right and left singular vectors respectively, $s_1, s_2, ..., s_r$ are the singular values, and r is the rank of the operator. We then have the right-singular vectors giving the best possible encodings (optimal encoding given by the first of these), left-singular values giving the best decodings (corresponding to the encodings), and the singular values giving the fidelity of the encoding/decoding pair. We can then use the largest singular value to tell us how good the transfer is.

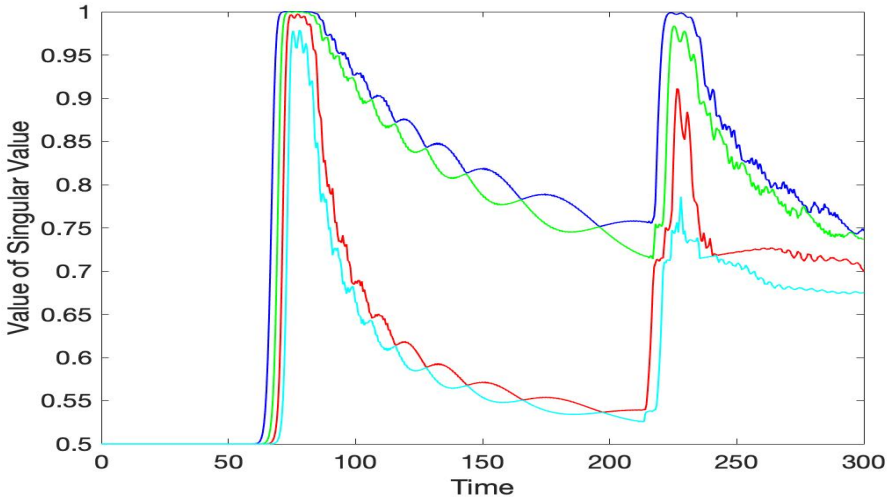

(a) *Reproduction of first 4 singular values of an N=300 chain with an encoding region of 20 qubits, calculated using our code*

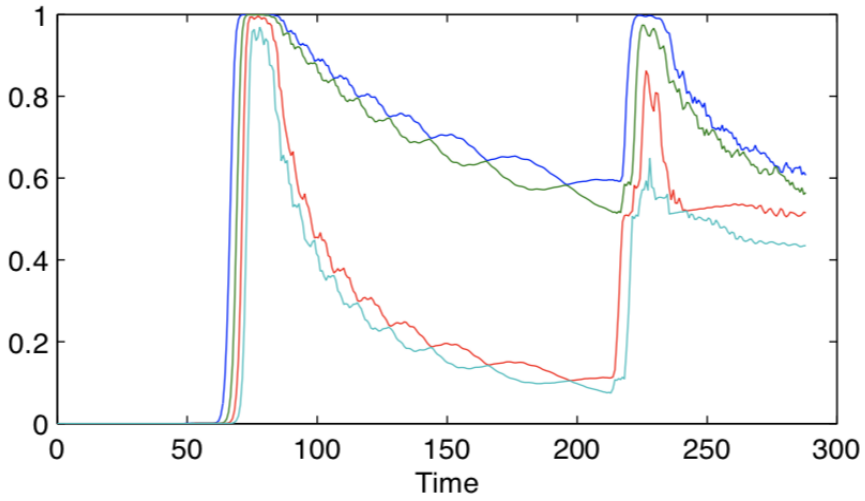

(b) Original figure from [29]

Figure 2.5: *Comparison of our results for the first 4 singular values of an N=300 chain with the results produced by Haselgrove in [29] for an N=300 chain*

As Haselgrove already introduced the optimal encoding scheme in the noise-free case, we can use some of the results produced in [29], to verify the numerics needed for our investigations. We start by building the encoding scheme he talks about and finding the largest singular values, as discussed above. The singular values in this case give the excitation transfer, and if we substitute this into Eq. (2.13), we therefore have the average fidelity as

$$\overline{F} = \frac{1}{2} + \frac{1}{3}\sqrt{s_1^2} + \frac{1}{6}s_1^2 \tag{2.80}$$

where s_1^2 is the first singular value squared. Using the results from [29] we can check our system is correctly calculating the singular values. We take the case of $N = 300$ with 20 spins each for the encoding and decoding regions, which Haselgrove displays in his results to compare with our own system. There will be some discrepancies due to a slight difference in the models we are using (we use the XX-Hamiltonian, whilst Haselgrove presents the Heisenberg Hamiltonian). The comparison of our own plot to that produced by Haselgrove is shown in Figs. 2.5a and 2.5b.

Chapter 3

Fabrication Defects

3.1 Introduction

Theoretically, perfect state transfer through quantum spin chains has been achieved for an arbitrary length of chain, by modulating the couplings between sites [31]. However, we ultimately aim to use spin chains in quantum computing devices and, as with any manufacturing process, there will be some fabrication defects associated with the physical realisation. It is essential to investigate how the system will react to these errors, and how we can attempt to mitigate these effects. Here, we discuss the types of random errors likely to appear in physical spin chains - namely proportional and additive errors, and show how these can be modelled. We then give an overview of the work already done on this subject, before introducing the technique we use to improve transfer in these conditions. We then demonstrate our technique on our example chains.

3.1.1 Random Errors

We now discuss how one can apply random errors to a system to mimic imperfect manufacture. Realistically, the nature of such errors will depend on the physical system. For the sake of demonstrating results, we have chosen a set of errors to present. We consider errors present on the spin sites themselves and errors in the couplings between spin sites. Particularly in the case of perfect transfer chains, such as that presented in [31], the couplings need to be precise to allow for PST, and any inaccuracies in the manufacture will lead to less-than-perfect transfer. The strengths of the couplings will depend on the specific system, but we scale all systems such that the maximum coupling strength is 1. When considering errors present on such system, we can consider both errors that are proportional to the coupling strengths and errors that are additive (and therefore do not depend on the coupling strengths). All on-site errors are additive as the error-free values are all 0.

Additive Errors

One method we may use to include errors in our system is to simply add some random value to each of the coupling strengths or on site energies (noting that this will be a different value for each coupling/site). Additive errors do not depend on the strength of the coupling itself and are errors that are simply added to all couplings and on-site energies with the same standard deviation. We give the coupling strengths with additive errors as

$$J_n^{\varepsilon} = J_n + \varepsilon_n, \tag{3.1}$$

where J_n^{ε} are the new coupling strengths after errors have been added and ε_n is the random error taken from the normal distribution with standard deviation of σ_J centered around 0. We have chosen the normal distribution as we believe it most closely models the errors likely to be found in experimental systems, in that smaller errors are more likely. However, our technique does not depend on the distribution we choose, and we have selected one solely so that we are able to demonstrate the technique. The errors on the sites themselves are given by

$$B_n^{\varepsilon} = B_n + \varepsilon_n, \tag{3.2}$$

where ε_n again comes from the normal distribution with standard deviation of σ_B, centered around 0.

Proportional Errors

Another method we could use to include errors in our system is to assume that errors will appear as a proportion of the coupling strengths (as the on-site energies are all 0, we use additive errors for those here). Proportional errors on the couplings are given by

$$J_n^{\epsilon} = J_n(1 + \epsilon_n), \tag{3.3}$$

where J_n^ϵ are the new couplings and they are different for each n. We take the random error values ϵ_n from the normal distribution centered 0, where standard deviation is given by σ_J. There are no proportional errors present on the sites, as these are all 0. We use additive errors here instead, which are given by Eq. (3.2).

We refer to these defects by their standard deviation, σ_B and σ_J, and use σ without a subscript when both values have the same standard deviation. It must be noted that there is a specific case where the coupling error is equal to the coupling strength, which could lead to the actual coupling strength being 0 – effectively creating separate chains. When creating the Hamiltonian containing the errors, it is essential that the $J_{nm} = J_{mn}^*$, but as the Hamiltonian must be real, these values are exactly equal and the Hamiltonian is symmetric. We have designed our system so that our error models can be easily changed according to experimental findings.

Proportional vs. Additive Error

To make a comparison between proportional and additive errors, we demonstrate a set of errors on each of the different systems we have chosen and apply it both additively (black) and proportionally (red) in Fig. 3.1. In the case of the Uniform chain, these are equivalent as all coupling strengths are 1. For all other chains the coupling strengths are much weaker at the ends of the chain compared to the central couplings. We can then expect that additive errors will be more damaging to these systems as they will more drastically alter these extremal couplings. We can demonstrate this by plotting the couplings with one random set of errors applied both proportionally and additively and compare then for different chains. We note that the errors on each chain are the same errors for both proportional and additive, but we apply a different set of random errors to each chain. We can see that additive errors are likely to be more damaging from Fig. 3.1b and 3.1d, where the proportional errors do not strongly alter the end couplings, but the additive errors do. The Apollaro chain demonstrates a mixture of the Uniform chain and the Linear/Quadratic chains in that the type of error does not affect the errors on the uniform portion of the chain, but at the ends we can see that the proportional errors are

slightly less damaging.

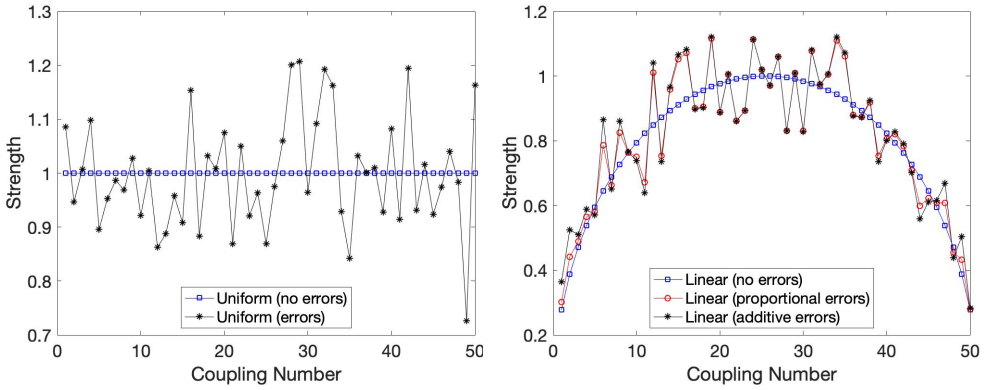

(a) *The Uniform chain*

(b) *Linear chain*

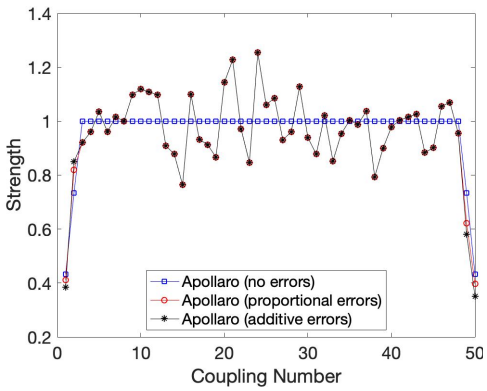

(c) *Apollaro chain*

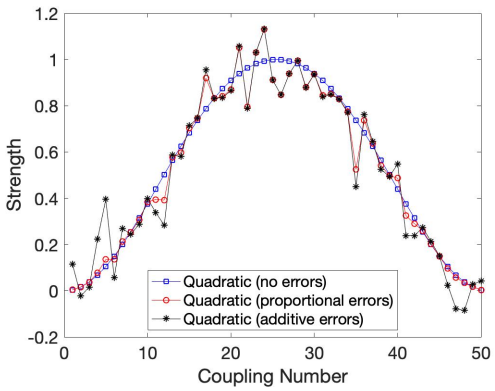

(d) *Quadratic chain*

Figure 3.1: *Plots showing how proportional and additive errors affect the coupling strengths for the four chains we have chosen, with an error having standard deviation* $\sigma_J = 0.1$

3.1.2 Overview of Previous Work

Among the first to consider spin systems subject to random errors were De Chiara *et. al.* in 2005 [49], who investigated static imperfections in an otherwise perfect state transfer chain. They considered the model presented in [31] (which allows PST and is referred to in this thesis as the *Linear PST Chain*, due to the nature of the eigenvalue spectrum) in the context of random variations of both the couplings and an externally applied magnetic field, although they do not attempt to mitigate the effects of these errors. They consider random errors on the couplings given by

$$J_k \to J_k(1+\delta_k) \tag{3.4}$$

where $\delta_k \in [-\varepsilon_J, \varepsilon_J]$ and these errors are therefore proportional to the strength of the couplings. The site energies of the model used here are 0 in the perfect case, so in the imperfect case, they become

$$B_k \rightarrow b_k \tag{3.5}$$

where $b_k \in [-\varepsilon_B, \varepsilon_B]$. As the disorder is random, the results are averaged over N_{Av} different disorder realisations. Results from [49] are shown in Fig. 3.2, where we can see that even a small amount of error on the couplings can be damaging, particularly for longer chains. We note here that the coupling strengths are not scaled, so the random fluctuations in site energies are less damaging to longer chains as the energies in the system are larger. This does not affect the coupling errors as these are proportional. In Fig. 3.2c we can see the effects of errors on both the couplings and sites, and the decrease in fidelity associated with these errors. We note that these figures use different notation from our own, such that $\overline{\mathcal{F}}(t_1)$ is the average fidelity at time t_1, ε_J and ε_B are equivalent to our ϵ for the couplings and ε for the sites. This reduction in fidelity due to random errors is exactly what we aim to improve.

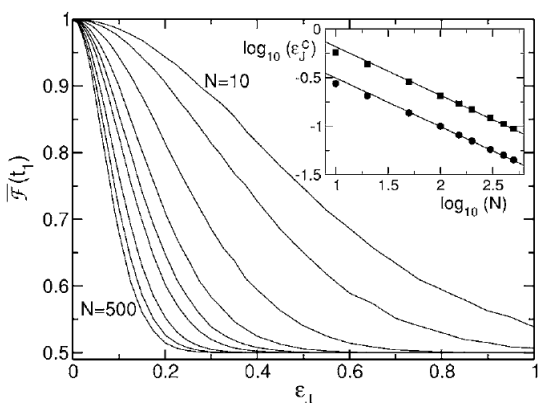

(a) *Coupling defects.*

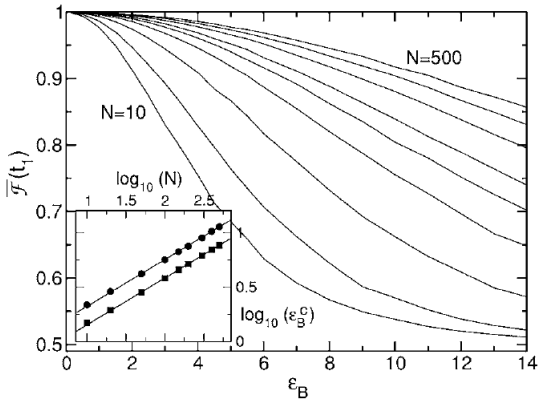

(b) *Site energy defects.*

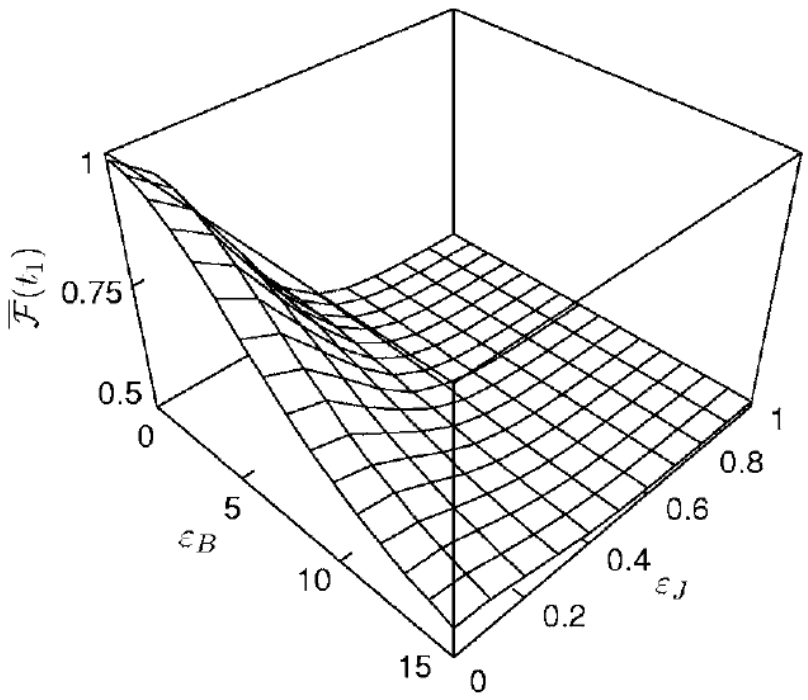

(c) *Average fidelity of transfer for different errors present on both couplings and sites for a chain length of N = 50.*

Figure 3.2: *Figures from [49] demonstrating the effect of different random errors on spin chains of varying lengths*

We can also consider how well different known systems react to random errors. In particular it is possible for the choice of eigenvalue spectrum in a spin system to make it more robust against fabrication errors, where [50] shows that the Linear spectrum, [31], is almost optimal. In [47], Zwick *et al.* consider which systems are most robust against the errors discussed in the previous literature, focusing specifically on coupling errors which are proportional to the desired coupling strengths, as in Eq. (3.4). They do not

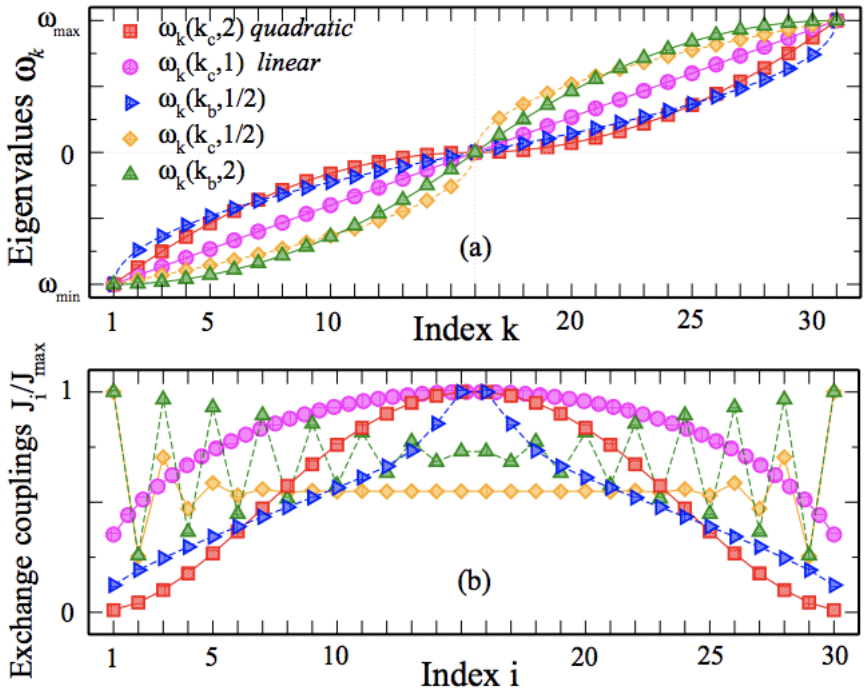

Figure 3.3: *Figure from [47] showing various eigenvalue spectra for a chain of* $N = 31$*, and the coupling strengths for the same chain length*

consider errors present on the sites themselves. The systems they consider all allow PST, but have different eigenvalue spacings. These spectra are shown in Fig. 3.3 where they specifically consider a chain of $N = 31$ sites. They found that the most robust systems are those where the eigenvalues are either linear or quadratic in their spread as demonstrated in Fig. 3.4. The eigenvalues for the PST couplings that we will use are those given as $\omega_k(k_c, 1)$ *linear* and $\omega_k(k_c, 2)$ *quadratic*, and are shown as magenta circles and red squares respectively.

Burgarth and Bose suggest a scheme to allow arbitrarily perfect state transfer even with random fluctuations [51]. They discuss multiple randomly coupled quantum chains in parallel, and how this system performs if the chains are not exactly identical to one another. This work can be extended to consider chains where the Hamiltonian is not exactly the same as that theorised. They conclude that dual-rail protocol makes a system more robust against errors and also allows the receiver to check whether the state they have received is correct or not. We, however, choose to look at the case where we have

a single 1-dimensional chain. Primarily this is so we can evaluate our technique on a simple to implement chain, but we also note that there is a significant size increase when one considers multiple chains, and we restrict to smaller spaces such that we can easily evaluate them numerically. Some static errors had been previously investigated for other quantum systems [52], [53], but not specifically for spin chains.

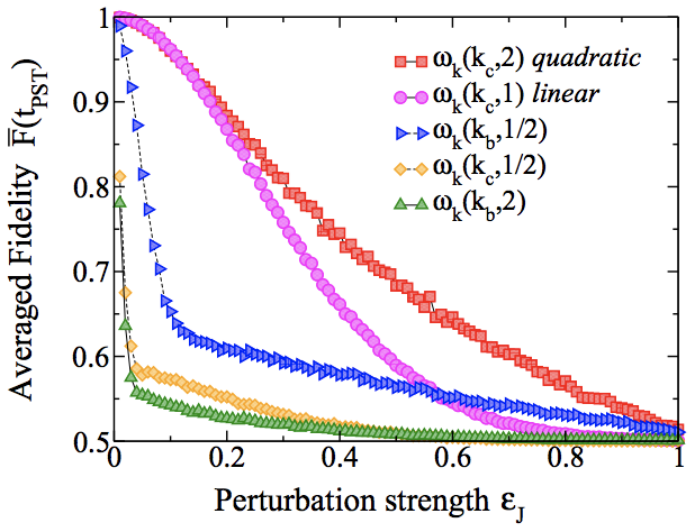

Figure 3.4: *From [47] compares different spreads of eigenvalues in the context of robustness against perturbations on the couplings, where here ε_J is the same as our σ_J*

3.2 Methods

3.2.1 Extraction Time

When the system is subject to fabrication defects, there is no longer a specific optimal time that we can expect to provide the highest fidelity. We therefore need to carefully consider how to deal with time. There are a few options in this regard, we present those options here, describe what we have chosen to do, and then demonstrate that we have made a reasonable choice. We could

- Optimise over time
- Select a specific extraction time
- Optimise over a specific time window.

We could choose to optimise each system over time, by evolving the system with small time steps, and choosing the time with the highest fidelity. Computationally this is possible, but difficult and time-consuming. We also note that realistically we will need to know the extraction time before we evolve, which is not possible for a system with random errors. Experimentally, we could build a set of chains, select the best of these and evolve it through time such that we know when the best arrival time would be. We can then repeat for all chains that produce fidelity in the upper quartile of all those made (or use any other method to select the best). Experimentally, this is possible as we will have a physical chain with only one set of random errors. However, computationally we want to average over a large set of errors, which would be computationally heavy as it involves finding the best arrival time for every chain. We can also decide on an extraction time before we evolve and choose to extract the state on all systems given by a certain Hamiltonian at that time. This is much easier computationally, but it is unlikely that we are able to find a reasonable time for all cases. We therefore choose to optimise over time, but within a specific time window given by the minimum and maximum arrival times as discussed in Section 2.5.5. We remind ourselves here that the latest arrival time comes from the arrival time for the swapping channel and is given

by $t_{max} = (N-1)\frac{\pi}{2}$. The earliest possible arrival time is taken from [44] and is given by $t_{min} = 0.34(N-1)+3.65$. As we are using a chain of $N = 51$ qubits, the time we evolve through is then

$$20.7 \leq t \leq 78.5, \tag{3.6}$$

where we use a time step of $\delta t = 0.1$. Although this time window gives us a well-defined minimum and maximum transfer time, we know from Section 2.5.5 that the arrival time for the Quadratic chain is much later than this, so we now evaluate whether the Quadratic chain is in fact a useful system to consider.

Quadratic PST Chain

The Quadratic PST chain is a system that allows PST, however, there is a long wait for extraction. In Fig 3.5a we show that the best extraction time is around $t_{Quad} = 1020$, which is a particularly long time to wait. Once we encode over 5 qubits at either end, we can see that the shape of this peak changes and that we can extract at a much earlier time at only a slightly lower fidelity. However, our problem is not to choose a suitable

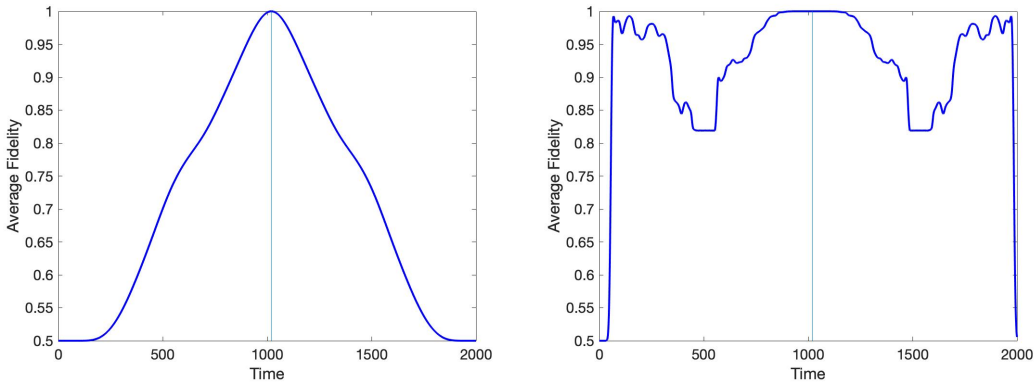

(a) *Quadratic PST chain showing extraction time.*

(b) *Quadratic PST with an encoding region of 5 qubits.*

Figure 3.5: *Plots showing the extraction time for the Quadratic PST Chain without encoding and with encoding for a chain of* $N = 51$

time for extraction in a perfect chain, but rather for one subject to fabrication defects. Therefore we can evaluate the same system subject to some random error, with and without encoding to select an appropriate extraction time. We apply random errors with standard deviation of $\sigma = 0.1$ for both sites and couplings and find that we have

minimum fidelity for these errors with no encoding (shown as the blue line along the x-axis in Fig. 3.6a). We repeat this 3 times for the case where we have encoded over 5 sites with the aim of revealing an extraction time. We can see the results of this in Fig. 3.5. It becomes clear that although the fidelity is improved by the encoding, it is difficult to find the best time to extract. However, as the best extraction time is no longer as late as the case without noise, we can consider looking in a smaller time window. We choose to look at the time window up to $t = 500$, as we can see from Fig. 3.5 that this is where we see the first peak. We then plot this system for the time window selected, repeating 5 times with a standard deviation of $\sigma = 0.1$ again. We can see from Fig. 3.6b that there is no clear time to extract the state from this system. This quadratic chain is then one that may benefit from physically constructing the chain and finding the specific arrival time for that chain. Due to the nature of this system and the lack of clear optimal time, we neglect this system from the rest of our results and focus on the Linear PST, Apollaro, and Uniform chains.

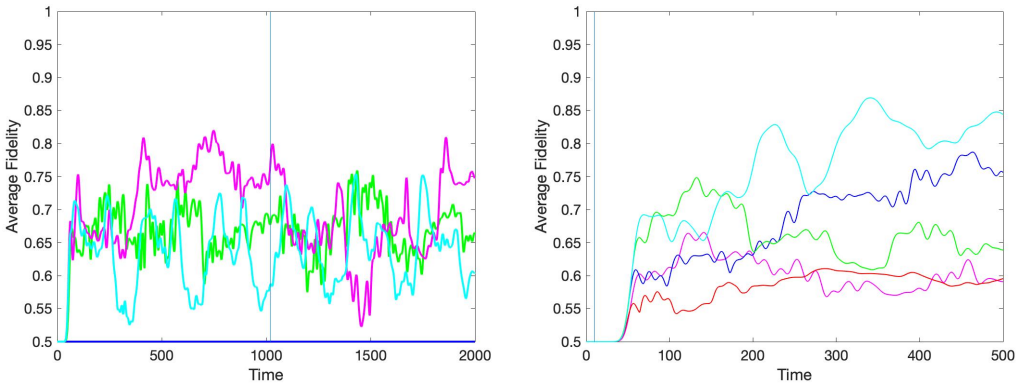

(a) (b)

Figure 3.6: *Plots showing how the quadratic chain evolves with random errors with standard deviation of* $\sigma = 0.01$. *(a) shows the evolution until* $t = 2000$*, (b) shows a shorter evolution time, until* $t = 500$. *Note that* $t_{max} = 78.5$

3.2.2 Numerics

Ultimately, the optimisation of the encoding region is complex and must be solved numerically. Therefore the problem can be simplified into a set of parameters we can choose, a set that are given, and a set we try to optimise. Particularly, there are several

variables that are dictated by experiment, such as: the length of the chain, the method for including errors, and the size of the encoding region we can use. We select values for these purely as a demonstration of our technique. The problem is then to find the encoding that maximises the fidelity of state transfer from one end of the chain to the other in the presence of fabrication defects. We must also consider time as a factor, where here we have chosen the use a time window given by a reasonable minimum and maximum.

We start by creating a Hamiltonian, with errors applied to the sites and couplings with the methods described above. Specifically we consider σ_B up to 0.9, in steps of 0.05, and values of σ_J up to 0.4 with the same steps of 0.05. Each of these Hamiltonians evolves the initial state, through the extraction time window, in steps of $\delta t = 0.1$, without any encoding and then compared to our desired state to give the average fidelity as given by Eq. (2.13). For the encoded system we use the scheme presented in Section 2.6 and take the square of the largest singular value as our measure of success to give an average fidelity given by Eq. (2.13). We repeat this process 1000 times and then choose the chain with the fidelity at the upper quartile. We choose the upper quartile as it is reasonable to assume one can take the best 25% of the manufactured chains and then the upper quartile provides a lower bound on the fidelity achieved. We then present our results as contour plots showing the fidelity of the upper quartile, averaged over input state, against the standard deviation for the errors on sites and couplings.

3.3 Demonstrations

In this section, we apply the random errors and encoding to three different Hamiltonians to demonstrate the scheme, these Hamiltonians being the Linear PST, Uniform, and Apollaro. We use a chain length of $N = 51$ for all systems and we encode and decode over 5 qubits at each end. We choose to first introduce errors that are proportional on the couplings and additive on the sites, then later, additive on sites and couplings. We choose the maximum standard deviation for the errors on the couplings to be $\sigma_J = 0.3$

and the maximum standard deviation of errors on the sites to be $\sigma_B = 0.6$. We repeat each set of random errors 1000 times and take the value at the upper quartile.

3.3.1 Proportional Errors

We first give a demonstration of the errors applied proportionally on the couplings, as given in Eq. (3.3).

Uniform Chain

The uniform chain is such that all couplings are equal to the maximum coupling strength 1. This system does not allow for PST in a system larger than $N = 3$, and additionally we saw in Section 2.5.1 that the fidelity is particularly low for a chain of $N = 51$. One might assume then that the Uniform chain would not be useful for transfer at these distances, however it has the benefit of not needing modulated couplings. Indeed, we can see from Fig. 3.7a that without encoding we cannot achieve a particularly high fidelity. However, this system that shows a particular improvement when we apply encoding. This could be very useful, as the Uniform chain has a very fast transfer time of $t_{Uni} \approx \frac{(N+0.8089N^{\frac{1}{3}})}{2J_{max}}$, and is easy to build due to the uniform couplings.

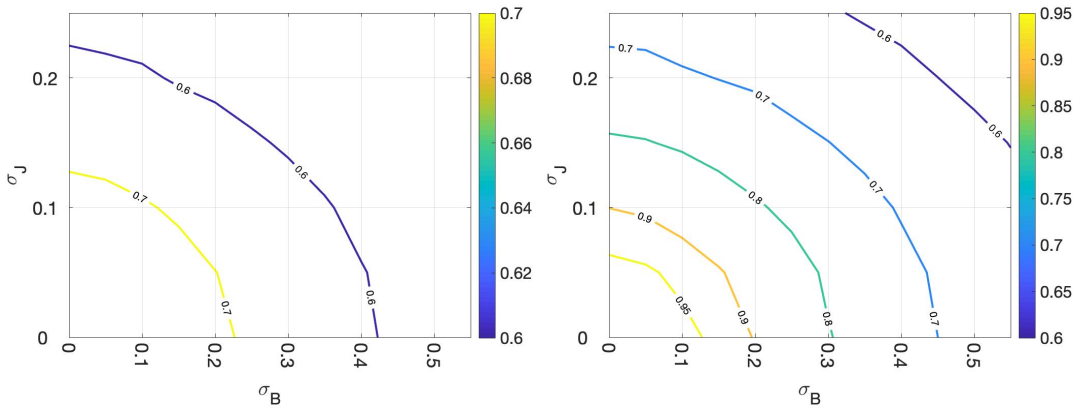

(a) *Uniform chain with no encoding or decoding present*

(b) *Uniform chain with an encoding and decoding regions of 5.*

Figure 3.7: *Plot showing encoding applied to a uniform chain in the presence of fabrication defects*

Linear PST Chain

The second chain we apply our encoding to is that presented in [31], which we call the *Linear PST Chain*. A particular benefit of this chain over others that allow for PST is that the transfer time is much earlier than other examples (such as the Quadratic Chain, which we choose not to present here).

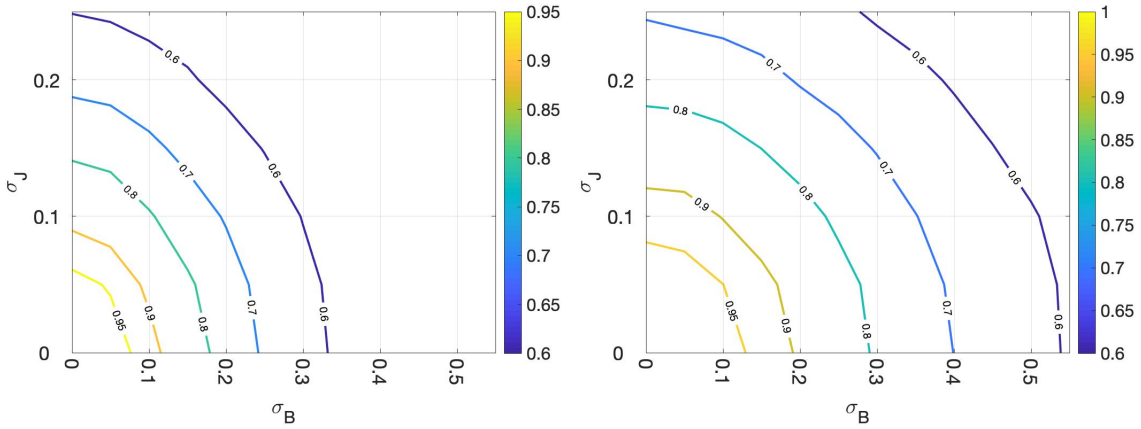

(a) *Linear chain with no encoding or decoding present*

(b) *Linear chain with an encoding and decoding regions of 5.*

Figure 3.8: *Plot showing encoding applied to a linear chain in the presence of fabrication defects applied proportionally*

We can see from Figs. 3.8 that through application of a relatively small encoding zone, we can already see substantial improvement.

Apollaro Chain

We expect the Apollaro Chain to be slightly more robust against errors, as the bulk of the chain is uniform and therefore these couplings are not tuned to specific values. We note that this is true, and that there is further improvement after applying encoding.

3.3.2 Additive Errors

We can also apply the errors additively, such that they are not dependent on the coupling strengths. We note that we expect these systems to perform slightly worse than when errors are proportional as we can see from Figs. 3.1 that the weaker coupling strengths are altered much more. We note that the on-site errors are added in the same way as

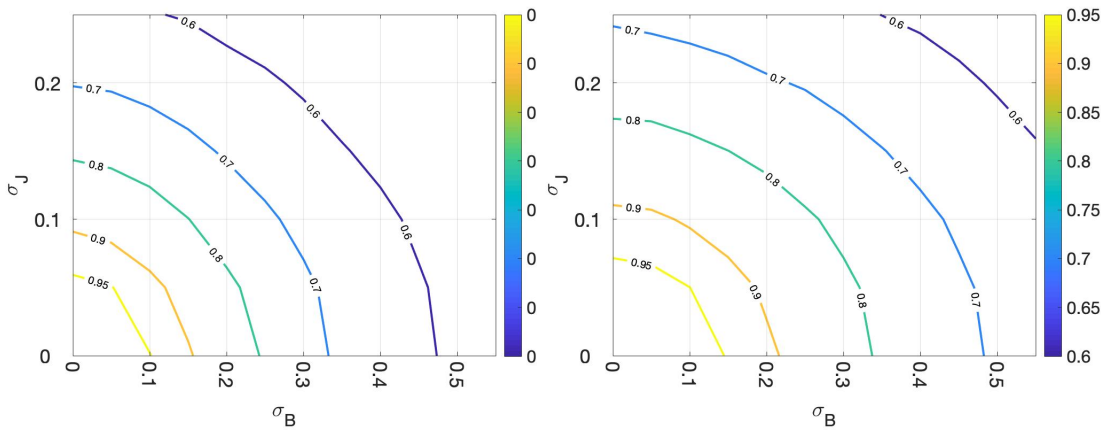

(a) *Apollaro chain with no encoding or decoding present*

(b) *Apollaro chain with an encoding and decoding regions of 5*

Figure 3.9: *Plot showing encoding applied to an Apollaro chain in the presence of fabrication defects applied proportionally*

previously, but there will be slight discrepancies as we are dealing with random errors. We do not present he Uniform chain here as the choice of additive/proportional errors is not relevant here where all coupling strengths are the same.

Linear Chain

The Linear chain is one that we expect to perform worse when we have additive errors compared to proportional errors, as the end couplings are much smaller. We note from Figs. 3.10 that this is true, and the performance is noticeably worse that that given in Figs. 3.8.

Apollaro Chain

The Apollaro chain is another chain where we expect to see a reduced fidelity as compared to when the errors are proportional to coupling strengths. We can see from Figs. 3.11 that the fidelity is reduced, but not significantly as in the case of the Linear chain. This is likely due to the fact that much of the Apollaro chain is uniform and so the additive errors are no different from proportional errors in the bulk of the chain.

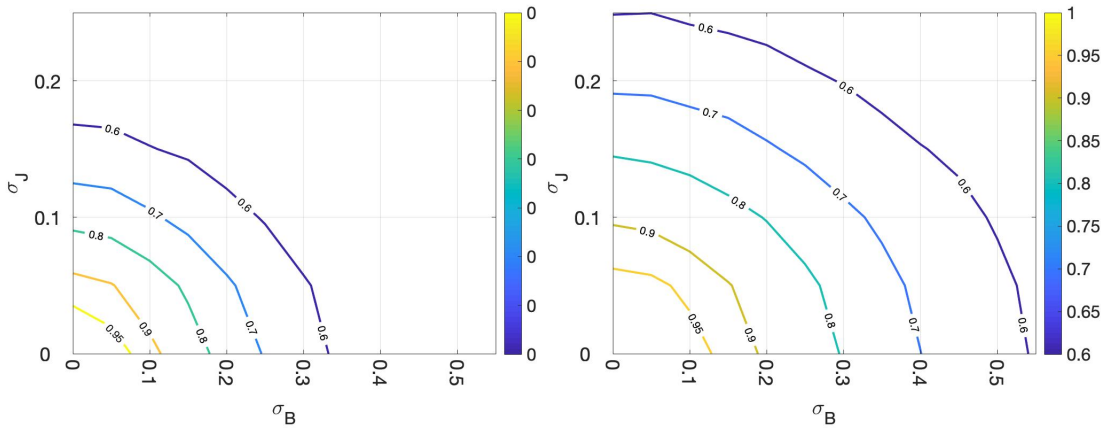

(a) *Linear chain with no encoding or decoding present*

(b) *Linear chain with an encoding and decoding regions of 5*

Figure 3.10: *Plot showing encoding applied to an Linear chain in the presence of fabrication defects that are applied additively*

3.4 Conclusion

We have demonstrated the effects of random errors to both the couplings and the sites themselves in different spin chain systems. We have shown that fabrication defects can be damaging and significantly reduce the fidelity of otherwise perfect systems. This is a very real issue that will be faced when attempting to build these systems. We have then introduced an encoding method that can reduce the effects of these defects and still produce reasonably good transfer in such chains. The technique is easily applicable and can be used in scenarios where the total number of qubits is low. It can also be applied to any Hamiltonian that is excitation preserving, making is very widely applicable. We have demonstrated the wide uses of this technique by applying our methods to three different chains and saw improvements over all. Perhaps the most useful result, from our demonstrations, is that applying this encoding scheme to a Uniform chain gives results close to that of a fully modulated chain that can give PST in an error-free system. It is also interesting to note that the average fidelities of the different systems after encoding are all relatively similar, regardless of their values before encoding. Our technique is easily applicable and the encoding zone can be adjusted to further increase fidelity or decreased to increase the bulk chain length (at the expense of higher quality transfer).

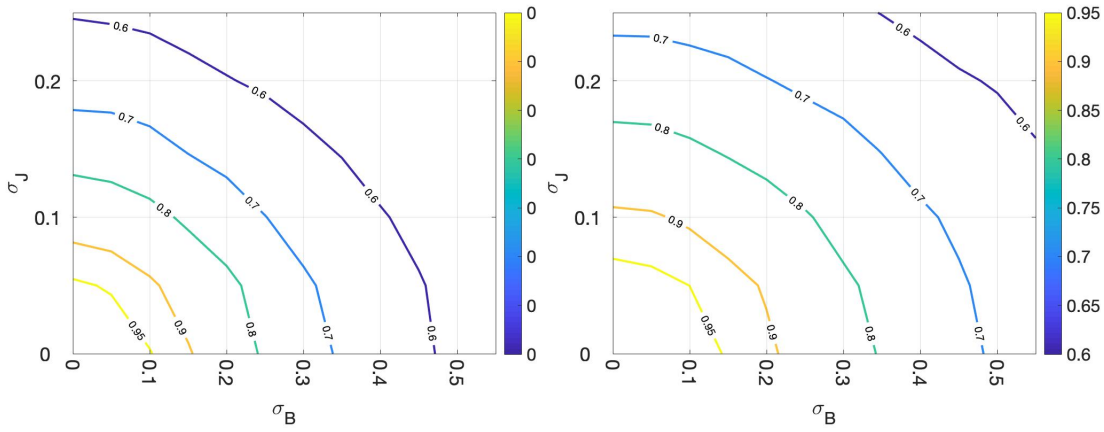

(a) *Apollaro chain with no encoding or decoding present*

(b) *Apollaro chain with an encoding and decoding regions of 5*

Figure 3.11: *Plot showing encoding applied to an Apollaro chain in the presence of fabrication defects applied additively*

3.5 Engineering Robust Chains

In the above sections, we chose specific chains to demonstrate that the encoding technique leads to improvements in fidelity. We now consider whether we can build a chain that is specifically designed to be robust against these errors. A natural starting point is to consider the random errors as pertubations to the Hamiltonian. Then, can we perturb the Hamiltonian in such a way that we can mitigate the effects of these? If we start with the Hamiltonian H, which has some perturbation V due to the random errors so that

$$H = H_0 + V, \tag{3.7}$$

where H_0 is the unperturbed Hamiltonian, then we aim to apply some δH to the Hamiltonian to (at least partially) remove the perturbations caused by the errors. For some set of random errors, given by some perturbation V, we can use the Dyson expansion of evolution [54] to show that the fidelity is given by

$$\begin{aligned} F = \langle N|e^{-iHt_0}|1\rangle - i\int \langle N|e^{-iH(t_0-t_1)}(V+\delta H)e^{-iHt_1}|1\rangle dt_1 \\ -\int \langle N|e^{-iH(t_0-t_1)}(V+\delta H)e^{-iH(t_1-t_2)}(V+\delta H)e^{-iHt_2}|1\rangle dt_1 dt_2 + \ldots, \end{aligned} \tag{3.8}$$

where $t_0 \geq t_1 \geq t_2$. We can see then that the errors due to V appear at the first order. This makes the problem more complex; given the random nature of the errors, we do not know them in advance, and therefore do not know them when we need to choose δH. It is possible for us to average over all errors such that we consider $\int \overline{F} dV$, but we then lose the first order V term (given that our errors are centered around 0, the average of the errors will be 0). The earliest our V will then appear is at the second order, and so we can only correct for second order V with our δH. This means that for any instance of V the first order term will still remain and cannot be corrected for. We then conclude that this is not a viable method for improving the robustness of our system against random errors and we have not pursued this further.

Chapter 4

Noisy Systems

4.1 Introduction

In Chapter 3, we discussed fabrication defects in experimental quantum spin chains, and how we can improve transfer in the presence of these errors with a simple to implement encoding technique. Here we extend this encoding technique to cover some systems that do not have unitary evolution. Any such quantum system, once created experimentally, will be subject to interaction with the environment. We call this interaction with the environment *noise*, or *decoherence*, and in Section 4.5, we will show how damaging this is. There are two types of noise that we will be considering in detail here. We will consider amplitude damping noise, which refers to the loss of information to the environment and is excitation decreasing, and dephasing, which refers to the loss of coherence in a quantum system. We can model amplitude damping noise analytically within the single excitation subspace, to show the scale of the decay to the environment, Section 4.5.3. Dephasing noise cannot be solved analytically. We then introduce a generalisation of the encoding technique that can improve transfer in the presence of noise.

Surprisingly little work has been done on noise within quantum systems, particularly in terms of mitigation. In [55], Hu and Lian consider systems with intrinsic decoherence modelled by the master equation, which is based on the research by Milburn in [56]. Some work has previously been done with respect to quantum error correction and noise in quantum spin chains [57]. Parallel spin chains have also been considered as systems appropriate for use in a noisy environment [58]. We specifically consider 1D spin chains of length up to 35 qubits. We chose 35 as it's unlikely that any experiment will exceed that length soon, and therefore we can provide a theoretical framework that is prepared for when experiments do reach that length. We also note that the noise becomes more damaging for longer chains, as transfer time increases. Our methods are easily scalable and we believe that these initial investigations show promising results.

In this chapter, we first give a very brief introduction to the types of noise we consider and introduce the idea of *error-correcting codes*, we then introduce some mathematical methods required to treat noisy systems. Then we introduce our noise, show how we

can evolve a system according to this, and provide results on how noise effects a system. We then introduce our encoding technique, aimed at improving transfer in the presence of noise. Finally, we demonstrate our technique with three different systems.

4.2 A (Very) Brief Introduction to Noise

First we present a short introduction to the idea of noise such that the reader can gain contextual information on the problem we are trying to solve. We introduce noise more thoroughly in Section 4.5. In this thesis, we consider two main types of noise: Amplitude damping and dephasing. Amplitude damping noise is perhaps easier to understand as it has many classical analogies. When we refer to amplitude damping, we are referring to the loss of energy from the system to the environment (due to interaction with the environment). Therefore, a system containing one excitation will decay to the zero excitation subspace over time as the energy is lost to its surroundings, and we can say that amplitude damping noise is *excitation decreasing*. Dephasing refers instead to the loss of *coherence* within a system, meaning that the relations between phases within the system are not exact, and we can no longer transfer states with high fidelity. Dephasing is therefore quantum mechanical in nature and has no simple classical analogy. This noise leads the state to spread throughout the system, but no energy is lost, so dephasing noise is *excitation preserving*.

4.3 Error-Correcting Codes

In classical communication, bits are used to store information, where the bits can be in either the state 1 or the state 0. An error on these bits, will manifest in a *bit flip* where the state 1 becomes 0 or vice versa. One of the simplest ways to detect if a bit-flip has occurred is to add additional bits and code each state onto a *codeword*. For example, the state 0 can be encoded with 000 and the state 1 can be encoded with 111. If the receiver receives the state 010, they can assume that the state 0 was sent, as long as the probability of a bit flip is low. This systems relies on the probability of one bit flip occurring being

much higher than the probability of two bit flips occurring, and therefore only allows us to correct for a single bit flip. Nevertheless, this allows us to introduce the theory of error-correction in classical systems. We now demonstrate how this can be adapted to quantum error-correcting codes. When we consider qubits instead of bits, quantum systems introduce another issue in that they cannot be directly measured without losing the information contained within a state, so a clever solution is needed. This solution appears in the addition of extra qubits to allow us to gain some information on the state without direct measurement of the state. We introduce the three-qubit code as an example of where these additional qubits are used, noting that this code only detects that a bit-flip error has occurred and cannot correct for it. For the three qubit code, we first introduce some assumptions:

1. Noise acts on each qubit independently
2. For each qubit, there is a probability $(1-p)$ of it remaining unchanged
3. The probability that a bit-flip occurs (by application of a Pauli-X operator) is $p \leq \frac{1}{2}$

To describe the protocol for the three-qubit code, we stick to the convention of using Alice as a sender and Bob as a receiver. Alice starts by preparing a qubit in the state $\alpha|0\rangle + \beta|1\rangle$ which she intends to send. She prepares an additional two qubits in the state $|0\rangle$, such that the initial state of all three qubits is

$$|\psi\rangle = \alpha|000\rangle + \beta|100\rangle. \tag{4.1}$$

Alice then operates a CNOT gate from the first qubit to the second (where the operation of a CNOT is to initiate a bit-flip on the target qubit if the control qubit is in the state 1), so that the state is now $|\psi\rangle = \alpha|000\rangle + \beta|110\rangle$. She then applies the CNOT from the first qubit to the third to arrive at the state $|\psi\rangle = \alpha|000\rangle + \beta|111\rangle$. Alice then sends the three qubits down the channel, and Bob receives them after the noise in the channel has

acted on them. The state of the qubits Bob receives is one of the following:

State	Probability
$\alpha\|000\rangle + \beta\|111\rangle$	$(1-p)^3$
$\alpha\|100\rangle + \beta\|011\rangle$	$p(1-p)^2$
$\alpha\|010\rangle + \beta\|101\rangle$	$p(1-p)^2$
$\alpha\|001\rangle + \beta\|110\rangle$	$p(1-p)^2$
$\alpha\|110\rangle + \beta\|001\rangle$	$p^2(1-p)$
$\alpha\|101\rangle + \beta\|010\rangle$	$p^2(1-p)$
$\alpha\|011\rangle + \beta\|100\rangle$	$p^2(1-p)$
$\alpha\|111\rangle + \beta\|000\rangle$	p^3.

Bob is unable to directly measure the state he receives or he will lose the information contained, so he adds two qubits of his own, prepared in the state $|00\rangle$, to the system. He then performs a CNOT from the first and second received qubits to the first of his added qubits, and from the first and third received qubits to the second of his. The state of all five qubits is then:

State	Probability
$(\alpha\|000\rangle + \beta\|111\rangle)\|00\rangle$	$(1-p)^3$
$(\alpha\|100\rangle + \beta\|011\rangle)\|11\rangle$	$p(1-p)^2$
$(\alpha\|010\rangle + \beta\|101\rangle)\|10\rangle$	$p(1-p)^2$
$(\alpha\|001\rangle + \beta\|110\rangle)\|01\rangle$	$p(1-p)^2$
$(\alpha\|110\rangle + \beta\|001\rangle)\|01\rangle$	$p^2(1-p)$
$(\alpha\|101\rangle + \beta\|010\rangle)\|10\rangle$	$p^2(1-p)$
$(\alpha\|011\rangle + \beta\|100\rangle)\|11\rangle$	$p^2(1-p)$
$(\alpha\|111\rangle + \beta\|000\rangle)\|00\rangle$	p^3.

Bob can then measure the additional qubits that he added to the system and decide his course of action depending on the state of such qubits. If he measures $|00\rangle$, then he does nothing. If he measures $|01\rangle$, $|10\rangle$, or $|11\rangle$ then he applies the Pauli-X operator to the third, second, or first qubit respectively. Then he either applies the operator such that he has the exact state that Alice sent, or he is a state of X out on all qubits. This protocol works on the assumption that one bit flip is much more likely than two, therefore Bob is more likely to correct to the state sent by Alice than one that is X out. This may seem like an elegant solution to the problem of quantum error correction, but this three-qubit code only corrects for bit-flip type errors, where quantum systems introduce another type of error. If we consider the Bloch sphere, shown in Fig. 1.1, we can see that there are countless possible states that can be received that were not the intended state, rather than a simple bit flip. This appears to make the task of error correction much more complex in the quantum case, however we are able to *digitise* the quantum case such that we can apply some of the same logic as in the classical case. We first note that any interaction between a qubit and the environment can be written as

$$|\psi\rangle|\phi_0\rangle_e \rightarrow \sum_i (E_i|\psi\rangle)|\phi_i\rangle_e \tag{4.2}$$

where the E_i are *error operators* and are tensor products of the Pauli operators [59], $|\psi\rangle$ is the initial state of the system, and $|\phi_i\rangle_e$ are the states of the environment. This shows us that any error that can occur can be expressed using the Pauli matrices, and furthermore we can express the Pauli-Y operator in terms of the Pauli-X and Pauli-Z operators (up to a phase) so that $-iY = XZ$. We can now remind ourselves that the Pauli-X operator is analogous to a bit flip, and the Pauli-Z operator enacts a phase change. Until now, we have been working in the computational basis $|0\rangle, |1\rangle$, but to consider the phase flips, we change to the conjugate basis $|+\rangle, |-\rangle$ where

$$|+\rangle = \frac{1}{\sqrt{2}}(|0\rangle + |1\rangle) \tag{4.3}$$

$$|-\rangle = \frac{1}{\sqrt{2}}(|0\rangle - |1\rangle) \tag{4.4}$$

and the phase flip (which happens via the Z operator) acts such that $Z|-\rangle = |+\rangle$ and $Z|-\rangle = |+\rangle$. We therefore need a code that is capable of detecting and correcting for both bit flips and phase flips. We now discuss how the theory of quantum error correcting codes has evolved. The first examples of quantum error-correcting codes are the CSS codes (Calderbank Shor Steane). Shor proved in [60] that 9 qubits could protect a single qubit , while in [61], Steane demonstrated that the same could be done with just 7 qubits. A more general theory for quantum error correcting codes was later given in [62] and [63]. A perfect 5 qubit code was later found [64], [65]. Although these perfect codes exist, they still require a large number of additional qubits, which is more difficult in practice. Given that the largest quantum computer currently in operation is a 53 qubit quantum computer created by IBM [66], it is useful to consider systems that can be robust against noise without using full-error correction, and therefore using fewer qubits. That is exactly what we present here.

4.4 Mathematical Methods

Before we discuss noise in detail, we introduce some of the mathematical methods required to consider noisy systems. First, we introduce *vectorisation* as a method whereby we rearrange the elements in a matrix to become a vector. This allows us to apply noise as superoperators to vector states. We then recalculate our average fidelity in this vectorised formalism to give us a measure of success for our technique.

4.4.1 Vectorisation

Here we introduce the *vectorisation* procedure that allows us to properly consider noisy systems. When we introduce noise to a system, we must consider mixed states. For this reason, we use the density operator

$$\rho = \sum_{ij} p_{ij} |i\rangle\langle j|, \tag{4.5}$$

where $\sum_i p_{ii} = 1$ and $p_{ij} = p^*_{ji}$.

This can be rewritten as a column vector by reorganising the elements

$$|\rho\rangle = \sum_{i,j} p_{ij}|i,j\rangle. \tag{4.6}$$

To apply this method to our work with spin systems and noise, we demonstrate how this works with operators.

Lemma 4.

$$|A\rho B\rangle = A \otimes B^T|\rho\rangle$$

Proof. Consider operators A and B, with the same dimensions. We can write these as

$$A = \sum_{kl} A_{kl}|k\rangle\langle l| \tag{4.7}$$

and

$$B = \sum_{kl} B_{kl}|k\rangle\langle l|, \tag{4.8}$$

where $A_{kl} = \langle k|A|l\rangle$ and $B_{kl} = \langle k|B|l\rangle$ so that

$$A = \sum_{kl} \langle k|A|l\rangle|k\rangle\langle l| \tag{4.9}$$

and

$$B = \sum_{kl} \langle k|B|l\rangle|k\rangle\langle l|. \tag{4.10}$$

Applying the same vectorisation process as above for the density operator, we have

$$|A\rho B\rangle = \sum_{kl} \langle k|A\rho B|l\rangle|k,l\rangle. \tag{4.11}$$

Then substituting in the Density Operator, Eq. (4.5), we get

$$|A\rho B\rangle = \sum_{ij}\sum_{kl} p_{ij}\langle k|A|i\rangle\langle j|B|l\rangle|k,l\rangle, \tag{4.12}$$

which can be rearranged to give

$$|A\rho B\rangle = \sum_{ij}\sum_{kl} p_{ij}|k,l\rangle\langle k|A|i\rangle\langle l|B^T|j\rangle = \sum_{kl}|k,l\rangle\langle k,l|A\otimes B^T\sum_{ij}p_{ij}|i,j\rangle. \quad (4.13)$$

Where the first summation gives the identity matrix and the final sum returns the vectorised density matrix. Therefore, we have

$$|A\rho B\rangle = A\otimes B^T|\rho\rangle. \quad (4.14)$$

□

This will allow us to treat noise superoperators as operators and therefore consider the evolution of a system subject to noise.

4.4.2 Average Fidelity in the Vectorised Formalism

We previously demonstrated how to calculate the average fidelity of state transfer for a system using the density operator, in Section 2.3.2. Now, we must consider how that translates to the vectorised form. If we start with an initial state

$$|\boldsymbol{\psi}\rangle = \alpha|\mathbf{0}\rangle + \beta|\mathbf{1}\rangle, \quad (4.15)$$

then, after some evolution, we have the state

$$|\boldsymbol{\psi}'\rangle = \alpha|\mathbf{0}\rangle + \beta\sum_{n=1}^{N}\eta_n|\mathbf{n}\rangle, \quad (4.16)$$

where the excitation can be spread over all sites. After we have allowed the system to evolve for some time t, we take the partial trace over all sites other than the final site (where we aim to extract the state). We therefore introduce some operator $\boldsymbol{\mathcal{C}}$ that takes the partial trace over sites 1 to $N-1$ such that

$$\boldsymbol{\mathcal{C}}e^{-iHt}|\rho\rangle = \mathrm{Tr}_{1,2,\ldots,N-1}|\rho'\rangle, \quad (4.17)$$

where $\rho' = |\psi'\rangle|\psi'^*\rangle$ is the density vector after evolution.

Example 4. The partial trace operator, $\mathcal{C}$ for $N = 3$ is given by

$$\mathcal{C} = \begin{array}{c} \\ |00\rangle \\ |01\rangle \\ |10\rangle \\ |11\rangle \end{array} \begin{array}{c} \begin{array}{cccccccccccccccc} |00\rangle & |01\rangle & |02\rangle & |03\rangle & |10\rangle & |20\rangle & |30\rangle & |11\rangle & |12\rangle & |13\rangle & |21\rangle & |22\rangle & |23\rangle & |31\rangle & |32\rangle & |33\rangle \end{array} \\ \begin{bmatrix} 1 & 0 & 0 & 0 & 0 & 0 & 0 & 1 & 0 & 0 & 0 & 1 & 0 & 0 & 0 & 0 \\ 0 & 0 & 0 & 1 & 0 & 0 & 0 & 0 & 0 & 0 & 0 & 0 & 0 & 0 & 0 & 0 \\ 0 & 0 & 0 & 0 & 0 & 0 & 1 & 0 & 0 & 0 & 0 & 0 & 0 & 0 & 0 & 0 \\ 0 & 0 & 0 & 0 & 0 & 0 & 0 & 0 & 0 & 0 & 0 & 0 & 0 & 0 & 0 & 1 \end{bmatrix} \end{array}, \tag{4.18}$$

where the first row (referring to the zero excitation subspace) will have 1's in the positions that refer to $|00\rangle$,$|11\rangle$,...,$|N-1, N-1\rangle$. Rows 2 and 3, will have 1's in the positions $|0N\rangle$ and $|N0\rangle$ respectively, and row 4, will have a 1 in position $|N, N\rangle$.

Taking the partial trace over of our density vector gives

$$\mathrm{Tr}_{1,2,\ldots,N-1}|\rho\rangle = |\rho_N\rangle = \begin{bmatrix} |\alpha|^2 + |\beta|^2(|\eta_1|^2 + \ldots + |\eta_{N-1}|^2) \\ \alpha\beta^*\eta_N^* \\ \alpha^*\beta\eta_N \\ |\beta|^2|\eta_N|^2 \end{bmatrix}, \tag{4.19}$$

where we can see that $|\eta_N|^2$ is the fidelity of excitation transfer, where we note that Eq. 4.19 is very similar to Eq. 2.69.

We recall that our fidelity is given by

$$F = \langle\psi|\rho_N|\psi\rangle, \tag{4.20}$$

which, in our vectorised format becomes

$$F = \langle\psi\psi^*|\rho_N\rangle, \tag{4.21}$$

so we have

$$F(\alpha, \beta) = (|\alpha|^2\langle 00| + \alpha^*\beta\langle 01| + \alpha\beta^*\langle 10| + |\beta|^2\langle 11|)(|\rho_N\rangle). \tag{4.22}$$

We expand this and replace $\alpha = \cos\left(\frac{\theta}{2}\right)$ and $\beta = \sin\left(\frac{\theta}{2}\right)e^{i\phi}$ respectively. To average over all possible input states, we integrate over all values of θ and ϕ on the Bloch sphere

$$\overline{F} = \int_0^{2\pi}\int_0^{\pi} F(\theta,\phi)\sin\theta d\theta d\phi. \tag{4.23}$$

The integration removes any terms with $e^{i\phi}$ or similar, so we are left with

$$\begin{aligned}\overline{F} = \tfrac{1}{6}[2+(|\eta_1|^2+\cdots+|\eta_{N-1}|^2))\langle 00|00\rangle + |\eta_N|^2\langle 00|11\rangle + \\ \eta_N^*\langle 01|01\rangle + \eta_N\langle 10|10\rangle + (1+2(|\eta_1|^2+\cdots+|\eta_N|^2)\langle 11|00\rangle + 2|\eta_N|^2\langle 11|11\rangle].\end{aligned} \tag{4.24}$$

We then compute the inner products so that now we have

$$\overline{F} = \frac{1}{6}(2+|\eta_1|^2+\cdots+|\eta_{N-1}|^2+\eta_N^*+\eta_N+2|\eta_N|^2). \tag{4.25}$$

Then, by applying a particular phase to $\eta_N^*+\eta_N$ we have $2|\eta_N|$. We can show this is true by considering the complex plane. As η_N^* and η_N are complex conjugates of each other we can write them as $(x+iy)+(x-iy)$. In polar coordinates we then have $re^{i\phi}+re^{-i\phi}$ where r is the absolute value and $e^{i\phi}$ gives us the angle from the positive real axis on the Argand diagram. We can then see that we have $r(2\cos\phi)$ where by applying some overall corrective phase $e^{-i\phi}$, we can retrieve the absolute value r. Finally our average fidelity of transfer is given by

$$\overline{F} = \frac{1}{6}(3+2|\eta_N|+|\eta_N|^2) \tag{4.26}$$

which is identical to the case without vectorisation. We extend this to the case of noise in Section 4.5.4.

4.5 Noise

We present here dephasing noise, $\mathcal{Q}_D$, (Section 4.5.2) and amplitude damping noise, $\mathcal{Q}_A$, (Section 4.5.3). We first demonstrate how a noisy system evolves through the

Lindblad Master Equation [67], then we use this and our vectorisation method to build the superoperators describing noise. Finally in this section, we demonstrate that dephasing noise evolves only in the single excitation subspace and that we can provide an analytical solution to amplitude damping noise.

4.5.1 The Lindblad Master Equation

When noise is introduced to a system, we are no longer confined to pure states and must also be able to consider mixed states. For this reason, we use the density matrix as given in Eq. (4.5). In this formalism, the Schrödinger equation for the noise-free case is given by

$$\frac{d\rho}{dt} = -i[H, \rho] \tag{4.27}$$

where $[A, B] = AB - BA$ gives the commutator of operators A and B. To model the noise, we use the Lindblad Master Equation

$$\frac{d\rho}{dt} = -i[H, \rho] + \sum_{n=1}^{N} (L_n \rho L_n^\dagger - \frac{1}{2} L_n^\dagger L_n \rho - \frac{1}{2} \rho L_n^\dagger L_n) \tag{4.28}$$

and substitute suitable operators in place of the Lindblad operators, L_n. These Lindblad operators are typically trace-free regardless of the trace of ρ, meaning that the sum of the eigenvalues does not change (and indeed is always 1). We also note that the Lindblad operators ensure that $\frac{d\rho}{dt}$ remains Hermitian so all the eigenvalues are real.

4.5.2 Dephasing Noise

Dephasing is the mechanism by which a quantum system becomes classical. For a quantum system to be useful as an information transfer system, there must be definite phase relations between states. When dephasing happens, this destroys the phase relation between states and therefore the separate states can no longer be defined and we have lost coherence in the system. This type of noise is excitation preserving and rather than losing energy to the environment (in the case of amplitude damping, Section 4.5.3), the energy is spread through the system and coherence between states is lost. In the case

of dephasing noise, the Lindblad operators are given by $L_n = \sqrt{\frac{\Gamma_z}{2}} Z_n$, where Γ_z gives the strength of the noise, and is related to the transverse relaxation process in NMR by $\Gamma_z = \frac{1}{T_2}$ [68]. Substituting this into Eq. (4.28), we can see that the Lindblad equation becomes

$$\frac{d\rho}{dt} = -i[H,\rho] + \frac{\Gamma_z}{2}\sum_{n=1}^{N}(Z_n\rho Z_n^\dagger - \frac{1}{2}Z_n^\dagger Z_n\rho - \frac{1}{2}\rho Z_n^\dagger Z_n). \tag{4.29}$$

We know that the Pauli matrices are hermitian, so this may be rewritten as

$$\frac{d\rho}{dt} = -i[H,\rho] + \frac{\Gamma_z}{2}\sum_{n=1}^{N}(Z_n\rho Z_n) - \frac{\Gamma_z}{2}\rho N. \tag{4.30}$$

Using the result from Lemma 4, we can vectorise each component. Starting with

$$|H\rho\rangle = (H\otimes\mathbb{1})|\rho\rangle, \tag{4.31}$$

and similarly

$$|\rho H\rangle = (\mathbb{1}\otimes H^T)|\rho\rangle, \tag{4.32}$$

where $H^T = H$ as long as H is real and symmetric. Then, without noise, our superoperator is given by

$$\boldsymbol{\mathcal{H}} = -iH\otimes\mathbb{1} + i\mathbb{1}\otimes H. \tag{4.33}$$

Finally,

$$|Z\rho Z^\dagger\rangle = (Z\otimes Z^*)|\rho\rangle. \tag{4.34}$$

Using these results, the Lindblad equation can be written as

$$\frac{d|\rho\rangle}{dt} = \boldsymbol{\mathcal{Q}}_D|\rho\rangle, \tag{4.35}$$

where

$$\boxed{\boldsymbol{\mathcal{Q}}_D = \boldsymbol{\mathcal{H}} + \frac{\Gamma_z}{2}\sum_{n=1}^{N} Z_n\otimes Z_n - \frac{\Gamma_z}{2}N\mathbb{1}\otimes\mathbb{1}}. \tag{4.36}$$

We can use the general solution for the above differential equation, giving the evolution of $|\rho\rangle$ as

$$|\rho(t)\rangle = e^{\mathcal{Q}_D t}|\rho(0)\rangle. \tag{4.37}$$

Using Eq. (4.36) we can build the superoperator for dephasing noise. Although this cannot be solved analytically, due to the diagonal perturbations, we can demonstrate that dephasing noise preserves excitation number through evolution. We first consider the component $\mathcal{H} = -iH \otimes \mathbb{1} + i\mathbb{1} \otimes H$ for the general case, taking each subspace separately. Taking first the S_{00} subspace, we need only apply this to the tensor product $|\mathbf{0}\rangle \otimes |\mathbf{0}\rangle$ which gives

$$-i(H|\mathbf{0}\rangle \otimes \mathbb{1}|\mathbf{0}\rangle) + i(\mathbb{1}|\mathbf{0}\rangle \otimes H|\mathbf{0}\rangle). \tag{4.38}$$

The identity operator returns the state unchanged and the Hamiltonian operator only has an effect on an excited states, so Eq. (4.38) gives us 0 for the S_0 subspace. Let's now consider the S_{01} subspace, $|\mathbf{0}\rangle \otimes |\mathbf{n}\rangle$, where we have the zero state tensored with a state that contains a single excitation at site n. Applying the same logic as above, we have

$$-i(H|\mathbf{0}\rangle \otimes \mathbb{1}|\mathbf{n}\rangle) + i(\mathbb{1}|\mathbf{0}\rangle \otimes H|\mathbf{n}\rangle). \tag{4.39}$$

This time we have a Hamiltonian operator acting on an excited state, therefore we return iH_1, where H_1 denotes the single excitation subspace of the Hamiltonian. We can also see that if we instead acted on $|\mathbf{n}\rangle \otimes |\mathbf{0}\rangle$ we would get $-iH_1$, therefore we know both subspaces S_{01} and S_{10}. Finally, we calculate the S_{11} subspace, giving $-i(H_1 \otimes \mathbb{1}) + i(\mathbb{1} \otimes H_1)$. The first component of $\mathcal{Q}_D$ is then given as

$$\mathcal{H} = \begin{array}{c} \\ \mathrm{S}_0 \\ S_{01} \\ S_{10} \\ S_{11} \end{array} \begin{array}{c} \begin{array}{cccc} S_0 & S_{01} & S_{10} & S_{11} \end{array} \\ \left[\begin{array}{c|c|c|c} 0 & 0 & 0 & 0 \\ \hline 0 & iH_1 & 0 & 0 \\ \hline 0 & 0 & -iH_1 & 0 \\ \hline 0 & 0 & 0 & -iH_1 \otimes \mathbb{1} + i\mathbb{1} \otimes H_1 \end{array}\right] \end{array}. \tag{4.40}$$

The noise in this case applies only to the diagonal components, and therefore preserves excitation number, so we can build the case for $N = 3$

$$\mathcal{Q}_D = \begin{array}{c|ccccccc|ccccccc|c} & |00\rangle & |01\rangle & |02\rangle & |03\rangle & |10\rangle & |20\rangle & |30\rangle & |11\rangle & |12\rangle & |13\rangle & |21\rangle & |22\rangle & |23\rangle & |31\rangle & |32\rangle & |33\rangle \\ \hline |00\rangle & 0 & 0 & 0 & 0 & 0 & 0 & 0 & 0 & 0 & 0 & 0 & 0 & 0 & 0 & 0 & 0 \\ |01\rangle & 0 & -\Gamma_z & i & 0 & 0 & 0 & 0 & 0 & 0 & 0 & 0 & 0 & 0 & 0 & 0 & 0 \\ |02\rangle & 0 & i & -\Gamma_z & i & 0 & 0 & 0 & 0 & 0 & 0 & 0 & 0 & 0 & 0 & 0 & 0 \\ |03\rangle & 0 & 0 & i & -\Gamma_z & 0 & 0 & 0 & 0 & 0 & 0 & 0 & 0 & 0 & 0 & 0 & 0 \\ |10\rangle & 0 & 0 & 0 & 0 & -\Gamma_z & -i & 0 & 0 & 0 & 0 & 0 & 0 & 0 & 0 & 0 & 0 \\ |20\rangle & 0 & 0 & 0 & 0 & -i & -\Gamma_z & -i & 0 & 0 & 0 & 0 & 0 & 0 & 0 & 0 & 0 \\ |30\rangle & 0 & 0 & 0 & 0 & 0 & -i & -\Gamma_z & 0 & 0 & 0 & 0 & 0 & 0 & 0 & 0 & 0 \\ \hline |11\rangle & 0 & 0 & 0 & 0 & 0 & 0 & 0 & 0 & i & 0 & -i & 0 & 0 & 0 & 0 & 0 \\ |12\rangle & 0 & 0 & 0 & 0 & 0 & 0 & 0 & i & -2\Gamma_z & i & 0 & -i & 0 & 0 & 0 & 0 \\ |13\rangle & 0 & 0 & 0 & 0 & 0 & 0 & 0 & 0 & i & -2\Gamma_z & 0 & 0 & -i & 0 & 0 & 0 \\ |21\rangle & 0 & 0 & 0 & 0 & 0 & 0 & 0 & -i & 0 & 0 & -2\Gamma_z & i & 0 & -i & 0 & 0 \\ |22\rangle & 0 & 0 & 0 & 0 & 0 & 0 & 0 & 0 & -i & 0 & i & 0 & i & 0 & -i & 0 \\ |23\rangle & 0 & 0 & 0 & 0 & 0 & 0 & 0 & 0 & 0 & -i & 0 & i & -2\Gamma_z & 0 & 0 & -i \\ |31\rangle & 0 & 0 & 0 & 0 & 0 & 0 & 0 & 0 & 0 & 0 & -i & 0 & 0 & -2\Gamma_z & i & 0 \\ |32\rangle & 0 & 0 & 0 & 0 & 0 & 0 & 0 & 0 & 0 & 0 & 0 & -i & 0 & i & -2\Gamma_z & i \\ |33\rangle & 0 & 0 & 0 & 0 & 0 & 0 & 0 & 0 & 0 & 0 & 0 & 0 & -i & 0 & i & 0 \end{array} \tag{4.41}$$

where we can see that the elements that allow movement between subspaces are all 0, therefore dephasing noise is excitation preserving.

4.5.3 Amplitude Damping Noise

Amplitude damping essentially refers to the relaxation of an excitation to the ground state through loss of energy to the environment. We can consider this to be analogous to a swinging pendulum. The systems we have considered in Chapter 3, without no noise present, are lacking in interaction with the environment. We can similarly consider a pendulum suspended in a vacuum, without any friction or other electrical or magnetic interactions. Such pendulum would continue to swing indefinitely, given that there is no energy being dissipated. However, if we consider the same pendulum, outside a vacuum, we know that due to the air resistance it encounters, it will lose energy to the environment and eventually stop. This description fits well with our spin system, where the interaction with the environment will cause some dissipation of energy and eventually the energy stored in our system will be lost to the environment. The Lindblad

operator for amplitude damping noise is given by

$$L_n = \sqrt{\frac{\Gamma_x}{2}}(X_n + iY_n), \tag{4.42}$$

where Γ_x is the strength of our noise, and is linked to the longitudinal relaxation time in NMR by $\Gamma_x = \frac{1}{T_1}$ [68]. Substituting these operators into the Lindblad equation gives

$$\boxed{\mathcal{Q}_A = \mathcal{H} + \frac{\Gamma_x}{2}\sum_{n=1}^{N}[(X_n + iY_n)\otimes(X_n + iY_n)^* - (\mathbb{1} - Z_n)\otimes\mathbb{1} - \mathbb{1}\otimes(\mathbb{1} - Z_n)]}. \tag{4.43}$$

We can then evolve our system according to amplitude damping noise as

$$|\rho'\rangle = e^{\mathcal{Q}_A t}|\rho\rangle. \tag{4.44}$$

We are able to gain a little more information from the case of amplitude damping. We can analytically calculate the evolution of each subspace of the density operator. We can also show why amplitude damping noise is excitation decreasing. It helps for us to show what the superoperator would look like in this case

$$\mathcal{Q}_A = \begin{array}{c} \\ S_{00} \\ S_{01} \\ S_{10} \\ S_{11} \end{array} \begin{array}{c} \begin{array}{cccc} S_{00} & S_{01} & S_{10} & S_{11} \end{array} \\ \left[\begin{array}{c|c|c|c} 0 & 0 & 0 & 2\Gamma_x\sum_k\langle\mathbf{kk}| \\ \hline 0 & iH_1 - \Gamma_x\mathbb{1} & 0 & 0 \\ \hline 0 & 0 & -iH_1 - \Gamma_x\mathbb{1} & 0 \\ \hline 0 & 0 & 0 & iH_1\otimes\mathbb{1} - i\mathbb{1}\otimes H_1 - 2\Gamma_x\mathbb{1} \end{array}\right] \end{array}, \tag{4.45}$$

where the upper right block exists as the $(X_n + iY_n)\otimes(X_n + iY_n)^*$ removed an excitation from both components and therefore has no effect on the S_{01},S_{10}, or S_{00} subspaces. We can see straight away that this is excitation decreasing as the components between the S_{11} and S_0 subspace are non-zero. Due to the block structure of Q_A, we can calculate the evolution of each of these subspaces separately. First, let's consider the S_{11} subspace.

If we take $W = \sum_j \langle jj|\rho_{11}\rangle$, from the above matrix (which is essentially the trace of the component in that subspace), we can see that

$$\frac{d|\rho_{11}\rangle}{dt} = (-2\Gamma_x \mathbb{1} + iH_1 \otimes \mathbb{1} - i\mathbb{1} \otimes H_1)|\rho_{11}\rangle. \tag{4.46}$$

Then

$$\frac{dW}{dt} = -2\Gamma_x W + i \sum_j \langle jj|(H_1 \otimes \mathbb{1} - \mathbb{1} \otimes H_1)|\rho_{11}\rangle. \tag{4.47}$$

The second term of this equation will be 0 as the two terms including H_1 will cancel one another out as $\mathrm{Tr}(H\rho_{11}) - \mathrm{Tr}(\rho_{11}H) = 0$ by the cyclic property of trace. We can then see that W evolves as $W(t) = W(0)e^{-2\Gamma_x t}$. Similarly, considering the ρ_{00} component, we can see from the matrix that

$$\frac{d|\rho_{00}\rangle}{dt} = -2\Gamma_x|00\rangle \sum_j \langle jj|\rho_{11}\rangle = -2\Gamma_x W|00\rangle. \tag{4.48}$$

We can solve this as a differential equation and we reach the result that if we let $|\rho_{00}\rangle = a(t)|00\rangle$ then

$$\frac{da}{dt} = -2\Gamma_x W = -2\Gamma_x W(0)e^{-2\Gamma_x t}. \tag{4.49}$$

We can then see that $a(t) = -W(0)e^{-2\Gamma_x t} + c$, and as $a(0) = \rho_{00}(0)$, then

$$a(t) = \rho_{00}(0) + W(0) - W(0)e^{-2\Gamma_x t}. \tag{4.50}$$

Finally we can see that our components evolve as

$$|\rho_{00}\rangle \to |\rho_{00}\rangle, \tag{4.51}$$

$$|\rho_{01}\rangle \to e^{-\Gamma_x 2t} e^{iH_1 t}|\rho_{01}\rangle, \tag{4.52}$$

$$|\rho_{10}\rangle \to e^{-\Gamma_x 2t} e^{-iH_1 t}|\rho_{10}\rangle, \tag{4.53}$$

$$|\rho_{11}\rangle \to e^{-2\Gamma_x t} e^{i(H_1 \otimes \mathbb{1} - \mathbb{1} \otimes H_1)t}|\rho_{11}\rangle + (1 - e^{-2\Gamma_x t})|\rho_{00}\rangle. \tag{4.54}$$

We can already see why this, unlike dephasing, is not excitation preserving by looking at the Γ_x entries in the 1^{st} row of Eq. (4.45). This Γ_x gives an indication of the scale of decay of the single excitation subspace to the zero excitation subspace. We can make predictions for this value, but realistically it would be experimentally determined. Completing this calculation gives the measure of decay to S_0 as $(1 - e^{-2\Gamma_x t})$. We have plotted this decay as the growth of the zero-excitation subspace for values of Γ_x from 0 to 1 against time for 5 units of time, Fig. 4.1.

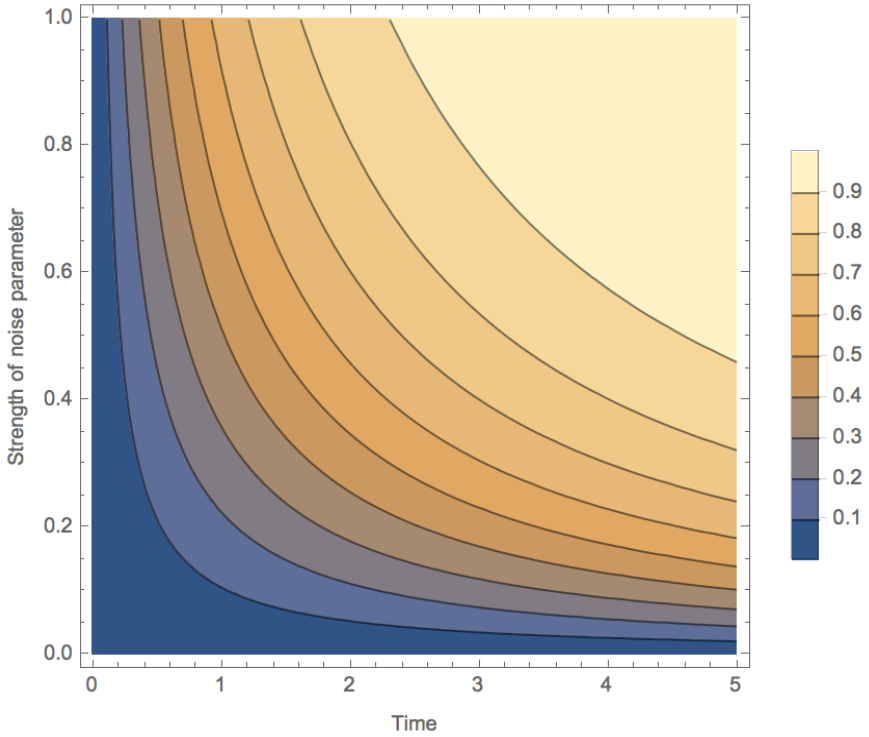

Figure 4.1: *State on the S_{00} subspace for amplitude damping noise parameter of Γ_x over time*

Most importantly, from the above calculations, the fidelity of excitation transfer at time t is given by $e^{-2\Gamma_x t} F_{ex}$ where F_{ex} is excitation transfer fidelity without noise. This then indicates that our only possibilities of improving transfer in the presence of noise is to make the transfer faster, or to improve F_{ex} with encoding.

4.5.4 Figure of Merit

Before we can consider how to improve these spin systems, we must define a measure of success. We have previously defined the average fidelity, so we can use this to give an

indicator of how well our noisy systems perform. We give our average fidelity calculation here in terms of $\mathcal{Q}$, which can subsequently be replaced with $\mathcal{Q}_D$ for dephasing noise or $\mathcal{Q}_A$ for amplitude damping noise. We can also apply both types of noise by using $\mathcal{Q}_D + \mathcal{Q}_A - \mathcal{H}$ where we take away $\mathcal{H}$ as it appears in both noise superoperators. We start with the initial state

$$|\psi\rangle = \alpha|\mathbf{0}\rangle + \beta|\mathbf{1}\rangle \tag{4.55}$$

then our initial density vector is given by

$$|\rho\rangle = |\psi, \psi^*\rangle = |\alpha|^2|\mathbf{00}\rangle + \alpha\beta^*|\mathbf{01}\rangle + \alpha^*\beta|\mathbf{10}\rangle + |\beta|^2|\mathbf{11}\rangle. \tag{4.56}$$

We demonstrated previously that the time evolution of the density operator is given by

$$|\rho'\rangle = e^{\mathcal{Q}t}|\rho\rangle. \tag{4.57}$$

After we have allowed the system to evolve for some time t, we take the partial trace over all sites other than the final site (where we aim to extract the state). We therefore remind ourselves of the operator $\mathcal{C}$ that takes the partial trace over sites 1 to $N-1$ such that

$$\mathcal{C}e^{\mathcal{Q}t}|\rho\rangle = \mathrm{Tr}_{1,2,\ldots,N-1}|\rho'\rangle \tag{4.58}$$

where $|\rho'\rangle$ is the density vector after evolution.

We define $\mathcal{Q}' = \mathcal{C}e^{\mathcal{Q}t}$ for simplicity. Then we take our fidelity as defined previously to get

$$F_{\alpha,\beta} = (|\alpha|^2\langle 00| + \alpha^*\beta\langle 01| + \alpha\beta^*\langle 10| + |\beta|^2\langle 11|)\mathcal{Q}'|\rho\rangle. \tag{4.59}$$

We then average over all input states to get the average fidelity of transfer, replacing $\alpha = \cos\frac{\theta}{2}$ and $\beta = e^{i\phi}\sin\frac{\theta}{2}$ and integrating over all points on the Bloch sphere

$$\overline{F} = \frac{1}{4\pi}\int_0^{2\pi}\int_0^{\pi} F(\theta,\phi)\sin\theta d\theta d\phi. \tag{4.60}$$

All components containing $e^{i\phi}$ or similar will vanish due to integration, so we are left

with

$$\overline{F} = \frac{1}{6}\left[\langle 00|\left(\mathcal{Q}'|\mathbf{11}\rangle + 2\mathcal{Q}'|\mathbf{00}\rangle\right) + \left(\langle 01|\mathcal{Q}'|\mathbf{01}\rangle + \langle 10|\mathcal{Q}'|\mathbf{10}\rangle\right) + \langle 11|\left(\mathcal{Q}'|\mathbf{00}\rangle + 2\mathcal{Q}'|\mathbf{11}\rangle\right)\right]. \tag{4.61}$$

Given that neither type of noise we are considering is excitation-increasing, we have that $\langle 00|\mathcal{Q}'|\mathbf{00}\rangle = 1$ and $\langle 11|\mathcal{Q}'|\mathbf{00}\rangle = 0$. This is evident as anything starting in the zero-excitation subspace must remain in the zero-excitation subspace and cannot increase excitation number. We can also identify that the trace of any state is 1, so $\langle 00|\mathcal{Q}'|\mathbf{11}\rangle + \langle 11|\mathcal{Q}'|\mathbf{11}\rangle = 1$. Again, we can explain this by noting that any state starting in the single-excitation subspace can only evolve to the single-excitation subspace or the zero-excitation subspace (where the latter is the decay of the state to the environment and only occurs for amplitude damping noise). This gives us a simplified version of the average fidelity

$$\overline{F} = \frac{1}{6}(3 + \langle 01|\mathcal{Q}'|\mathbf{01}\rangle + \langle 10|\mathcal{Q}'|\mathbf{10}\rangle + \langle 11|\mathcal{Q}'|\mathbf{11}\rangle). \tag{4.62}$$

The part $\langle 01|\mathcal{Q}'|\mathbf{01}\rangle + \langle 10|\mathcal{Q}'|\mathbf{10}\rangle$ appears to simplify to $2\mathrm{Re}(\langle 01|\mathcal{Q}'|\mathbf{01}\rangle)$ but as we can apply an arbitrary phase to the final state, we can apply this phase such that we get $|\langle 01|\mathcal{Q}'|\mathbf{01}\rangle|$. We are then able to use this average fidelity to see how well systems perform under different noise strength parameters. We have already indicated that we can analytically calculate the extent of the decay to the environment with the case of amplitude damping, but now we are able to provide numerical solutions.

4.5.5 Preliminary Results

Now that we have a way to measure success, we can see what this noise looks like. So far, our work is applicable to any system governed by a Hamiltonian that is excitation preserving, but we now select a specific Hamiltonian to demonstrate our methods. For now, we choose the Hamiltonian presented in [31], where the coupling strengths are given by $J_n = \frac{2\sqrt{n(N-n)}}{\sqrt{N^2-1}}$. We choose this system as without noise, it gives PST, so we can

clearly see the damage due to noise. Later we show how our technique can be applied to different Hamiltonians. Using the figure of merit as described above, we can plot an example of the decay over time due to noise for $N = 5$ and $N = 11$ and amplitude damping and dephasing strength parameters of $\Gamma_{x,z} = 0.1$. We choose $N = 5$ and $N = 11$ to show how the noise affects different chain lengths, but with small enough N to show multiple peaks. We also evolve the longer chain over a longer time to provide clearer results.

Amplitude Damping

We first plot the cases with no noise present, and compare that to the case where we have just amplitude damping noise present.

It is quite clear from our results in Fig. 4.2 that even a small chain of just 5 qubits suffers noticeably from amplitude damping, and that these effects worsen as the chain increases in length, since transfer time $\approx N$. We also note here that extracting the state on its first revival gives the best average fidelity and all subsequent revivals will show a decrease. Given how damaging amplitude damping noise can be to a system, due to the $-\Gamma_x t$ factor, it is important that we find a way to mitigate this damage.

Dephasing

We then use our figure of merit to demonstrate how dephasing noise effects our system. Where amplitude damping preserves the coherence of our system but we have reduced peaks due to energy leaking to the environment, dephasing does not leak energy to the system but instead we lose coherence. This means that the excitation spreads evenly over all sites and can no longer be located on a single site. We have plotted $N = 5$ and $N = 11$ for a dephasing noise parameter of $\Gamma_z = 0.1$ and a system including both types of noise, both with strength parameter $\Gamma_{x,z} = 0.1$ These results are shown in Fig. 4.3.

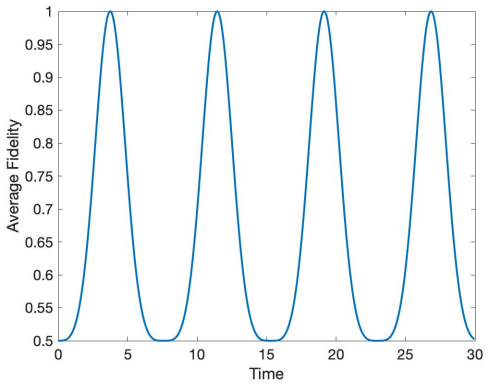

(a) $N = 5, \Gamma_{x,z} = 0$

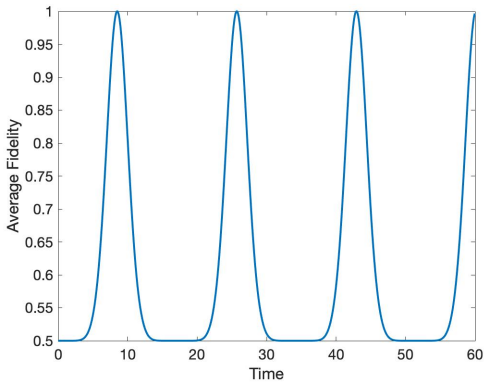

(b) $N = 11, \Gamma_{x,z} = 0$

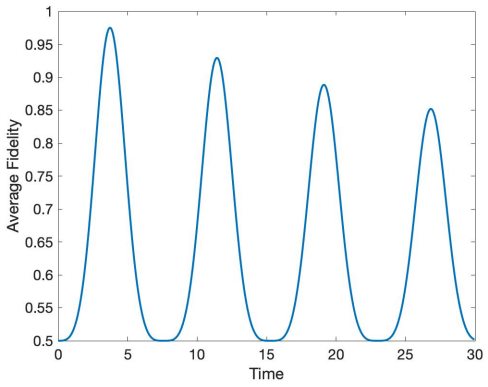

(c) $N = 5, \Gamma_x = 0.01$

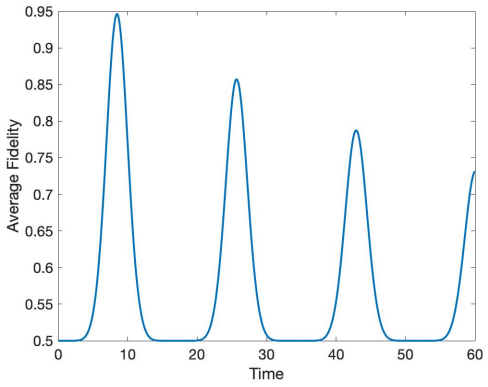

(d) $N = 11, \Gamma_x = 0.01$

Figure 4.2: *Results showing how amplitude damping noise effects chains of different lengths. We show chain lengths of* $N = 5$ *and* $N = 11$*, with no noise and an amplitude damping parameter of* $\Gamma_x = 0.01$

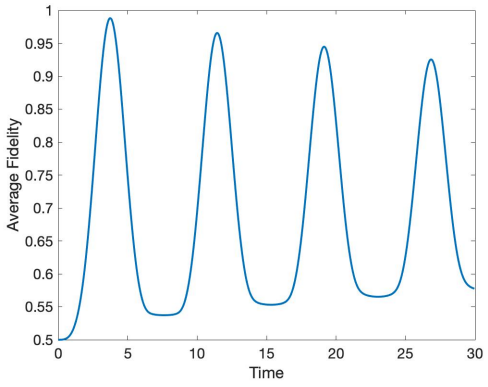

(a) $N = 5, \Gamma_z = 0.01$

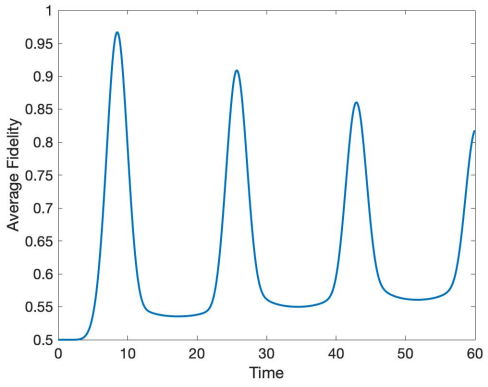

(b) $N = 11, \Gamma_z = 0.01$

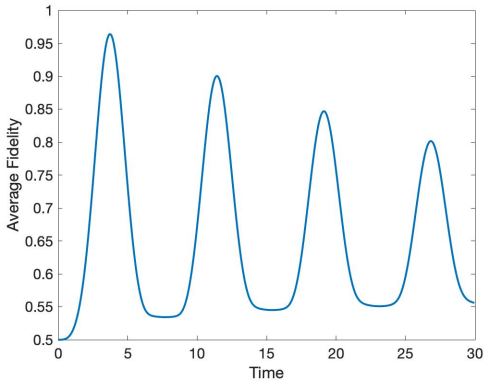

(c) $N = 5, \Gamma_x, \Gamma_z = 0.01$

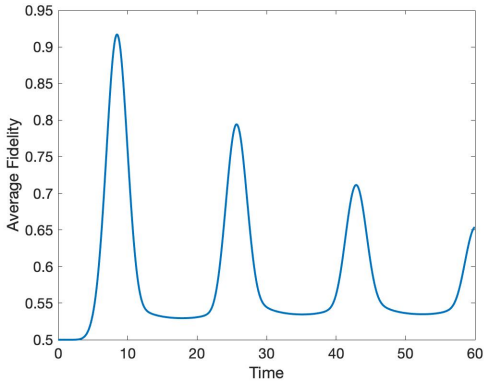

(d) $N = 11, \Gamma_x, \Gamma_z = 0.01$

Figure 4.3: *Results showing how dephasing noise effects chains of different lengths. We show chain lengths of* $N = 5$ *and* $N = 11$*, with dephasing noise and both amplitude damping and dephasing noise. Noise parameters of* $\Gamma_x, \Gamma_z = 0.01$

4.6 Encoding and Decoding

We have shown how noise affects transfer of states through quantum spin chains, and how the effects become worse over time and for longer chains. This is then an important problem to find a realistic solution for, as this interaction with the environment will always be present in physical spin systems. So far, with respect to noisy spin systems, we have only considered sending a state from one qubit to another qubit (at opposite ends of a 1D chain). However, we can consider encoding a state over a number of spins and decoding over a number of spins at the other end. This allows us to collect the excitation that may be spread out among a few qubits at the end of the chain and apply a unitary to 'move' the state onto the final qubit before extracting. Therefore, we are increasing the zone we can 'catch' the excitation from. Our work here builds on that of Haselgrove in [29] where we extend his scheme into noisy system. For now, we restrict ourselves to encoding within the single excitation subspace to see what improvement we can achieve. Later, in Chapter 5, we extend this to consider encoding across the 1- and 2-excitation subspaces.

4.6.1 Technique

Previously we have introduced our initial state as

$$|\psi\rangle = \alpha|\mathbf{0}\rangle + \beta|\mathbf{1}\rangle \tag{4.63}$$

where we have a superposition of the $|0\rangle$ state and the $|1\rangle$ state over the first qubit and all remaining qubits are in the $|0\rangle$ or relaxed state. Our scheme remains in the single excitation subspace, rather than encoding with multiple excitations as in error correction. We aim then to see what improvements can be made on a noisy systems with a much simpler to implement scheme. Instead of confining the excitation on the first qubit, we now spread it over a number of qubits such that we have

$$|\psi\rangle = \alpha|\mathbf{0}\rangle + \beta|\psi\rangle \tag{4.64}$$

where $|\psi\rangle = \sum_{n=1}^{M} \delta_n |\mathbf{n}\rangle$. M is the number of qubits we encode over and the optimal $|\psi\rangle$ is something to be determined. Also we have that $M < \frac{N}{2}$ such that we still have part of the chain that forms the bulk and is not included in either the encoding or decoding region. Generally, encoding over a larger number of qubits will give a higher average fidelity, as the arrival peak will be wider so we have the opportunity to extract at an earlier time, but will reduce the bulk length of the chain. Therefore we aim to find a balance between a large enough encoding zone to achieve high fidelity transfer and large enough bulk such that the transfer distance is meaningful. As we are dealing with noise, and therefore mixed states, we must use the density operator formalism to evolve our system over time. Referring to Section 4.4.1, we also continue to use the vectorised format of the density operator. Our density operator is then given by

$$|\rho\rangle = (\alpha|\mathbf{0}\rangle + \beta|\psi\rangle)(\alpha^*|\mathbf{0}\rangle + \beta^*|\psi^*\rangle). \tag{4.65}$$

We have already shown evolution through time is given by applying the superoperator $e^{\mathcal{Q}t}$ to the density vector, $|\rho\rangle$ where $\mathcal{Q}$ is the superoperator that describes noise and can be replaced with either $\mathcal{Q}_A$ or $\mathcal{Q}_D$. We define our density vector at a later time as

$$|\rho'\rangle = e^{\mathcal{Q}t}(\alpha|\mathbf{0}\rangle + \beta|\psi\rangle)(\alpha^*|\mathbf{0}\rangle + \beta^*|\psi^*\rangle). \tag{4.66}$$

As mentioned previously, the state we can extract deteriorates over time with noise, so we must choose the optimal time for extraction. This optimal time will depend on our choice of Hamiltonian, and we will consider this in more detail in Section 4.7.1. To calculate our fidelity, we need to compare the state on the final qubit to our desired state and then average over all input states. Therefore, we need to take only the state on the final qubit. We can achieve this by applying a unitary, U, to the decoding region to move any excitation to the final qubit and then trace off all remaining states. Then our fidelity is given by

$$F = (\alpha^*\langle 0| + \beta^*\langle 1^*|)(\alpha\langle 0| + \beta\langle 1|)\mathcal{C}(U \otimes U^T)|\rho'\rangle \tag{4.67}$$

where $\mathcal{C}$ is as previously defined, and traces over all sites but N. We previously demonstrated how to find the average fidelity of transfer by integrating over all possible input states, and we apply the same action here such that

$$\overline{F} = \int_0^{2\pi} \int_0^{\pi} F \sin\theta d\theta d\phi = \frac{1}{6}(3 + \langle 10|\mathcal{A}|\psi\mathbf{0}\rangle + \langle 01|\mathcal{A}|\mathbf{0}\psi^*\rangle + \langle 11|\mathcal{A}|\psi\psi^*\rangle), \quad (4.68)$$

where $\mathcal{A} = \mathcal{C}(U \otimes U^T e^{\mathfrak{Q}t}$. Our aim now is to choose the best encoding and unitary operator to maximise the average transfer fidelity. To maximise $\overline{F}$ we initially maximise the components $\langle 10|\mathcal{A}|\psi\mathbf{0}\rangle$ and $\langle 11|\mathcal{A}|\psi\psi^*\rangle$ separately. We are then able to combine our methods to achieve the near-optimal average fidelity.

Let us first consider how to maximise $\langle 11|\mathcal{A}|\psi\psi^*\rangle$ by choosing the optimal encoding $|\psi\rangle$ and unitary U. As above, we defined our initial encoding as $|\psi\rangle = \sum_{n=1}^{M} \delta_n |\mathbf{n}\rangle$, so we can write

$$e^{\mathfrak{Q}t}|\psi\psi^*\rangle = \gamma_{00}|\mathbf{00}\rangle + \sum_{n=1}^{N} \gamma_n |\mathbf{n0}\rangle + \sum_{m=1}^{N} \gamma_m |\mathbf{0m}\rangle + \sum_{n,m=1}^{N} \gamma_{nm} |\mathbf{nm}\rangle, \quad (4.69)$$

where the $\{\gamma_n\}$ are the time evolved constants, and we may have components belonging to the zero-excitation subspace as our noise is excitation decreasing. To utilise our decoding zone, we must apply a unitary to those sites to move the excitation to the final site. However, as we have completed the evolution and we are only interested in the decoding region, we can first trace off any spins that are not part of our decoding region. For simplicity, we introduce the notation Λ to represent the set of spins in the decoding region, and $\mathcal{C}_{\overline{\Lambda}}$ as the trace operator that traces off any states not belonging to the decoding region. Similarly we introduce $\mathcal{C}_{\Lambda_{\overline{N}}}$ to represent the trace operator over all sites in the decoding region apart from the final site N. We are then looking for

$$\mathcal{A}|\psi\psi^*\rangle = \mathcal{C}_{\Lambda_{\overline{N}}}(U \otimes U^T)\mathcal{C}_{\overline{\Lambda}}\left(\gamma_{00}|\mathbf{00}\rangle + \sum_{n=1}^{N} \gamma_n |\mathbf{n0}\rangle + \sum_{m=1}^{N} \gamma_m |\mathbf{0m}\rangle + \sum_{n,m=1}^{N} \gamma_{nm} |\mathbf{nm}\rangle\right). \quad (4.70)$$

We can see that we later take the overlap with the state $\langle 11|$ and notice that only the term $\sum_{n,m=1}^{N} \gamma_{nm}|\mathbf{nm}\rangle$ can overlap, so we can neglect any other terms. We can consider each

of the three operations separately, so we first trace off all sites that do not belong to the decoding region. Therefore Eq. (4.70) becomes

$$\mathcal{C}_{\overline{\Lambda}} e^{\mathcal{Q}_t} |\psi\psi^*\rangle \sim \sum_{n,m\in\Lambda} \gamma_{nm} |\mathbf{nm}\rangle, \tag{4.71}$$

where we have neglected terms that do not overlap with $\langle 11|$. We now consider the action of the unitary operator U on the decoding region. We can make some assumptions on what this unitary will look like, by noting that anything that belongs to the zero-excitation subspace must remain in that subspace after the action of the unitary, therefore we choose

$$U|\mathbf{0}\rangle = |\mathbf{0}\rangle. \tag{4.72}$$

Consequently, anything not within the decoding zone remains unchanged by the unitary operator so

$$U|\mathbf{n}\rangle = |\mathbf{n}\rangle, \forall n \in \bar{\Lambda}. \tag{4.73}$$

All other states certainly arise from an excitation being input, so should decode to $|1\rangle$ on the output qubit. Without any further loss in generality, we denote that application of the unitary operator will give

$$U|\mathbf{n}\rangle = |N, \boldsymbol{\phi}_n\rangle, \forall n \in \Lambda \tag{4.74}$$

where $|\boldsymbol{\phi}_n\rangle$ is a superposition of the all zero state $|\mathbf{0}\rangle$ over all sites other than N, and $\{|\mathbf{m}\rangle\}$ over sites $\Lambda_{\overline{N}}$. More information on the Unitary, along with an example, can be found in Appendix B. Therefore, we can see that the action of the unitary, U, on $\mathcal{C}_{\overline{\Lambda}} e^{\mathcal{Q}_t} |\psi\psi^*\rangle$ is given by

$$(U \otimes U^T)\mathcal{C}_{\overline{\Lambda}} e^{\mathcal{Q}_t} \sim \sum \gamma_{nm} |N, \boldsymbol{\phi}_n\rangle |N, \boldsymbol{\phi}_m^*\rangle. \tag{4.75}$$

Now we have used out unitary to ‘move’ the excitation from the decoding region to the final site, we can take the partial trace over the remaining sites to leave us with only the

state on the final site. We can show that $|\boldsymbol{\phi}_m^*\rangle$ and $|\boldsymbol{\phi}_n\rangle$ are orthogonal states by noting that $\langle \boldsymbol{m}|\boldsymbol{n}\rangle = \langle \boldsymbol{m}|U^\dagger U|\boldsymbol{n}\rangle = \langle N, \boldsymbol{\phi}_m|N, \boldsymbol{\phi}_n\rangle$, we can see that $\langle \boldsymbol{\phi}_m|\boldsymbol{\phi}_n\rangle = \delta_{nm}$, which then gives us

$$\boldsymbol{\mathcal{A}}|\psi\psi^*\rangle \sim \sum |1,1\rangle\gamma_{nm}\langle \boldsymbol{\phi}_m|\boldsymbol{\phi}_n\rangle = \left(\sum \gamma_{nn}\right)|1,1\rangle. \tag{4.76}$$

Taking the overlap then with the state we want to extract, gives us

$$\langle 1,1|\boldsymbol{\mathcal{A}}|\psi\psi^*\rangle = \sum_{n\in\Lambda} \gamma_{nn}. \tag{4.77}$$

This allows us to see that our choice of U is irrelevant (beyond our earlier assumptions), for the $\langle 11|\boldsymbol{\mathcal{A}}|\psi\psi^*\rangle$ component. All that's left for us to do now, is to work out how to choose the input state to maximise $\sum \gamma_{nn}$. If we label our output sites (the decoding region) as k, then we can sum over such output states as

$$R_{ij} = \sum_{k\in\Lambda} \langle k,k|e^{\mathcal{Q}t}|i,j\rangle. \tag{4.78}$$

We then have

$$R = \sum_{i,j=1}^{M} R_{ij}|j\rangle\langle i|, \tag{4.79}$$

such that $\sum \gamma_{nn} = \langle\psi|R|\psi\rangle$, and are able to maximise $\sum \gamma_{nn}$ by selecting the eigenvector of R with the maximum eigenvalue.

We then need to maximise our other component. It is sufficient to maximise only $\langle 10|\boldsymbol{\mathcal{A}}|\psi\mathbf{0}\rangle$ as this can always be made real by application of an arbitrary phase incorporated into the unitary, so $\langle 10|\boldsymbol{\mathcal{A}}|\psi\mathbf{0}\rangle = \langle 01|\boldsymbol{\mathcal{A}}|\mathbf{0}\psi^*\rangle$.

Following the same method as before, after evolution we have the state

$$e^{\mathcal{Q}t}|\psi\mathbf{0}\rangle = \gamma_{00}|\mathbf{00}\rangle + \sum_{n=1}^{N} \gamma_n|\mathbf{n0}\rangle. \tag{4.80}$$

We then take the partial trace such that we remove the states on any sites other than

those belonging to the decoding region.

$$\mathcal{C}_{\overline{\Lambda}} e^{\mathcal{Q}_t} |\psi \mathbf{0}\rangle = \gamma_{00} |\mathbf{00}\rangle + \sum_{n \in \Lambda} \gamma_n |\mathbf{n0}\rangle. \tag{4.81}$$

We once again apply the unitary operator to our system

$$(U \otimes U^T) \mathcal{C}_{\overline{\Lambda}} e^{\mathcal{Q}_t} |\psi \mathbf{0}\rangle \sim \sum_{n \in \Lambda} \gamma_n |N, \boldsymbol{\phi}_n\rangle |\mathbf{0}\rangle, \tag{4.82}$$

where we have again neglected any terms that will not overlap with $\langle 10|$. We trace off all remaining states in the decoding region, leaving only the state on the final site.

$$\mathcal{A} |\psi \mathbf{0}\rangle \sim \sum_{n \in \Lambda}^{N} \gamma_n |10\rangle \langle \mathbf{0}_{\Lambda_{\overline{N}}} | \boldsymbol{\phi}_n \rangle \tag{4.83}$$

where $\langle \mathbf{0}_{\Lambda_{\overline{N}}}|$ indices that this is the zero components over all sites in the decoding region excluding site N. We then take the overlap with our desired state

$$\langle 10 | \mathcal{A} | \psi \mathbf{0} \rangle = \sum_{n \in \Lambda} \gamma_n \langle \mathbf{0}_{\Lambda_{\overline{N}}} | \boldsymbol{\phi}_n \rangle. \tag{4.84}$$

We see now that if we want to maximise this quantity, we are actually maximising $\langle \mathbf{0} | U_{\Lambda_{\overline{N}}} \sum_{n \in \Lambda_{\overline{N}}} \gamma_n |\mathbf{n}\rangle$ over U because once we have 'moved' any excitation from the encoding region to the final site we expect to maximise the overlap of the decoding region with $\langle \mathbf{0}|$. We are therefore looking for $(\langle \mathbf{0}|U)^\dagger$ parallel to $\sum \gamma_n |\mathbf{n}\rangle$ so

$$\langle \mathbf{0} | \boldsymbol{\phi}_n \rangle = \frac{\gamma_n^*}{\sqrt{\sum_{m \in \Lambda} |\gamma_m|^2}} \tag{4.85}$$

and finally we can say that

$$\langle 10 | \mathcal{A} | \psi \mathbf{0} \rangle = \sqrt{\sum_{m \in \Lambda} |\gamma_m|^2} = \langle 01 | \mathcal{A} | \mathbf{0} \psi^* \rangle. \tag{4.86}$$

We can now maximise our input state $|\psi\rangle$ by saying that

$$S = |(P_{out} \otimes \langle 0|)e^{\mathcal{Q}t}(|\psi\rangle \otimes |\mathbf{0}\rangle)|. \tag{4.87}$$

Therefore our encoding $|\psi\rangle$ will be the largest right singular vector of

$$(P_{out} \otimes \langle 0|)e^{\mathcal{Q}t}(P_{in} \otimes |0\rangle) \tag{4.88}$$

where P_{in} and P_{out} are projectors projecting onto the encoding region and decoding region respectively.

4.6.2 Comparison to Haselgrove

If we consider a system with no noise such that $\mathcal{Q} = -iH \otimes \mathbb{1} + i\mathbb{1} \otimes H$ then we can rewrite Eq. (4.88) as $S = (P_{out}e^{-iHt}P_{in}) \otimes (\langle 0|e^{iHt}|0\rangle)$. We can see that the second component will always be equal to 1 as the zero component will always evolve to itself under an excitation preserving Hamiltonian. Looking at Eqs. (4.51), for amplitude damping noise, we can see that when we are considering a noisy system, all we need to do it take $|\rho'_{10}\rangle \to e^{-\frac{\Gamma_x^2}{2}t}e^{-iH_1t}|\rho_{10}\rangle$. Therefore in our formalism we simply have $|\rho'_{10}\rangle \to e^{-\frac{\Gamma_x^2}{2}t}(P_{out}e^{-iHt}P_{in}) \otimes \langle 0|e^{iHt}|0\rangle$. If we look at the R component, we have

$$R = \sum_{i,j}\sum_{n} |j\rangle\langle i|\langle n|e^{-iHt}|i\rangle\langle n|e^{iH^*t}|j\rangle, \tag{4.89}$$

where H is hermitian, so $\langle n|e^{iH^*t}|j\rangle = \langle j|e^{iHt}|n\rangle$. Then R can be rewritten as

$$\sum_{i,j}\sum_{n} |j\rangle\langle j|e^{iHt}|n\rangle\langle n|e^{-iHt}|i\rangle\langle i| = P_{in}e^{iHt}P_{out}e^{-iHt}P_{in} = S^\dagger S. \tag{4.90}$$

We then see that our result coincides with the result Haselgrove obtained when there is no noise in our system. We also note that in a system without noise, if we start with a pure state, our system will only evolve to pure states and so the components of R that represent mixed states will be 0. When we consider a system with amplitude damping

noise, this just becomes $e^{-\Gamma_x t}\mathbb{1}$. Therefore we can see that our result at a fixed time is the same as that which Haselgrove obtained, with an additional factor of $e^{-\frac{\Gamma_x}{2}t}$ to account for the noise, and we note that in the noiseless case, our encoding is entirely dependent on the S_{01} subspace.

4.6.3 Optimising Over Components

In the previous section, we have described how to find the optimal encoding to maximise each element of the average fidelity of transfer. Although in some cases (such as amplitude damping noise), these results will coincide, they generally will not - such as in the case of dephasing noise. We now consider how we can combine these encodings such that we maximise the average fidelity. We remember that for the component $\langle 11|\boldsymbol{\mathcal{A}}|\psi\psi^*\rangle$ our optimal encoding is given by the maximum eigenvector of $R = \sum R_{i,j}|i\rangle\langle j|$ and our optimal encoding for the $\langle 10|\boldsymbol{\mathcal{A}}|\psi\mathbf{0}\rangle$ component is given by the maximum right singular vector of $S = (P_{out}\otimes\langle 0|)e^{\boldsymbol{\mathcal{Q}}t}(P_{in}\otimes|0\rangle)$. Instead of finding the maximum right singular vector of S, we can find the maximum eigenvector of $S^\dagger S$. Combining the two terms, we want to maximise

$$\overline{F} = \frac{1}{2} + \frac{1}{3}\sqrt{\langle\psi|S^\dagger S|\psi\rangle} + \frac{1}{6}\langle\psi|R|\psi\rangle \tag{4.91}$$

over all $|\psi\rangle$, which, assuming that $|\boldsymbol{\psi}\rangle$ is close to an eigenvector of $S^\dagger S$, can be written as

$$\overline{F} \approx \frac{1}{2} + \frac{1}{6}\langle\psi|(2\sqrt{S^\dagger S} + R)|\psi\rangle \tag{4.92}$$

which is just the maximum eigenvector of

$$2\sqrt{S^\dagger S} + R. \tag{4.93}$$

Then we can either evaluate Eq. (4.91) or approximate our average fidelity from Eq. (4.92), which after finding the maximum eigenvalue of Eq. (4.93), which we call X,

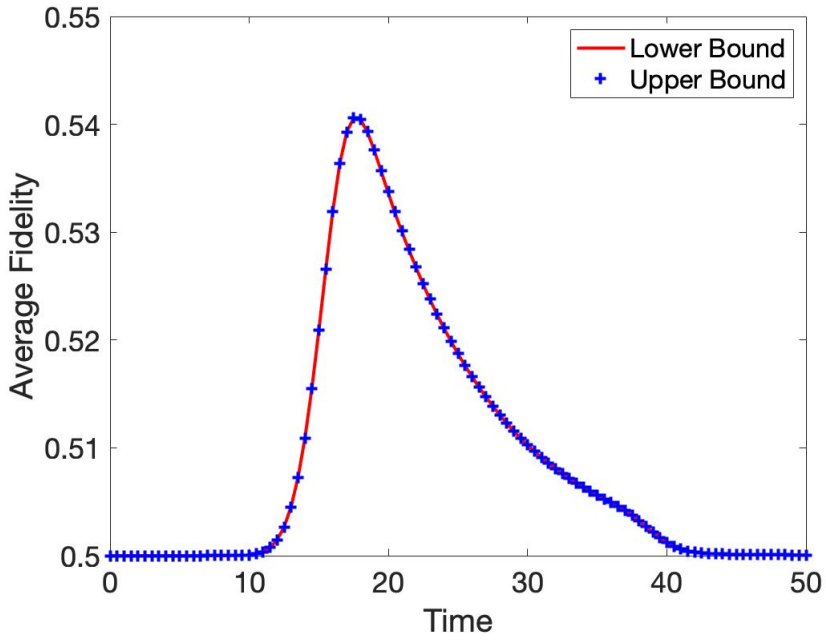

Figure 4.4: *Demonstration of the upper and lower bounds on fidelity of encoded state. Noise parameters are* $\Gamma_{x,z} = 0.3$

becomes

$$\overline{F} \approx \frac{1}{2} + \frac{X}{6}. \tag{4.94}$$

This gives us a lower bound on the best transfer fidelity we can achieve. We will maximise $S^\dagger S$ and R separately to obtain an upper bound and compare the results. We present the results of the upper and lower bounds in Fig. 4.4 for a chain of $N = 35$ and both noise parameters $\Gamma_{x,z} = 0.3$, where we can see that the upper and lower bound essentially coincide. Our approximation that $|\psi\rangle$ is close to an eigenvector of $S^\dagger S$ is a good one, even at the excessive noise levels, and any weaker noise can be expected to give a better approximation.

4.7 Demonstrations

The techniques presented in this chapter are applicable to any excitation preserving Hamiltonian and excitation non-increasing noise. We select three such Hamiltonians to demonstrate the application of our technique. The specific Hamiltonians we select are the Uniform Hamiltonian, Linear PST Hamiltonian, and Apollaro Hamiltonian. These

systems are described in more detail in Section 2.5. We choose these as the Linear PST chain provides perfect transfer in a reasonable time, the Uniform chain provides fast transfer (at the expense of high quality transfer), and the Apollaro chain is a compromise between these two qualities. One might assume that it is best to start with a system that can already allow perfect state transfer, but we can see from Eqs. (4.51-4.54) that a faster arrival time will be less affected by noise. We first give the extraction time windows we have chosen and demonstrate that these times are reasonable. We then show the improvement in average fidelity for a system with encoding, for the three systems we have selected.

4.7.1 Extraction Time

Given that we are hoping for these systems to be experimentally realisable, it is useful to consider what the best extraction time would be. We therefore need to look at each of our systems and evolve them through time with our noise parameters to find out when we are likely to achieve the best fidelity. We note that the encoded systems show a broader peak, which allows us to extract earlier, and therefore reduce the effects of noise. However, we need to be able to extract at the start of this peak or we lose a lot of this potential benefit. We choose to evolve through a particular time window to find a good extraction time, noting that this is a slightly easier task than with our fabrication errors, as we no longer have to deal with randomness. We can therefore choose a time window that surrounds the best arrival time for different strengths of noise. We demonstrate that these time windows are appropriate in the following sections.

Uniform

The Uniform chain is the fastest of the three and, from Eq. (2.54) gives an extraction time of $t_{Uni} \approx 18.8$ for $N = 35$. We evolve the system through time with different noise parameters and choose a time window of $10 \leq t_{Uni} \leq 25$. We can see from Fig. 4.5 that this is appropriate even for high levels of noise, where the optimal extraction time is earlier that in the case with no noise.

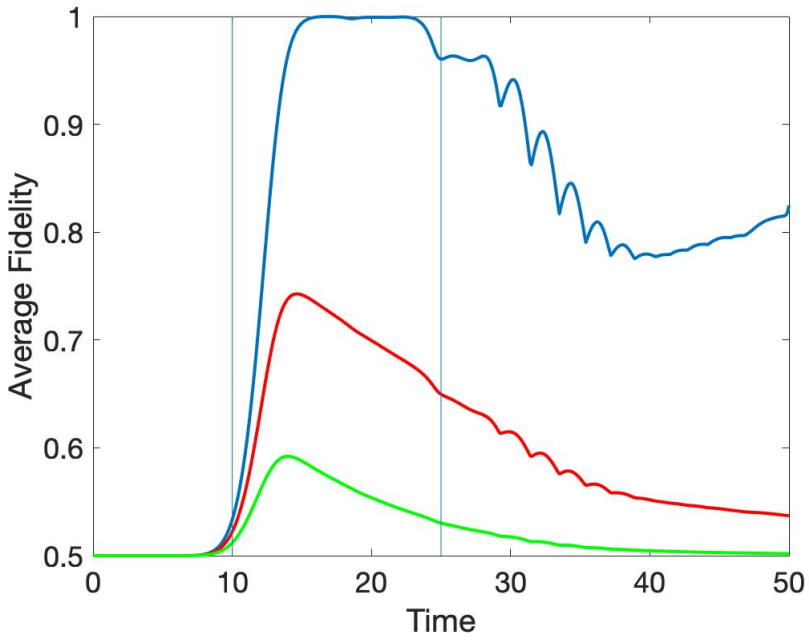

Figure 4.5: *Uniform chain demonstrating that the time window (vertical blue lines) we have chosen is reasonable. Noise free case is given in blue,* $\Gamma_{x,z} = 0.02$ *in red, and* $\Gamma_{x,z} = 0.05$ *in green. Encoding region of* $M = 7$

Linear PST

Next we consider the linear PST chain, where we know that the optimal transfer time in the absence of noise is given by $t_{PST} = \frac{\pi}{4}\sqrt{N^2 - 1}$, and for $N = 35$ this gives an extraction time of $t_{Lin} \approx 27.5$. We choose to evolve over a time window $10 \leq t_{Lin} \leq 25$, as we know we need to extract at the start of the broad encoding peak. From Figs. 4.6 we can see that this time window is reasonable, and that the addition of noise moves the extraction time slightly earlier.

Apollaro

The Apollaro chain is a modified version of the Uniform chain, where the two extremal couplings at each end are given specific values to allow near perfect transfer for arbitrary N in the absence of noise. The best extraction time for a chain of $N = 35$ without encoding or noise is $t_{App} \approx 22$. We choose the extraction window for the encoded case to be the same as the previous case where we have $10 \leq t \leq 25$, and demonstrate in Fig. 4.7 that this is reasonable.

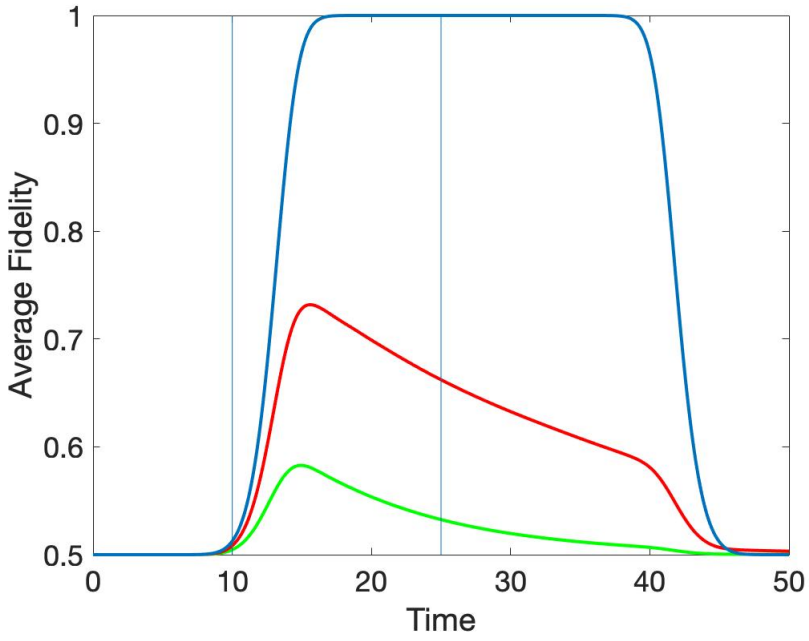

Figure 4.6: *Linear chain demonstrating that the time window we have chosen is reasonable. Noise free case is given in blue,* $\Gamma_{x,z} = 0.02$ *in red, and* $\Gamma_{x,z} = 0.05$ *in green. Encoding region of* $M = 7$

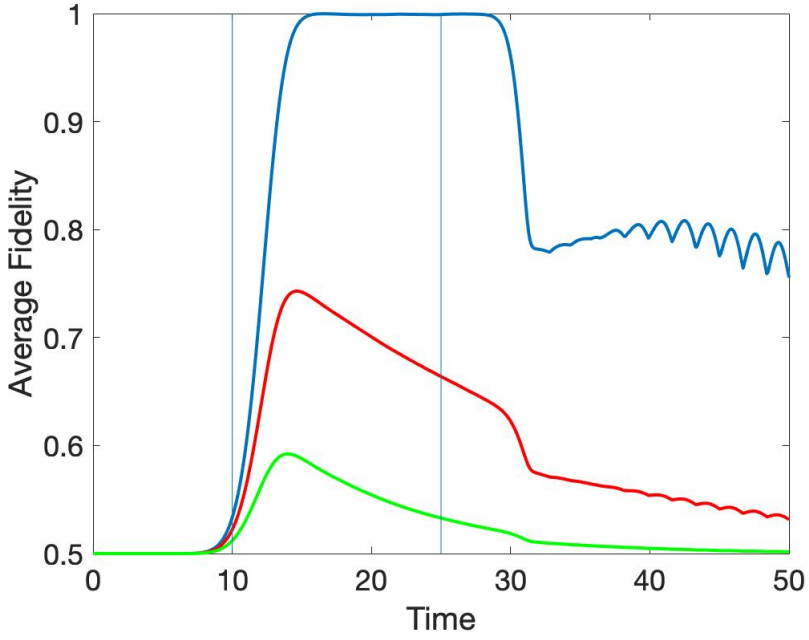

Figure 4.7: *Apollaro chain demonstrating that the time window we have chosen is reasonable. Noise free case is given in blue,* $\Gamma_{x,z} = 0.02$ *in red, and* $\Gamma_{x,z} = 0.05$ *in green.Encoding region of* $M = 7$

Now we have demonstrated that the time windows we have chosen are reasonable, we can apply our different noise parameters to the system with various values to get a clearer picture of how noise affects our systems and how much improvement we can see from introducing encoding and decoding regions.

4.7.2 Encoding

Using the methods we have developed in the previous section, we can work out the optimal encoding for a system. We present here a chain of $N = 35$ with noise parameters of Γ_x, Γ_z taking values from 0 to 0.05 for both parameters, with intervals of 0.005. We chose $N = 35$, as it is longer than most experimentally realisable systems, but can still be simulated in a reasonable time. We present our technique applied to different Hamiltonians. The images in the left column show the systems without encoding in the order: Uniform, Linear PST, Apollaro. The right column shows the encoded counterparts in the same order. It is expected that these plots would show straight lines as the effect of amplitude damping is to add an $e^{-\Gamma_x}$ term and the dominant term in dephasing noise is an $e^{-\Gamma_z}$ term. Overall we have $e^{-(\Gamma_x+\Gamma_z)t} \approx F$, so constant noise values will give constant F. We note that without encoding, the chain to perform the worse is the Uniform system. This is expected as it does not perform well in a reasonable time for longer systems without noise. The Linear PST and Apollaro both perform relatively well - the Apollaro slightly better than the Linear PST. When we apply our encoding, we can see that the Apollaro and Uniform chains perform equally well, and slightly better than the PST chain. This result is very positive, as it demonstrates that simpler-to-build systems actually show great improvement in the presence of noise when encoding is applied.

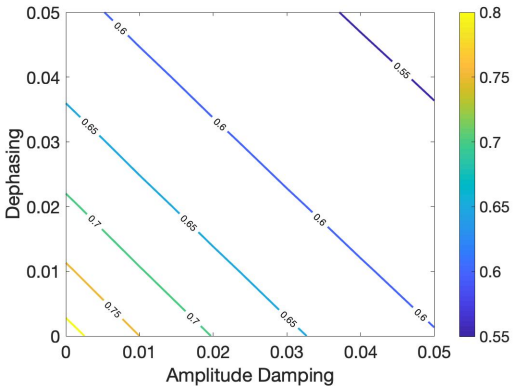

(a) No encoding, Uniform

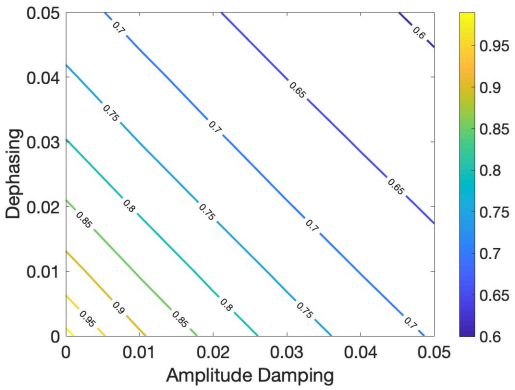

(b) Encoding over 7 sites, Uniform

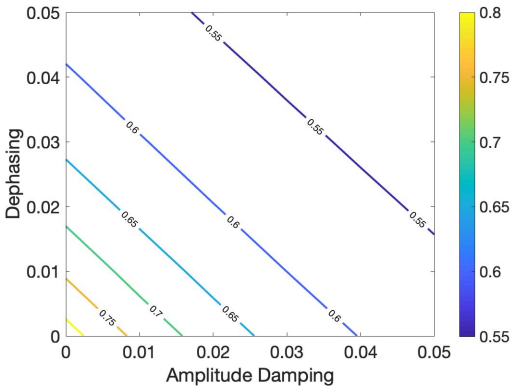

(c) No encoding, linear PST

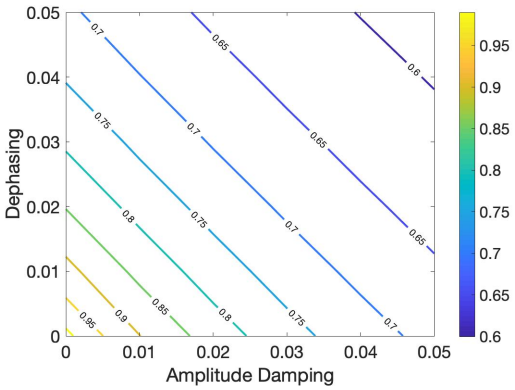

(d) Encoding over 7 sites, linear PST

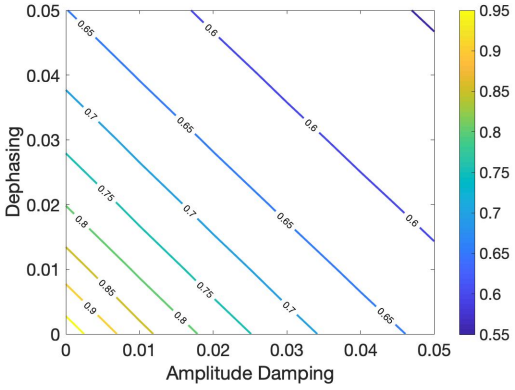

(e) No encoding, Apollaro

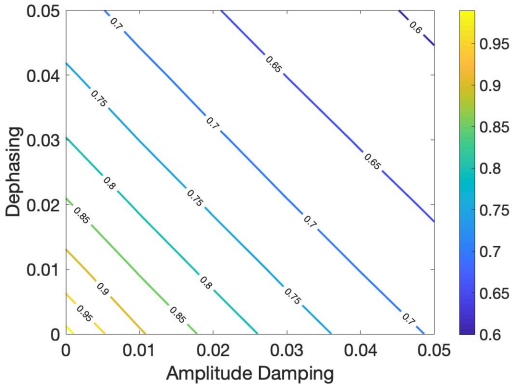

(f) Encoding over 7 sites, Apollaro

Figure 4.8: *Results from encoding over 7 sites for the linear PST, Apollaro, and Uniform Hamiltonians, of length* $N = 35$. *Maximum values of* $\Gamma_{x,z} = 0.05$

.

4.8 Conclusion and Further Work

We have introduced a technique for reducing the effects of noise in quantum spin systems that is simpler to implement than full error correction. Our results show a significant improvement on the fidelity achievable, particularly in simpler chains, such as the Uniform chain and the Apollaro chain presented in [40]. Our technique is scalable and can be applied to any Hamiltonian that is excitation non-increasing. Further improvements could be made by finding a more accurate extraction time. We can further optimise the chains for the specific scenario of encoding - the x and y values in the Apollaro chain are optimised for end to end transfer and we could consider optimising these values for encoded transfer. We have also only encoded in the single excitation subspace. In the next chapter, we will extend this to consider higher subspaces.

Chapter 5

Higher Excitation Subspaces

5.1 Introduction

Quantum computation is on the horizon and promises to revolutionise many aspects of human life. However, one of the biggest challenges we currently face before quantum computation can be fully realised, is the problem of noise. We have already seen in Chapter 4 that both amplitude damping noise and dephasing noise lead to a significant reduction in fidelity. We have introduced an encoding technique that aims to reduce the effects of this noise and demonstrated that significant improvements can be made to the fidelity. Now we want to see whether we can further improve this scheme. In Section 4.5.3, we saw that amplitude damping noise is excitation decreasing, so one might question why we should not attempt to transfer more than one excitation? For example, the probability of receiving at least one excitation is higher when the input state includes three excitations that when it only includes one. Nevertheless, it is not clear that encoding with multiple excitations will perform better than encoding with just one, as arrival probabilities decrease for multiple excitations in the absence of noise [29]. Previously we restricted ourselves to the single and zero-excitation subspaces, to introduce a technique that was easy to implement, but now we start to consider higher excitation subspaces to see what further improvements we can make. In the following sections, we extend our scheme to include the second excitation subspace - but we note that we can also extend to higher excitation subspaces.

5.2 Technique

We now extend the noisy encoding technique introduced in Section 4.6 such that we can encode across higher excitation subspaces. We introduce K as the excitation number, where we can encode over subspaces up to and including the K^{th} excitation subspace. We begin with the same equation for the average fidelity of state transfer, restating it here for clarity

$$\overline{F} = \frac{1}{2} + \frac{1}{3}|\langle 10|\mathcal{A}|\psi\mathbf{0}\rangle| + \frac{1}{6}\langle 11|\mathcal{A}|\psi\psi^*\rangle, \tag{5.1}$$

where we remember that $\mathcal{A} = \mathcal{C}_{\Lambda_{\overline{N}}}(U \otimes U^T)\mathcal{C}_{\overline{\Lambda}} e^{\mathcal{Q}t}$ and we maximise the two components, 10 and 11, separately. As we are now moving into higher excitation subspaces, we need to define our initial state to include such subspaces. We therefore use

$$|\psi\rangle = \sum_{x \in V_M \setminus 00...0} \gamma_{x\mathbf{0}} |x\rangle, \tag{5.2}$$

where $V_M = \{0,1\}^M$ (a binary string of length M, and weight $\leq K$, and we have M as the size of the encoding region - and assume that the decoding region is the same size. $V_M \setminus 00...0$ indicates that we do not include the all zero state.). An example of this is the binary string 01100, which gives an encoding region of 5, with excitations present at sites 2 and 3. The subscript $\mathbf{0}$ of γ refers to the sites not included in the encoding region. We also note that our $\mathcal{Q}$ now includes the subspaces belonging to all excitation subspaces from the zero excitation subspace up to the K^{th}. Let us first consider how to maximise the component $\langle 11|\mathcal{A}|\psi\psi^*\rangle$, where we apply each of these operations in turn, beginning with the time evolution of the initial state

$$e^{\mathcal{Q}t}|\psi\psi^*\rangle = \sum_{x,y \in V_N} \eta_{x,y} |x, y\rangle, \tag{5.3}$$

where now $V_N = \{0,1\}^N$ and the excitations can be spread over all sites. The next operator we apply is $\mathcal{C}_{\overline{\Lambda}}$, which traces off all states not belonging to the encoding region, so that we are left with

$$\mathcal{C}_{\overline{\Lambda}} \sum_{x,y \in V_N} \eta_{x,y} |x, y\rangle = \sum_{\substack{k,l \in V_{|\Lambda|} \\ z \in V_{N-|\Lambda|}}} \eta_{kz,lz} |k, l\rangle, \tag{5.4}$$

where Λ is the set of sites belonging to the decoding region, and we are careful to note that k and l only cover Λ. Next, we take a brief detour to consider what our unitary operator should look like. We first use the constraint that when applying the unitary to

the all zero state within the decoding region, we want to return the all zero state so that

$$U|\mathbf{0}\rangle_\Lambda = |\mathbf{0}\rangle_\Lambda. \tag{5.5}$$

If there is an excitation within the decoding region, then we want this to be moved to site N, and leave a set of orthogonal states on the remaining sites within the decoding zone

$$U|\boldsymbol{k}\rangle = |N, \boldsymbol{\phi}_k\rangle, \forall k \in V_\Lambda \setminus 00...0, \tag{5.6}$$

where we note that we are assuming that $|\boldsymbol{k}\rangle \neq |\mathbf{0}\rangle$. As we have orthogonal states over $\Lambda \setminus N$ we know that $\langle \boldsymbol{\phi_k} | \boldsymbol{\phi_l} \rangle = \delta_{kl}$. To allow these orthogonal states, we have to introduce some constraints to the size of the encoding region and excitation number. The dimensions of the space that we require these states to be orthogonal over is $2^{|\Lambda|-1}$ as we are working in the decoding zone, but excluding the final site. Therefore, we need the dimensions of our Hilbert space to be less than or equal to this value. If we are working in the K^{th} excitation subspace, then we can encode over excitation number up to and including K, so that the size of our Hilbert space is $\sum_{i=1}^{K} \binom{M}{i}$.

Then we have enough space as long as we impose the constraint that

$$K < \frac{M}{2}, \tag{5.7}$$

since $\sum_{i=1}^{k} \binom{M}{i} = 2^k - 1$, and assuming that our encoding and decoding regions are the same size. Now we apply the unitary, which must follow the constraints above but can otherwise be arbitrary, to get

$$U \otimes U^T \sum_{\substack{k,l \in V_{|\Lambda|} \\ z \in V_{N-|\Lambda|}}} \eta_{kz,lz} |\boldsymbol{k}, \boldsymbol{l}\rangle \sim \sum_{\substack{k,l \in V_{|\Lambda|} \\ z \in V_{N-|\Lambda|}}} \eta_{kz,lz} |N, \boldsymbol{\phi_k}\rangle |N, \boldsymbol{\phi_l}\rangle, \tag{5.8}$$

where we have neglected any terms that will vanish when we take the overlap with $\langle 11|$. Now we have used the unitary to 'move' any excitation within Λ to the final site, we can

trace off all other sites

$$\mathcal{C}_{\Lambda_{\overline{N}}} \sum_{\substack{k,l\in V_{|\Lambda|} \\ z\in V_{N-|\Lambda|}}} \eta_{kz,lz}|N,\boldsymbol{\phi_k}\rangle|N,\boldsymbol{\phi_l}\rangle = \sum_{\substack{k\in V_{|\Lambda|} \\ z\in V_{N-|\Lambda|}}} \eta_{kz,kz}|11\rangle, \tag{5.9}$$

where we see that again our choice of U is arbitrary as long as we stick to the earlier constraints. Now all that remains is to take the overlap, giving

$$\langle 11|\mathcal{A}|\boldsymbol{\psi}\boldsymbol{\psi}^*\rangle = \sum_{\substack{k\in V_{|\Lambda|} \\ z\in V_{N-|\Lambda|}}} \eta_{kz,kz}, \tag{5.10}$$

so that it is clear that to maximise this components, we need to maximise $\sum_{\substack{k\in V_{|\Lambda|} \\ z\in V_{N-|\Lambda|}}} \eta_{kz,kz}$. To maximise this we use the same method as the case in the single excitation subspace where we have

$$\sum_{\substack{k\in V_{|\Lambda|} \\ z\in V_{N-|\Lambda|}}} \eta_{kz,kz} = \sum_{\substack{k\in V_{|\Lambda|} \\ z\in V_{N-|\Lambda|}}} \langle \boldsymbol{kz},\boldsymbol{kz}|e^{\mathcal{Q}t}|\boldsymbol{\psi}\boldsymbol{\psi}^*\rangle, \tag{5.11}$$

where the $\boldsymbol{k}$ are the output binary strings, and introduce

$$R = \sum_{x,y\in V_M} \sum_{\substack{k\in V_{|\Lambda|} \\ z\in V_{N-|\Lambda|}}} |\boldsymbol{y}\rangle\langle\boldsymbol{x}|\langle \boldsymbol{kz},\boldsymbol{kz}|e^{\mathcal{Q}t}|\boldsymbol{x0},\boldsymbol{y0}\rangle. \tag{5.12}$$

Then

$$\sum \eta_{kz,kz} = \langle\boldsymbol{\psi}|R|\boldsymbol{\psi}\rangle \tag{5.13}$$

and this is maximised by choosing the eigenvector with the largest eigenvalue for $|\boldsymbol{\psi}\rangle$.

We now consider how we can maximise the $\langle 10|\mathcal{A}|\boldsymbol{\psi 0}\rangle$ component, which is done in the same way as the previous component, by applying each of the operators in turn. We start with the time evolution operator such that

$$e^{\mathcal{Q}t}|\boldsymbol{\psi 0}\rangle = \sum_{x\in V_N} \eta_x|\boldsymbol{x0}\rangle, \tag{5.14}$$

where again we have the excitation spread over all sites in this subspace. We now apply

the first trace operator and the unitary operator, giving

$$U \otimes U^T \mathcal{C}_{\overline{\Lambda}} \sum_{x \in V_N} \eta_x |\boldsymbol{x}\mathbf{0}\rangle \sim \sum_{k \in V_{|\Lambda|}} \eta_{k0} |N, \boldsymbol{\phi}_k\rangle |\mathbf{00}\rangle, \tag{5.15}$$

where, again, we have neglected any terms that will disappear when we take the overlap with the $\langle 10|$ state. We now trace off the states on all remaining sites so that

$$\mathcal{C}_{\overline{N}} \sum \eta_{k0} |N, \boldsymbol{\phi}_k\rangle |\mathbf{00}\rangle = \sum \eta_{k0} |10\rangle \langle \mathbf{0}|\boldsymbol{\phi_k}\rangle. \tag{5.16}$$

Finally we take the overlap with this to get

$$\langle 10| \sum \eta_{k0} |10\rangle \langle \mathbf{0}|\boldsymbol{\phi_k}\rangle = \sum \eta_{k0} \langle \mathbf{0}|\boldsymbol{\phi}_k\rangle, \tag{5.17}$$

which is exactly what we need to maximise. To maximise this, we then have

$$\langle \mathbf{0}|\boldsymbol{\phi}_k\rangle = \frac{\eta^*_{k0,00}}{\sqrt{\sum_{l \in V_M} |\eta_{l0,00}|^2}}, \tag{5.18}$$

where

$$\eta_{k,l} = \langle k, l | e^{\mathcal{Q}t} | \boldsymbol{\psi}\mathbf{0}\rangle \tag{5.19}$$

and we are maximising

$$\sqrt{\sum |\eta_{k0}|^2}. \tag{5.20}$$

This is completed by setting

$$S = \sum_{k \in V_{|\Lambda|}} |k\rangle\langle k0,00| e^{\mathcal{Q}t} \sum_{x \in V_{|\Lambda|}} |x0,00\rangle\langle x| = (P_{out} \otimes \langle 0|) e^{\mathcal{Q}t} (P_{in} \otimes |0\rangle). \tag{5.21}$$

Previously, in Section 4.6, we combined the two components using an approximation. It is less clear whether the approximation is still valid for all cases. By optimising separately, we have an upper bound on what can be achieved, and the approximation gives a lower bound on what is certainly achievable. It is less clear if we expect these

curves to coincide, and in Section 5.4.1, we show that, in general, they do not.

5.3 Required Qubits

One might ask why we might encode over higher excitation subspaces rather than using error-correction. We discuss here the additional qubits required for each of these techniques. Introducing higher excitation subspaces means that we have a certain minimum size of the encoding region as given in Eq. (5.7), meaning that we are required to use more qubits to achieve an improvement in fidelity. Even increasing to the second excitation subspace, where we have $K = 2$ requires encoding and decoding regions of at least $M = 5$ each, where we then have 10 qubits that are not included in the bulk of the chain. However, this does not necessarily scale with the length of the chain. A longer chain could benefit from a larger encoding region, but adding qubits to the bulk of the chain does not mean we are required to add qubits to the encoding and decoding region to improve the fidelity in the presence of noise. We compare this to quantum error correction where smallest possible code is a five-qubit code [69], meaning that for each logical qubit, we require 5 physical qubits. Error correcting codes for noisy spin chains are discussed in more detail in [34], [57], where the smallest error correcting code is shown to be 7 qubits. Our technique shows that improvement can be made with encoding regions smaller than $M = 7$, with chains of $N = 51$. It is expected that the encoding region will need to be larger to see similar improvements on larger chains, but this can be adjusted depending on exactly how much improvement one wants.

5.4 Noise Superoperators

The superoperators of noise presented in Sections 4.5.2 and 4.5.3 are still valid here such that dephasing is given by

$$\mathcal{Q}_D = \mathcal{H} + \frac{\Gamma_z}{2} \sum_{n=1}^{N} Z_n \otimes Z_n - \frac{\Gamma_z}{2} N \mathbb{1} \otimes \mathbb{1}, \tag{5.22}$$

and evolves the density vector as

$$|\rho'\rangle = e^{\mathcal{Q}_D t}|\rho\rangle.$$

The superoperator for amplitude damping is given as

$$\mathcal{Q}_A = \mathcal{H} + \frac{\Gamma_x}{2}\sum_{n=1}^{N}[(X_n + iY_n)\otimes(X_n + iY_n)^* = (\mathbb{1} - Z_n)\otimes\mathbb{1} - \mathbb{1}\otimes(\mathbb{1} - Z_n)], \tag{5.23}$$

and the evolution is given by

$$|\rho'\rangle = e^{\mathcal{Q}_A t}|\rho\rangle.$$

We can demonstrate what the Hamiltonian component of this will look like in the subspaces up to and including the $K = 2$, and we see that we have

$$\mathcal{H}_{0,1,2} = \begin{array}{c|ccc|c|cc|cc|c}
 & S_0 & S_{01} & S_{10} & S_{11} & S_{02} & S_{20} & S_{12} & S_{21} & S_{22} \\
\hline
S_0 & 0 & 0 & 0 & 0 & 0 & 0 & 0 & 0 & 0 \\
\hline
S_{01} & 0 & iH_1 & 0 & 0 & 0 & 0 & 0 & 0 & 0 \\
S_{10} & 0 & 0 & -iH_1 & 0 & 0 & 0 & 0 & 0 & 0 \\
\hline
S_{11} & 0 & 0 & 0 & -iH_1\otimes\mathbb{1} + i\mathbb{1}\otimes H_1 & 0 & 0 & 0 & 0 & 0 \\
\hline
S_{02} & 0 & 0 & 0 & 0 & iH_2 & 0 & 0 & 0 & 0 \\
S_{20} & 0 & 0 & 0 & 0 & 0 & -iH_2 & 0 & 0 & 0 \\
\hline
S_{12} & 0 & 0 & 0 & 0 & 0 & 0 & -iH_1\otimes\mathbb{1} + i\mathbb{1}\otimes H_2 & 0 & 0 \\
S_{21} & 0 & 0 & 0 & 0 & 0 & 0 & 0 & -iH_1\otimes\mathbb{1} + i\mathbb{1}\otimes H_2 & 0 \\
\hline
S_{22} & 0 & 0 & 0 & 0 & 0 & 0 & 0 & 0 & -iH_2\otimes\mathbb{1} + i\mathbb{1}\otimes H_2
\end{array}. \tag{5.24}$$

Now we know what the Hamiltonian looks like in the subspaces we are interested in, we can see what the dephasing and amplitude damping superoperators look like. We start with the dephasing superoperator (where we have not included $\mathcal{H}$ due to the size

of the matrix).

$$\mathcal{Q}_D - \mathcal{H} = \begin{array}{c|cccc|cccc|c} & S_0 & S_{01} & S_{10} & S_{11} & S_{02} & S_{20} & S_{12} & S_{21} & S_{22} \\ \hline S_0 & 0 & 0 & 0 & 0 & 0 & 0 & 0 & 0 & 0 \\ \hline S_{01} & 0 & \Gamma_z\mathbb{1} & 0 & 0 & 0 & 0 & 0 & 0 & 0 \\ S_{10} & 0 & 0 & -\Gamma_z\mathbb{1} & 0 & 0 & 0 & 0 & 0 & 0 \\ \hline S_{11} & 0 & 0 & 0 & -2\Gamma_z\sum_{k\neq j}\langle \mathbf{kj}|\mathbb{1} & 0 & 0 & 0 & 0 & 0 \\ \hline S_{02} & 0 & 0 & 0 & 0 & -2\Gamma_z\mathbb{1} & 0 & 0 & 0 & 0 \\ S_{20} & 0 & 0 & 0 & 0 & 0 & -2\Gamma_z\mathbb{1} & 0 & 0 & 0 \\ \hline S_{12} & 0 & 0 & 0 & 0 & 0 & 0 & -\Gamma_z\mathbb{1} & 0 & 0 \\ S_{21} & 0 & 0 & 0 & 0 & 0 & 0 & 0 & -\Gamma_z\mathbb{1} & 0 \\ \hline S_{22} & 0 & 0 & 0 & 0 & 0 & 0 & 0 & 0 & -2\Gamma_z\sum_{k,l\neq j,m}\langle \mathbf{kl,jm}|\mathbb{1} \end{array}. \tag{5.25}$$

We can see then that dephasing noise remains excitation preserving in the second excitation subspace, just as it does in the single excitation subspace.

We can also give the amplitude damping superoperator as

$$\mathcal{Q}_A - \mathcal{H} = \begin{array}{c|cccc|cccc|c} & S_0 & S_{01} & S_{10} & S_{11} & S_{02} & S_{20} & S_{12} & S_{21} & S_{22} \\ \hline S_0 & 0 & 0 & 0 & \Gamma_x\sum_k\langle \mathbf{kk}| & 0 & 0 & 0 & 0 & 0 \\ \hline S_{01} & 0 & -\frac{\Gamma_z}{2}\mathbb{1} & 0 & 0 & 0 & 0 & \mathbf{A} & 0 & 0 \\ S_{10} & 0 & 0 & -\frac{\Gamma_z}{2}\mathbb{1} & 0 & 0 & 0 & 0 & \mathbf{B} & 0 \\ \hline S_{11} & 0 & 0 & 0 & -\Gamma_z\mathbb{1} & 0 & 0 & 0 & 0 & \mathbf{C} \\ \hline S_{02} & 0 & 0 & 0 & 0 & -\Gamma_z\mathbb{1} & 0 & 0 & 0 & 0 \\ S_{20} & 0 & 0 & 0 & 0 & 0 & -\Gamma_z\mathbb{1} & 0 & 0 & 0 \\ \hline S_{12} & 0 & 0 & 0 & 0 & 0 & 0 & -\frac{3\Gamma_z}{2}\mathbb{1} & 0 & 0 \\ S_{21} & 0 & 0 & 0 & 0 & 0 & 0 & 0 & -\frac{3\Gamma_z}{2}\mathbb{1} & 0 \\ \hline S_{22} & 0 & 0 & 0 & 0 & 0 & 0 & 0 & 0 & -2\Gamma_z\mathbb{1} \end{array}, \tag{5.26}$$

where the elements of A are given by $\langle 0,k|i,jk\rangle = \Gamma_x\delta_{ij}$ and $\langle 0,j|i,jk\rangle = \Gamma_x\delta_{ik}$. We have the elements of B given by $\langle j,0|ij,k\rangle = \Gamma_x\delta_{ik}$ and $\langle i,0|ij,k\rangle = \Gamma_x\delta_{jk}$. Finally, we have that elements of C are $\langle i,k|ij,kl\rangle = \Gamma_x\delta_{jl}$, $\langle j,l|ij,kl\rangle = \Gamma_x\delta_{ik}$, $\langle i,l|ij,kl\rangle = \Gamma_x\delta_{jk}$, and $\langle j,k|ij,kl\rangle = \Gamma_x\delta_{il}$. These are the elements that cause amplitude damping noise to be excitation decreasing.

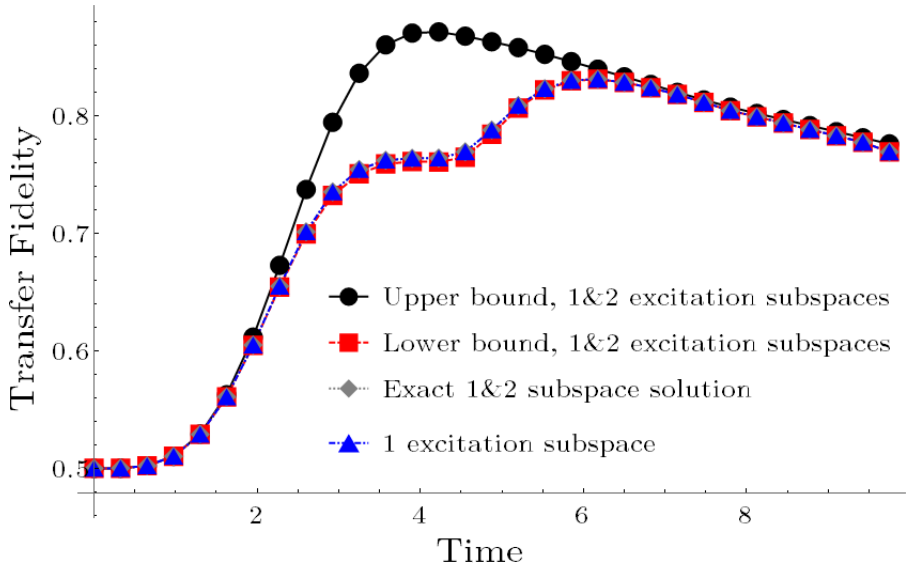

Figure 5.1: *Comparison of the upper and lower bounds of the approximation introduced in Section 4.6 for a Uniform chain. We also include the encoding in the single excitation subspace. Chain of* $N = 13$ *with encoding region of 5.*

5.4.1 Structure of S and R

In Section 5.2, we have given expressions for S and R when we consider multiple excitations. However, one cannot optimise these separately as we must have one single input state. In Section 4.6.3, we demonstrated an optimisation that works in the single excitation subspace, and we now consider whether this is still a valid approximation. In Fig. 5.1, we show the evolution of an $N = 13$ Uniform system with encoding regions of $M = 5$, and we encode across subspaces up to and including $K = 2$. We also include the evolution in only the single excitation subspace (blue). We can see here that there is no improvement from encoding in the second excitation subspace. We note that the separate optimisation implies that there may be a better approximation. To make sense of this plot, we consider the structure of S and R. We first consider S in the context of excitation preserving noise, and then amplitude damping noise. The matrix, S, essentially shows us how our input states evolve to our output states, such that we are considering the evolution

$$|\psi_{in}\mathbf{0}\rangle \otimes |\mathbf{0}\rangle \rightarrow |\mathbf{0}\psi_{out}\rangle \otimes |\mathbf{0}\rangle. \tag{5.27}$$

If our noise is excitation preserving, then a 2 excitation input will evolve to a 2 excitation output and similarly, a 1 excitation input will evolve to a 1 excitation output. Then we

have some block structure to the S matrix, separating excitation subspaces as so

$$S = \begin{array}{c} \\ S_{10} \\ S_{20} \end{array} \begin{array}{c} \begin{array}{cc} S_{10} & S_{20} \end{array} \\ \left[\begin{array}{c|c} 1Ex & 0 \\ \hline 0 & 2Ex \end{array}\right] \end{array}. \tag{5.28}$$

We must also consider what happens when noise is excitation decreasing (as in the case of amplitude damping noise). If we refer back to Eq. (5.23), we can see that the part that makes this excitation decreasing is $(X_n + iY_n) \otimes (X_n + iY_n)^*$. This requires that we are able to remove an excitation from both components of the tensor product $|\psi\rangle \otimes |\mathbf{0}\rangle$, which we cannot, as the second component does not contain an excitation. We can also see this clearly from Eq. (5.26), where the blocks belonging to these components are all 0 (other than those on the diagonal, which are excitation preserving).

If we consider R in the excitation preserving case, we can show that it also exhibits this block structure. Our input state looks like $|\psi_{in_1}\mathbf{0}\rangle \otimes |\psi_{in_2}\mathbf{0}\rangle$, and our output components are given by $\sum_{kz} \langle kz| \otimes \langle kz|$. Then we can see that if $|\psi_{in_1}\rangle$ contains 2 excitations, it will evolve to a state $\langle kz|$ with 2 excitations. Since we only take pure states as output, the other $\langle kz|$ components must contain 2 excitations, and therefore must come from an input state $|\psi_{in_2}\rangle$ containing 2 excitations. The same is true for 1 excitation. If refer to Eq. (5.26), which is excitation decreasing, we can see that the output components $\langle nn|$ only come from the input components $|mm\rangle$ for $m \geq n$. Within those components there are no $|ij\rangle$ terms for $i \neq j$, so we still have some block structure.

5.5 Conclusion

We have demonstrated that our encoding scheme is not restricted to the single excitation subspace and that we can extend it to higher subspaces as long as our encoding region is large enough that we can have orthogonal states on all sites within the encoding region, not including the final site. We demonstrated this with a short chain of $N = 13$, with an encoding region of $M = 5$ and we encode up to and including the 2^{nd} excitation subspace.

We expected this to show a significant improvement over encoding in the single excitation subspace, as our amplitude damping noise is excitation decreasing. Instead, we saw that the optimal encoding was found in the single excitation subspace. Our scheme does not allow for full error-correction, but it does lead to significant improvements in transfer fidelity with fewer additional qubits, when we encode in the single excitation subspace, which can be useful for devices where a large number of qubits is not available. We are unable to directly compare our scheme to the error correcting codes in [34] and [57] as those systems require simulation of too large a Hilbert space to be practical. We note that these error correcting codes are only designed to tolerate a single errors and the stored information could be completely destroyed if a second error is present. Our technique does not have such a rigid threshold and may be likely to perform better in certain scenarios.

Chapter 6

Summary and Further Work

6.1 Summary

Full scale quantum computation is on the horizon and will introduce significant improvements on classical computation, therefore leading to leaps in our understanding of various other topics. Quantum spin chains have been introduced as systems used to transfer states within quantum devices. There has been much theoretical study of these spin chains and we have already shown above that they can provide fast, high quality transfer. By selecting particular couplings, they can even provide perfect state transfer for any length of chain. However, we know that any physical implementation of these devices will be subject to manufacturing errors and noise.

In this thesis, we have presented particular problems with the physical implementation of these spin chains and introduced a technique than can improve transfer fidelity in the presence of such issues. We first demonstrated how the energies within a system are affected by imperfect manufacture, and how one can model such errors. We then introduced the encoding scheme given in [29] and applied it to such systems, showing significant improvement. Briefly, we considered how one might build a chain that is robust against these defects. We then presented a method whereby one can model noisy evolution within quantum spin chains. The results of this showed that even low levels of noise can be damaging to the fidelity of state transfer that these systems are able to achieve. Our encoding technique was extended to treat non-unitary evolution such that we could apply it to these noisy systems, and we demonstrated that improvements were made over all systems we considered. Finally, we discussed the possibility of encoding over higher excitation subspaces, and developed the encoding scheme such that it can be used as such. The main results are summarised as follows

- Fabrication defects lead to a significant reduction in fidelity for spin chains
- We can improve the fidelity of these spin chains in the presence of errors, by using the encoding scheme presented in [29]
- We are able to treat the density operator as a vector and therefore evaluate the effects of noise on a system, where both types of noise considered lead to a

reduction in fidelity even at low levels

- The encoding technique can be extended to consider non-unitary evolution and can then be applied to noisy systems
- Such encoding leads to significant improvements in fidelity in the presence of both types of noise, with a lower number of qubits than error-correction
- Encoding in higher subspaces leads to a slight improvement in fidelity for the Uniform chain, but no improvement in the linear chain

Our methods provide a way to deal with the errors and noise that will occur in physical implementations of quantum spin systems, without needing full error correction techniques. We have demonstrated the flexibility of our technique and its applicability to various scenarios. Numerical simulations are provided to demonstrate the improvement that can be made in particular scenarios, but we note these are a small set of the potential applications of this technique.

6.2 Further Work

6.2.1 Building Robust Chains

In Section 3.5, we took a brief detour to consider how one could build chains that are more robust against fabrication defects. We showed that adding a perturbation to the Hamiltonian to mitigate the effects of the errors would not be possible, due to the random nature of such defects. There may, however, be other ways to make systems more robust against random errors in the presence of encoding. We have not considered here how to build a chain that is more robust against noise. We note that in a noisy system, faster transfer is likely to lead to better fidelity, and that the uniform chain is the fastest. We saw from the demonstrations in Chapter 4, that the Uniform and Apollaro chains perform equally well after encoding. The x and y values for the Apollaro chain are optimised for end-to-end transfer, and there may be a possibility to improve transfer by optimising

these in the encoding regime and/or optimising them in the presence of noise. We then see that work could be done to further improve these systems, by considering the construction of these chains.

6.2.2 Higher Subspaces

In Chapter 5, we considered the use of multiple excitation encodings. We have demonstrated that our encoding technique can be applied in this scenario, although demonstrations showed only mild improvement in the case of the uniform chain and no improvement in the case of the Linear chain. We restricted ourselves to 2 excitations, but there is a possibility that further improvement can be made from higher subspaces (although this would require a larger encoding region). Our technique was demonstrated on the Uniform and Linear chains, and it is possible that other types of chains may show better results.

6.3 Final Conclusion

In this thesis, we have introduced the reader to quantum state transfer through spin chains and the issues we are required to overcome to realise such systems. We have presented a technique that leads to significant improvement in state transfer fidelity, and is widely applicable. Demonstrations show that the technique works well in various scenarios and can be extended to noisy systems and higher subspaces. Finally, we have shown that there is further work that may be done on these areas.

Appendix A

The Partial Trace

The partial trace is a method by which we can trace off the states on a set of qubits, leaving only the states on the qubits we are interested in. It is given formally in [48] as

$$(\mathrm{Tr} \otimes \mathbb{1}_{L(y)})(X \otimes Y) = \mathrm{Tr}(X)Y, \tag{A.1}$$

for all operators $X \in L(x)$ and $Y \in L(y)$. If we have a chain of N qubits, we often want to know the state of a single qubit rather than the whole chain. For example, if we have completed a state transfer protocol and want to extract from the last site, it is useful to consider the state of that final site independently from the rest of the chain.

Example 5. We take a simple example for $N = 3$, where our chain is in the state

$$|\psi\rangle = \alpha|\mathbf{0}\rangle + \beta|\mathbf{3}\rangle \tag{A.2}$$

meaning that the excitation is located on the 3rd site (in this case, the final site). We then want to take the partial trace over all sites apart from the N^{th}. We start by constructing the density matrix, which is given by

$$\rho = |\psi\rangle\langle\psi| = |\alpha|^2|000\rangle\langle 000| + \alpha\beta^*|000\rangle\langle 001| + \alpha^2\beta|001\rangle\langle 000| + |\beta|^2|001\rangle\langle 001|. \tag{A.3}$$

We then take the inner product of all the sites other than the site we want the state of

$$|\alpha|^2|0\rangle\langle 0|\langle 00|00\rangle + \alpha\beta^*|0\rangle\langle 1|\langle 00|00\rangle + \alpha^*\beta|1\rangle\langle 0|\langle 00|00\rangle + |\beta|^2|0\rangle\langle 0|\langle 00|00\rangle \quad \text{(A.4)}$$

where we know that the inner product $\langle 00|00\rangle = 1$ so we are left with

$$|\alpha|^2|0\rangle\langle 0| + \alpha\beta^*|0\rangle\langle 1| + \alpha^*\beta|1\rangle\langle 0| + |\beta|^2|0\rangle\langle 0| = \begin{bmatrix} |\alpha|^2 & \alpha\beta^* \\ \alpha^*\beta & |\beta|^2 \end{bmatrix}. \quad \text{(A.5)}$$

This gives us the state just on the final qubit.

Appendix B

The Unitary

Relevant to Section 4.6.1. A unitary operator is an operator that maps a set of mutually orthogonal states onto another set of mutually orthogonal states, and the existence of such unitary can be proven in general using Gram-Schmidt [70]. Here, we demonstrate that apart from some restraints on the unitary operator, we are free to choose any operator that satisfies such restraints. Let's consider a decoding region of size 3, which requires a unitary operator of size 8×8. After evolution, the state of this region can be given by

$$|\psi\rangle = \alpha_2|\mathbf{N\text{-}2}\rangle + \alpha_1|\mathbf{N\text{-}1}\rangle + \alpha_0|\mathbf{N}\rangle, \tag{B.1}$$

where as always, N is the length of our chain. To demonstrate the action of the unitary operator, we choose the constants $\{\alpha_2, \alpha_1, \alpha_0\}$ to be $\{\sqrt{\frac{2}{3}}, 0, \frac{1}{\sqrt{3}}\}$ respectively. As mentioned above, the job of our unitary is to map a set of orthogonal states onto another set of orthogonal states. Given that the aim of our unitary is to 'move' the excitation contained within the encoding zone to the final site, we can see that the act of the unitary on $|\psi\rangle$ should be

$$U|\psi\rangle = |\mathbf{N}\rangle. \tag{B.2}$$

We can then introduce 2 new states that are orthogonal to $|\boldsymbol{\psi}\rangle$ and to one another. We are free to choose these states, and we ensure they are normalised. We therefore choose

$$|\boldsymbol{\psi}_1^{\perp}\rangle = \frac{1}{\sqrt{3}}|\mathbf{N\text{-}2}\rangle - \sqrt{\frac{2}{3}}|\mathbf{N}\rangle, \tag{B.3}$$

and

$$|\boldsymbol{\psi}_2^{\perp}\rangle = |\mathbf{N\text{-}1}\rangle. \tag{B.4}$$

Then after application of the unitary, we require

$$U|\boldsymbol{\psi}_1^{\perp}\rangle = |\mathbf{N,N\text{-}1}\rangle \tag{B.5a}$$

$$U|\boldsymbol{\psi}_2^{\perp}\rangle = |\mathbf{N,N\text{-}2}\rangle. \tag{B.5b}$$

This information then allows us to fill in some elements of our unitary operator. For our particular case, we therefore have some known elements. We choose to label the elements of our unitary operator as $\{000, 001, 010, 100, 011, 101, 110, 111\}$, where the position of the 1 indicates that there is some portion of excitation present on that site, and 001 refers to site $|\mathbf{N\text{-}2}\rangle$ and 100 refers to $|\mathbf{N}\rangle$. We first know that we require

$$\sqrt{\frac{2}{3}}|\mathbf{N\text{-}2}\rangle + 0|\mathbf{N\text{-}1}\rangle + \frac{1}{\sqrt{3}}|\mathbf{N}\rangle \rightarrow |\mathbf{N}\rangle, \tag{B.6}$$

and can therefore fill in the corresponding elements.

$$U = \begin{array}{c} \\ 000 \\ 001 \\ 010 \\ 100 \\ 011 \\ 101 \\ 110 \\ 111 \end{array} \begin{array}{c} \begin{array}{cccccccc} 000 & 001 & 010 & 100 & 011 & 101 & 110 & 111 \end{array} \\ \begin{pmatrix} u_{1,1} & u_{1,2} & u_{1,3} & u_{1,4} & u_{1,5} & u_{1,6} & u_{1,7} & u_{1,8} \\ u_{2,1} & u_{2,2} & u_{2,3} & u_{2,4} & u_{2,5} & u_{2,6} & u_{2,7} & u_{2,8} \\ u_{3,1} & u_{3,2} & u_{3,3} & u_{3,4} & u_{3,5} & u_{3,6} & u_{3,7} & u_{3,8} \\ 0 & \sqrt{\frac{2}{3}} & 0 & \frac{1}{\sqrt{3}} & 0 & 0 & 0 & 0 \\ u_{15,1} & u_{5,2} & u_{5,3} & u_{5,4} & u_{5,5} & u_{5,6} & u_{5,7} & u_{5,8} \\ u_{6,1} & u_{6,2} & u_{6,3} & u_{6,4} & u_{6,5} & u_{6,6} & u_{6,7} & u_{6,8} \\ u_{7,1} & u_{7,2} & u_{7,3} & u_{7,4} & u_{7,5} & u_{7,6} & u_{7,7} & u_{7,8} \\ u_{8,1} & u_{8,2} & u_{8,3} & u_{8,4} & u_{8,5} & u_{8,6} & u_{8,7} & u_{8,8} \end{pmatrix} \end{array}. \tag{B.7}$$

We can similarly use the other known transfers of states to fill in further elements of the unitary. Considering also that the matrix must be orthonormal, we can fill in the other elements that must be 0. We can also add the assumption that $U|\mathbf{0}\rangle \rightarrow |\mathbf{0}\rangle$ by giving that element the value of 1 (it must transfer to itself)

$$U = \begin{array}{c} \\ 000 \\ 001 \\ 010 \\ 100 \\ 011 \\ 101 \\ 110 \\ 111 \end{array} \begin{array}{c} \begin{array}{cccccccc} 000 & 001 & 010 & 100 & 011 & 101 & 110 & 111 \end{array} \\ \begin{pmatrix} 1 & 0 & 0 & 0 & 0 & 0 & 0 & 0 \\ 0 & 0 & 0 & 0 & u_{2,5} & u_{2,6} & u_{2,7} & u_{2,8} \\ 0 & 0 & 0 & 0 & u_{3,5} & u_{3,6} & u_{3,7} & u_{3,8} \\ 0 & \sqrt{\frac{2}{3}} & 0 & \frac{1}{\sqrt{3}} & 0 & 0 & 0 & 0 \\ 0 & 0 & 0 & 0 & u_{5,5} & u_{5,6} & u_{5,7} & u_{5,8} \\ 0 & 0 & 1 & 0 & 0 & 0 & 0 & 0 \\ 0 & \frac{1}{\sqrt{3}} & 0 & -\sqrt{\frac{2}{3}} & 0 & 0 & 0 & 0 \\ 0 & 0 & 0 & 0 & u_{8,5} & u_{8,6} & u_{8,7} & u_{8,8} \end{pmatrix} \end{array}. \tag{B.8}$$

Finally, we can choose the other elements freely. We choose to have $|111\rangle$ transfer to itself and construct the matrix so that there is some symmetry with the remaining

elements. Our final U is then

$$U = \begin{array}{c} \\ 000 \\ 001 \\ 010 \\ 100 \\ 011 \\ 101 \\ 110 \\ 111 \end{array} \begin{array}{c} \begin{array}{cccccccc} 000 & 001 & 010 & 100 & 011 & 101 & 110 & 111 \end{array} \\ \begin{pmatrix} 1 & 0 & 0 & 0 & 0 & 0 & 0 & 0 \\ 0 & 0 & 0 & 0 & \sqrt{\frac{2}{3}} & 0 & \frac{1}{\sqrt{3}} & 0 \\ 0 & 0 & 0 & 0 & 0 & 1 & 0 & 0 \\ 0 & \sqrt{\frac{2}{3}} & 0 & \frac{1}{\sqrt{3}} & 0 & 0 & 0 & 0 \\ 0 & 0 & 0 & 0 & \frac{1}{\sqrt{3}} & 0 & -\sqrt{\frac{2}{3}} & 0 \\ 0 & 0 & 1 & 0 & 0 & 0 & 0 & 0 \\ 0 & \frac{1}{\sqrt{3}} & 0 & -\sqrt{\frac{2}{3}} & 0 & 0 & 0 & 0 \\ 0 & 0 & 0 & 0 & 0 & 0 & 0 & 1 \end{pmatrix} \end{array}. \tag{B.9}$$

This is just an example of a Unitary operator that we could use. However, as long as we stick to our previously mentioned constraints, we are relatively free to choose any appropriate Unitary.

Bibliography

[1] N. Tredennick, "Microprocessor-based computers," *Computer*, vol. 29, pp. 27–37, Oct. 1996.

[2] H. Ma, M. Govoni, and G. Galli, "Quantum simulations of materials on near-term quantum computers," *npj Computational Materials*, vol. 6, p. 85, Dec. 2020.

[3] J. Preskill, "Quantum computing and the entanglement frontier," *arXiv:1203.5813 [cond-mat, physics:quant-ph]*, Nov. 2012.

[4] B. M. Terhal, "Quantum supremacy, here we come," *Nature Physics*, vol. 14, pp. 530–531, June 2018. Number: 6 Publisher: Nature Publishing Group.

[5] R. P. Feynman, "Simulating physics with computers," *International Journal of Theoretical Physics*, vol. 21, pp. 467–488, June 1982.

[6] A. Cho, "Google claims quantum computing milestone," *Science*, vol. 365, pp. 1364–1364, Sept. 2019.

[7] R. Courtland, "Google aims for quantum computing supremacy [News]," *IEEE Spectrum*, vol. 54, pp. 9–10, June 2017. Conference Name: IEEE Spectrum.

[8] M. Steffen, D. P. DiVincenzo, J. M. Chow, T. N. Theis, and M. B. Ketchen, "Quantum computing: An IBM perspective," *IBM Journal of Research and Development*, vol. 55, pp. 13:1–13:11, Sept. 2011.

[9] T. Hey, "Quantum computing: An introduction," *Computing & Control Engineering Journal*, vol. 10, pp. 105–112, Sept. 1999.

[10] J. Preskill, "Quantum Computing in the NISQ era and beyond," *Quantum*, vol. 2, p. 79, Aug. 2018.

[11] M. A. Nielsen and I. L. Chuang, *Quantum computation and quantum information*. Cambridge ; New York: Cambridge University Press, 10th anniversary ed., 2010.

[12] N. Gershenfeld and I. L. Chuang, "Quantum Computing with Molecules," *Scientific American*, vol. 278, pp. 66–71, June 1998.

[13] R. Marx, A. F. Fahmy, J. M. Myers, W. Bermel, and S. J. Glaser, "Approaching five-bit NMR quantum computing," *Physical Review A*, vol. 62, p. 012310, June 2000. Publisher: American Physical Society.

[14] J. Zhang, G. L. Long, W. Zhang, Z. Deng, W. Liu, and Z. Lu, "Simulation of a Heisenberg XY- chain and realization of a perfect state transfer algorithm using liquid nuclear magnetic resonance," *arXiv:quant-ph/0503199*, Mar. 2005.

[15] D. G. Cory, R. Laflamme, E. Knill, L. Viola, T. F. Havel, N. Boulant, G. Boutis, E. Fortunato, S. Lloyd, R. Martinez, C. Negrevergne, M. Pravia, Y. Sharf, G. Teklemariam, Y. S. Weinstein, and W. H. Zurek, "NMR Based Quantum Information Processing: Achievements and Prospects," *Fortschritte der Physik*, vol. 48, no. 9-11, pp. 875–907, 2000.

[16] J. A. Jones, "Quantum Computing with NMR," *Progress in Nuclear Magnetic Resonance Spectroscopy*, vol. 59, pp. 91–120, Aug. 2011.

[17] J. I. Cirac and P. Zoller, "Quantum Computations with Cold Trapped Ions," *Physical Review Letters*, vol. 74, pp. 4091–4094, May 1995. Publisher: American Physical Society.

[18] T. P. Harty, D. T. C. Allcock, C. J. Ballance, L. Guidoni, H. A. Janacek, N. M. Linke, D. N. Stacey, and D. M. Lucas, "High-fidelity preparation, gates, memory and readout of a trapped-ion quantum bit," *Physical Review Letters*, vol. 113, p. 220501, Nov. 2014.

[19] D. J. Wineland, M. Barrett, and et al, "Quantum information processing with trapped ions," *The Royal Society*, p. 13, 2003.

[20] J. M. Pino, J. M. Dreiling, C. Figgatt, J. P. Gaebler, S. A. Moses, M. S. Allman, C. H. Baldwin, M. Foss-Feig, D. Hayes, K. Mayer, C. Ryan-Anderson, and B. Neyenhuis, "Demonstration of the trapped-ion quantum CCD computer architecture," *Nature*, vol. 592, pp. 209–213, Apr. 2021.

[21] G. Wendin, "Quantum information processing with superconducting circuits: a review," *Reports on Progress in Physics*, vol. 80, p. 106001, Oct. 2017.

[22] C. Bennett and Bishop, Lev, "The qubit," July 2021.

[23] A. Romito, R. Fazio, and C. Bruder, "Solid-state quantum communication with Josephson arrays," *Physical Review B*, vol. 71, p. 100501, Mar. 2005.

[24] I. D'Amico, "Quantum dot-based quantum buses for quantum computer hardware architecture," *Microelectronics Journal*, vol. 37, pp. 1440–1441, Dec. 2006.

[25] D. Loss and D. P. DiVincenzo, "Quantum computation with quantum dots," *Physical Review A*, vol. 57, pp. 120–126, Jan. 1998.

[26] M. Bellec, G. M. Nikolopoulos, and S. Tzortzakis, "A Faithful Communication Hamiltonian in Photonic Lattices," *Optics Letters*, vol. 37, p. 4504, Nov. 2012. arXiv: 1210.1009.

[27] A. Perez-Leija, R. Keil, A. Kay, H. Moya-Cessa, S. Nolte, L.-C. Kwek, B. M. Rodríguez-Lara, A. Szameit, and D. N. Christodoulides, "Coherent Quantum Transport in Photonic Lattices," *Physical Review A*, vol. 87, p. 012309, Jan. 2013.

[28] R. J. Chapman, M. Santandrea, Z. Huang, G. Corrielli, A. Crespi, M.-H. Yung, R. Osellame, and A. Peruzzo, "Experimental perfect state transfer of an entangled photonic qubit," *Nature Communications*, vol. 7, p. 11339, Sept. 2016.

[29] H. L. Haselgrove, "Optimal state encoding for quantum walks and quantum communication over spin systems," *Physical Review A*, vol. 72, Dec. 2005.

[30] S. Bose, "Quantum Communication Through an Unmodulated Spin Chain," *Physical Review Letters*, vol. 91, Nov. 2003.

[31] M. Christandl, N. Datta, A. Ekert, and A. J. Landahl, "Perfect State Transfer in Quantum Spin Networks," *Physical Review Letters*, vol. 92, p. 187902, May 2004.

[32] P. Karbach and J. Stolze, "Spin chains as perfect quantum state mirrors," *Physical Review A*, vol. 72, p. 030301, Sept. 2005. Publisher: American Physical Society.

[33] A. Kay, "A Review of Perfect State Transfer and its Application as a Constructive Tool," *International Journal of Quantum Information*, vol. 08, pp. 641–676, June 2010.

[34] A. Kay, "Perfect Coding for Dephased Quantum State Transfer," *Physical Review A*, vol. 97, p. 032317, Mar. 2018.

[35] M.-H. Yung, "Quantum speed limit for perfect state transfer in one dimension," *Physical Review A*, vol. 74, p. 030303, Sept. 2006.

[36] G. M. L. Gladwell, "Inverse Problems in Vibration," *Applied Mechanics Reviews*, vol. 39, pp. 1013–1018, July 1986.

[37] L. Vinet and A. Zhedanov, "Almost perfect state transfer in quantum spin chains," *Physical Review A*, vol. 86, p. 052319, Nov. 2012.

[38] L. Banchi, G. Coutinho, C. Godsil, and S. Severini, "Pretty good state transfer in qubit chains—The Heisenberg Hamiltonian," *Journal of Mathematical Physics*, vol. 58, p. 032202, Mar. 2017.

[39] M. Christandl, N. Datta, T. C. Dorlas, A. Ekert, A. Kay, and A. J. Landahl, "Perfect transfer of arbitrary states in quantum spin networks," *Physical Review A*, vol. 71, Mar. 2005.

[40] T. J. G. Apollaro, L. Banchi, A. Cuccoli, R. Vaia, and P. Verrucchi, "99-fidelity ballistic quantum-state transfer through long uniform channels," *Physical Review A*, vol. 85, p. 052319, May 2012.

[41] A. Zwick, G. Alvarez, J. Stolze, and O. Osenda, "Quantum state transfer in disordered spin chains: How much engineering is reasonable?," *Quantum Information & Computation*, vol. 15, pp. 582–600, May 2015.

[42] C. Albanese, M. Christandl, N. Datta, and A. Ekert, "Mirror Inversion of Quantum States in Linear Registers," *Physical Review Letters*, vol. 93, p. 230502, Nov. 2004.

[43] M. Oskin, F. Chong, I. Chuang, and J. Kubiatowicz, "Building quantum wires: the long and the short of it," in *30th Annual International Symposium on Computer Architecture, 2003. Proceedings.*, pp. 374–385, June 2003. ISSN: 1063-6897.

[44] M. Murphy, S. Montangero, V. Giovannetti, and T. Calarco, "Communication at the quantum speed limit along a spin chain," *Physical Review A*, vol. 82, p. 022318, Aug. 2010.

[45] T. Caneva, M. Murphy, T. Calarco, R. Fazio, S. Montangero, V. Giovannetti, and G. E. Santoro, "Optimal Control at the Quantum Speed Limit," *Physical Review Letters*, vol. 103, p. 240501, Dec. 2009.

[46] A. Kay, "A Note on the Speed of Perfect State Transfer," *arXiv:1609.01854 [quant-ph]*, Sept. 2016. arXiv: 1609.01854.

[47] A. Zwick, G. A. Álvarez, J. Stolze, and O. Osenda, "Robustness of spin-coupling distributions for perfect quantum state transfer," *Physical Review A*, vol. 84, p. 022311, Aug. 2011.

[48] J. Watrous, "The Theory of Quantum Information," May 2018.

[49] G. De Chiara, D. Rossini, S. Montangero, and R. Fazio, "From perfect to fractal transmission in spin chains," *Physical Review A*, vol. 72, p. 012323, July 2005.

[50] A. Kay, "Perfect state transfer: Beyond nearest-neighbor couplings," *Physical Review A*, vol. 73, p. 032306, Mar. 2006.

[51] D. Burgarth and S. Bose, "Perfect quantum state transfer with randomly coupled quantum chains," *New Journal of Physics*, vol. 7, pp. 135–135, May 2005.

[52] B. Georgeot and D. L. Shepelyansky, “Emergence of quantum chaos in the quantum computer core and how to manage it,” *Physical Review E*, vol. 62, pp. 6366–6375, Nov. 2000.

[53] G. Benenti, G. Casati, S. Montangero, and D. L. Shepelyansky, “Efficient Quantum Computing of Complex Dynamics,” *Physical Review Letters*, vol. 87, p. 227901, Nov. 2001.

[54] N. Zagury, A. Aragao, J. Casanova, and E. Solano, “Unitary expansion of the time evolution operator,” *Physical Review A*, vol. 82, p. 042110, Oct. 2010.

[55] M. L. Hu and H. L. Lian, “State transfer in intrinsic decoherence spin channels,” *The European Physical Journal D*, vol. 55, pp. 711–721, Dec. 2009.

[56] G. J. Milburn, “Intrinsic decoherence in quantum mechanics,” *Physical Review A*, vol. 44, pp. 5401–5406, Nov. 1991.

[57] A. Kay, “Quantum Error Correction for State Transfer in Noisy Spin Chains,” *Physical Review A*, vol. 93, p. 042320, Apr. 2016.

[58] D. Burgarth and S. Bose, “Conclusive and arbitrarily perfect quantum-state transfer using parallel spin-chain channels,” *Physical Review A*, vol. 71, p. 052315, May 2005.

[59] A. M. Steane, “A Tutorial on Quantum Error Correction, Proceedings of the International School of Physics "Enrico Fermi", Course CKXII, "Quantum Computers, Algorithms and Chaos,",” *IOS Press, Amsterdam 2006*, p. 24.

[60] P. W. Shor, “Scheme for reducing decoherence in quantum computer memory,” *Physical Review A*, vol. 52, pp. R2493–R2496, Oct. 1995. Publisher: American Physical Society.

[61] A. M. Steane, “Error Correcting Codes in Quantum Theory,” *Physical Review Letters*, vol. 77, pp. 793–797, July 1996.

[62] A. R. Calderbank and P. W. Shor, "Good Quantum Error-Correcting Codes Exist," *Physical Review A*, vol. 54, pp. 1098–1105, Aug. 1996.

[63] A. Steane, "Multiple-particle interference and quantum error correction," *Proceedings of the Royal Society of London. Series A: Mathematical, Physical and Engineering Sciences*, vol. 452, pp. 2551–2577, Nov. 1996.

[64] C. H. Bennett, D. P. DiVincenzo, J. A. Smolin, and W. K. Wootters, "Mixed State Entanglement and Quantum Error Correction," *Physical Review A*, vol. 54, pp. 3824–3851, Nov. 1996.

[65] R. Laflamme, C. Miquel, J. P. Paz, and W. H. Zurek, "Perfect Quantum Error Correction Code," *arXiv:quant-ph/9602019*, Feb. 1996.

[66] E. Pednault and J. Gunnels, "On "Quantum Supremacy"," Oct. 2019. IBM Research Blog.

[67] D. Manzano, "A short introduction to the Lindblad Master Equation," *arXiv:1906.04478 [cond-mat, physics:quant-ph]*, June 2019.

[68] H. Singh, Arvind, and K. Dorai, "Using a Lindbladian approach to model decoherence in two coupled nuclear spins via correlated phase-damping and amplitude damping noise channels," *Pramana*, vol. 94, p. 160, Dec. 2020. arXiv: 2007.12972.

[69] E. Knill, R. Laflamme, R. Martinez, and C. Negrevergne, "Benchmarking Quantum Computers: The Five-Qubit Error Correcting Code," *Physical Review Letters*, vol. 86, pp. 5811–5814, June 2001.

[70] S. J. Leon, Björck, and W. Gander, "Gram-Schmidt orthogonalization: 100 years and more," *Numerical Linear Algebra with Applications*, vol. 20, no. 3, pp. 492–532, 2013. _eprint: https://onlinelibrary.wiley.com/doi/pdf/10.1002/nla.1839.